COPY NUMBER 16

NASA CR-137959
REPORT NUMBER • MDC A4434

GROUND TEST OF THE "D" SHAPED VENTED THRUST VECTORING NOZZLE

ISSUE DATE 15 OCTOBER, 1976

CONTRACT NUMBER NAS 2-8663

PREPARED BY D.W. ESKER

MCDONNELL AIRCRAFT COMPANY

Box 516, Saint Louis, Missouri 63166

MCDONNELL DOUGLAS CORPORATION

TABLE OF CONTENTS

LIST OF PAGES

Title
ii through xi
1 through 70
A-1 and A-2

SUMMARY

Static ground tests of a large scale lift/cruise thrust vectoring nozzle were conducted at the NASA-Ames Research Center outside test facility to establish (1) vectoring performance "in" and "out" of ground effect, (2) thrust spoilage capability, (3) compatibility of the nozzle with a turbotip fan, and (4) the nozzle structural temperature distribution. The purpose of the tests was the experimental determination of vectoring performance of a short coupled, vented nozzle design on a large scale, 60%, basis and to establish a comparison with small scale, 4.5%, test nozzle results. The test nozzle was a "boiler-plate" model of the MCAIR "D" vented nozzle configured for operation with the LF336/J85 turbotip lift fan system. Calibration of the LF336/J85 test fan with a simple convergent nozzle was performed with four different nozzle exit areas to establish reference thrust, nozzle pressure ratio, and nozzle corrected flow characteristics for comparison with the thrust vectoring nozzle data. Thrust vectoring tests with the "D" vented nozzle were conducted over the range of vector angles between 0° and 117° for several different nozzle exit areas.

Analysis of the large scale test data and comparisons with small scale performance showed:

- The effects of model scale between 4.5% and 60% on longitudinal and VTO performance out of ground effect are small. Agreement within 1% to 2% was obtained over the range of nozzle variables tested.
- In ground effect, the vented nozzle design was found to exhibit an increase in effective exit area as the ratio of ground height to fan diameter was reduced to 1.60. An increase in thrust performance was recorded during ground height reduction at 90% fan speed, the maximum speed tested, whereas a decrease in thrust was measured at lower fan speeds.
- Thrust reduction modulation (TRM), by porting exhaust flow through the top of the nozzle, is an effective thrust spoilage technique. The TRM tests with the "D" vented design showed a capability to reduce the nozzle thrust coefficient to 0.70 at the 90° vector angle.
- Compatibility of the nozzle design with a turbotip fan during thrust vectoring and spoilage operations was demonstrated by successful completion of the nozzle test program without detectable adverse effects on fan operation.

- Measurement of nozzle wall temperature distributions indicated that significant mixing of the fan flow with the high temperature (700°K) turbine exhaust takes place within the nozzle such that the temperature on the hood elements remained below 400°K (260°F).

LIST OF FIGURES

LIST OF FIGURES (Cont'd)

SYMBOLS

A_{FAN}	Cross sectional area at traversing probe location for integration of fan exit flow properties, 4776 cm^2
A_{NOZ}	Nozzle exit geometric area, cm^2
A_o	Nozzle entrance flow area, 6284 cm^2
A_{TRM}	Thrust reduction modulation port open area, 100% open area = 1581 cm^2
$A_{TURBINE}$	Cross sectional area at traversing probe location for integration of turbine exit flow properties, 2465 cm^2
C_T	Nozzle thrust coefficient, resultant gross thrust/reference thrust with Calibration Nozzle
D_F	LF336 fan diameter, 91.44 cm
F_G	Resultant gross thrust, newtons
h	Ground plane height, cm
N_F	Fan speed, RPM
NPR	Nozzle entrance total pressure ratio, $(P_T)_{NOZ}/P_A$
P_A	Ambient pressure, newtons/cm^2
P_S	Nozzle internal wall pressure, newtons/cm^2
P_T	Total pressure, newtons/cm^2
P_{T1-4}	Total pressure recorded on traversing probes 1 through 4, newtons/cm^2
$(P_T)_{FAN}$	Area weighted total pressure at fan exit, newtons/cm^2
$(P_T)_{NOZ}$	Mass weighted total pressure at nozzle entrance, newtons/cm^2
R	Gas Constant, 2.8696 X 10^6 cm^2/sec - K°
R_H	Hub centerbody radius at traversing probe location, 23.88 cm
R_M	Turbine midbox center radius at traversing probe location, 45.72 cm
R_T	Nozzle wall radius at traversing probe location, 53.62 cm
R_o	Normal distance between thrust vector and hood pivot point, cm
r	Radial position of traversing probe, cm
T_A	Ambient temperature, °K

SYMBOLS (Continued)

T_T	Total temperature, °K
T_{T1-4}	Total temperature recorded on traversing probes 1 through 4, °K
u_{ise}	Isentropic exit velocity, cm/sec
W_{FAN}	Fan mass flow rate, kg/sec
W_{GG}	Gas generator mass flow rate, kg/sec
W_{TOT}	Nozzle mass flow rate, kg/sec
δ	Relative absolute pressure ratio, ambient pressure/standard pressure
δ_t	Relative total pressure ratio, Total pressure/standard pressure
θ	Relative absolute temperature ratio, ambient temperature/standard temperature
θ_t	Relative total temperature ratio, Total temperature/standard temperature
θ_v	Thrust vector angle, degrees
ψ	Yaw vector angle, degrees
γ	Ratio of specific heats, C_p/C_v

ABBREVIATIONS

cm	Centimeters
N	Newtons
°K	Degrees Kelvin
kg	Kilograms
°R	Degrees Rankine
T/C	Thermocouple

CONVERSIONS

Newtons = 4.4482 pounds force

Kilograms = .4536 pounds mass

Centimeter = 2.54 inches

°Kelvin = 1.8 °Rankine

1. INTRODUCTION

Development of a high performance V/STOL aircraft for military and civil applications has been established as a major near term R&D program by both NASA and Navy. The Navy requires a multimission V/STOL aircraft in the 1980's capable of sea control operations from many platforms as well as ship to shore and shore to ship functions. Civil applications for V/STOL aircraft include short haul transports and utility aircraft for remote site operations.

McDonnell Aircraft Company (MCAIR), as a result of extensive studies of various V/STOL aircraft designs over the past decade, has identified the lift fan powered aircraft as a configuration which provides significant improvements in range/payload, speed, and mission adaptability over either rotary wing or other proposed V/STOL designs. The MCAIR lift/cruise fan aircraft (Figure 1-1) is a fixed wing vehicle powered by three interconnected single stage fans, two lift/cruise fans and one forward fuselage lift fan, which are used for powered lift flight modes. For cruise mode operations, the forward fan unit is shut down and the two lift/cruise fans provide thrust for conventional flight. Interconnection of the three fan units and the engines required to power them may be accomplished mechanically via gears and shafting or pneumatically by means of hot gas ducting and fan mounted tip turbines.

A key feature of this three fan arrangement is the utilization of two fan units for both vertical and cruise flight modes. Lift/cruise vectoring nozzles are used to vector fan thrust between the horizontal and vertical directions. The vectoring nozzles are also used to provide a portion of the aircraft attitude control forces required during low speed powered lift operation where there is insufficient aerodynamic control. The performance of the vectoring nozzle, particularly in the 90° vector position (VTO), impacts strongly on aircraft performance. For example, a 1% improvement in VTO thrust vectoring efficiency results in a 1% increase in aircraft gross takeoff weight capability and a corresponding 5% to 10% increase in payload range capability. As a consequence, the development of a high performance thrust vectoring nozzle is of primary importance to the successful development of the lift fan V/STOL aircraft.

The "D" vented thrust vectoring nozzle is a design which MCAIR has selected for extensive in-house developmental testing. This nozzle configuration is illustrated in Figure 1-2 in each of its primary functional modes, high speed cruise, low speed cruise, longitudinal vectoring, yaw vectoring, and thrust

FIGURE 1-1
MCAIR LIFT/CRUISE FAN AIRCRAFT

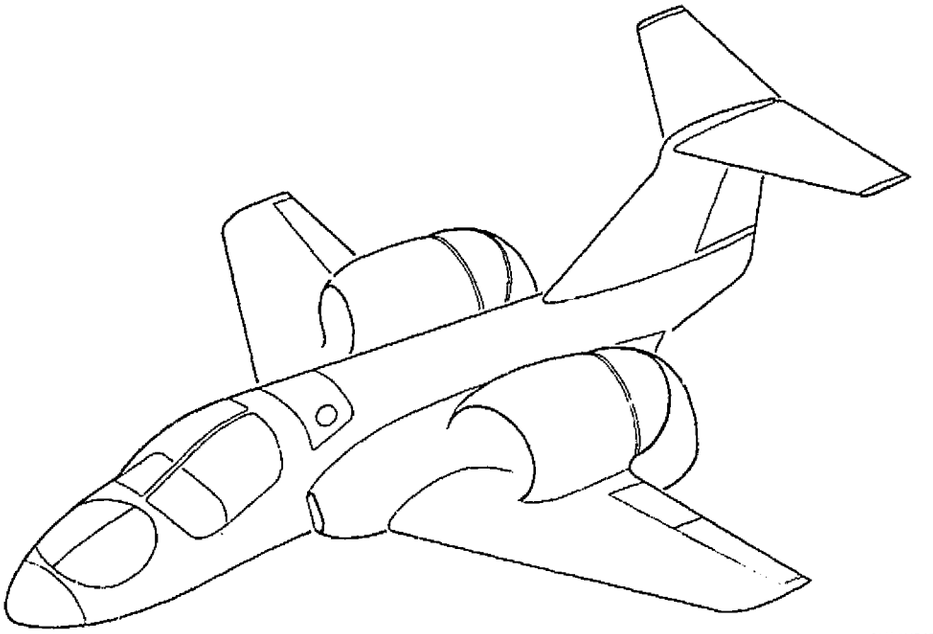

FIGURE 1-2
"D" VENTED LIFT/CRUISE VECTORING NOZZLE

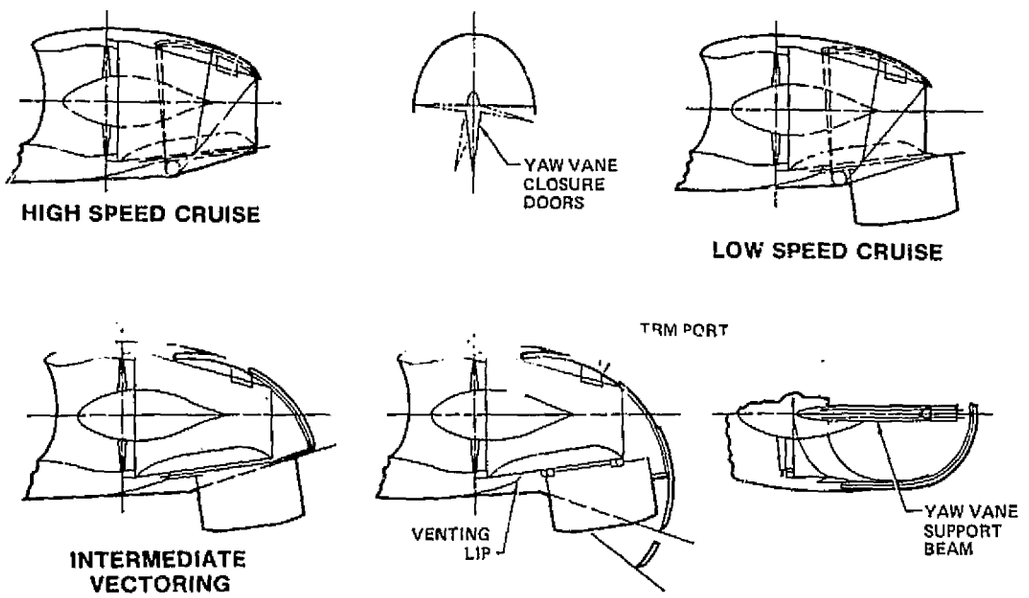

reduction modulation (spoilage). The designation, "D" vented, is used primarily to identify the shape of the nozzle exit in its cruise and VTO positions and the open or "vented" lower elbow corner which is formed in the VTO position. The venting feature, on the basis of small scale test results, provides entrainment of ambient air into the lower elbow corner region of the nozzle flow and results in improved 90° vectoring performance over an unvented design. This feature was also found in the small scale tests to provide a constant effective nozzle exit area when operated in ground effect.

A series of small scale model (3" entrance diameter) tests have been conducted at MCAIR to establish the performance envelope of the "D" vented nozzle over a range of nozzle entrance conditions, thrust vectoring angles, and nozzle exit geometries. As noted, VTO performance is of major importance and the small scale tests have been focused primarily on defining the VTO performance map for the "D" vented nozzle. Figure 1-3 depicts the VTO performance map which has resulted from the small scale tests in terms of thrust coefficient, C_T, specific nozzle entrance corrected flow rate, $(W\sqrt{\theta_t}/\delta_t A_o)$, and nozzle entrance pressure ratio (NPR). To utilize the map of Figure 1-3, nozzle entrance flow, total pressure, total temperature and entrance flow area data are required and are usually available from fan and engine performance decks for a particular fan system. The above data are used to calculate nozzle pressure ratio and specific nozzle entrance corrected flow parameter with which the map is entered to obtain a value of VTO thrust coefficient. This procedure has been carried out for the gas driven fan system presently being considered for the MCAIR Model 260 multimission lift fan aircraft, the General Electric LCF459/J97 lift cruise fan, Reference (1). The LCF459/J97 VTO operating point has been spotted on Figure 1-3 and indicates that a VTO thrust coefficient of 0.94 is achievable with the "D" vented nozzle using the small scale data base. The variation of nozzle thrust coefficient with vectoring angle as measured via the small scale models is shown in Figure 1-4 and indicates that the cruise mode thrust coefficient of the "D" vented nozzle is 0.985. The VTO and cruise mode thrust coefficients defined from the scale model tests provide the MCAIR Model 260 multimission lift fan aircraft with excellent vertical takeoff gross weight capability and efficient cruise operating characteristics.

Recognizing the need to establish the validity of the small scale nozzle data base with large scale test data, the NASA Research Center, with Navy support, contracted with MCAIR to design and test a "boilerplate" version of

FIGURE 1-3
VTO PERFORMANCE MAP FOR "D" VENTED NOZZLE
Small Scale Test Data

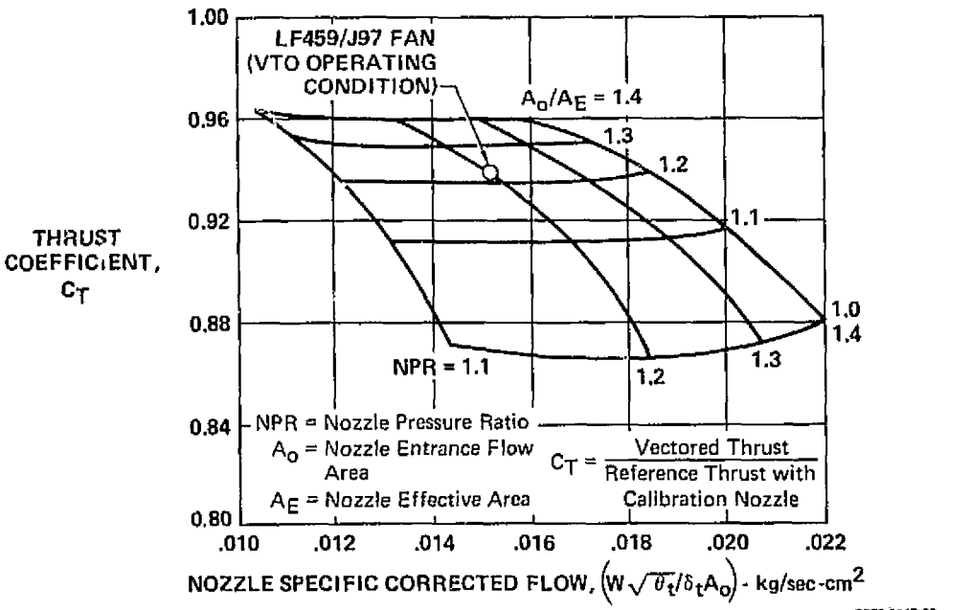

GP76-0867-33

FIGURE 1-4
THRUST VECTORING PERFORMANCE FOR "D" VENTED NOZZLE
Small Scale Test Data

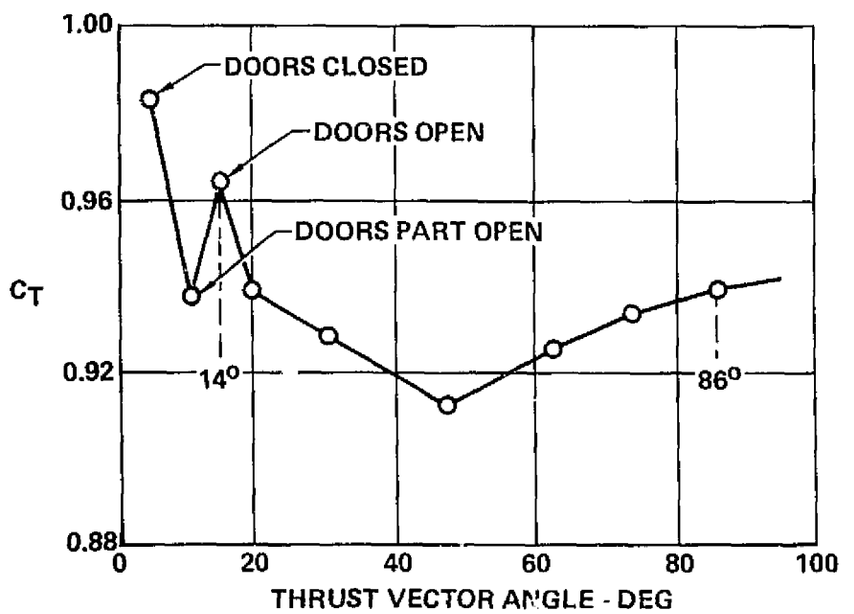

GP76-0867-90

the "D" vented vectoring nozzle under static ground conditions. The objectives of the test program were the experimental determination of (1) the "D" vented nozzle vectoring performance "in" and "out" of ground effect, (2) the thrust spoilage capability, (3) the compatibility of the "D" vented nozzle with a turbotip fan, and (4) the vectoring nozzle structural temperature distribution. An additional objective was a comparison of scale effects on nozzle performance.

The propulsion system used for the large scale nozzle test program was a General Electric LF336/J85 turbotip lift fan. The LF336 is a 91.44 cm (36 in.) diameter fan with an aerodynamic design pressure ratio of 1.3, and a design fan flow of 98.88 kg/sec (218 lb/sec). The LF336 is driven by the exhaust flow of one J85 gas generator which provides a system overall bypass ratio of 5.0.

The design pressure ratio of the LF336 fan is representative of the LCF459 fan being considered for the full scale lift fan aircraft; however, the overall bypass ratio of the LF336/J85 system is approximately 60% lower than the LCF459/J97 system. The difference in overall bypass ratio is a result of the reduced gas power per unit exhaust flow produced by the J85 compared to the J97 gas generator. The difference in gas generators results in a specific nozzle corrected flow for the LF336/J85 which is approximately 20% higher than the LCF459/J97 system at the same nozzle pressure ratio. This difference in specific nozzle corrected flow will result in lower VTO nozzle performance than expected for the full scale aircraft propulsion system. Consequently, large scale nozzle tests with the LF336/J85 are not completely representative of the full scale system; however, testing with this system provides a valid comparison of nozzle scale effects over the range of nozzle pressure ratios and specific nozzle corrected flow developed by the LF336/J85 system. In order to produce a large variation in specific nozzle corrected flow, a total of five different VTO nozzle exit areas were evaluated during the test program.

The large scale "boilerplate" nozzle was designed to approximate the internal flow geometry of the "D" vented design developed during the small scale tests, consistent with low cost fabrication techniques. A welded segment design using a combination of flat plate and single curvature segments was selected. As a result of this design approach, several deviations from the small scale internal contours were required in the large scale model. The primary deviations were in the downstream contour of the fixed structure element and in the thickness and internal nesting of the rotating hood elements. The

effect of these deviations caused some reduction in performance for the large scale nozzle when compared with the small scale test data.

The overall program was conducted under Contract NAS2-8663 with Mr. L. Stewart Rolls of NASA Ames Research Center serving as program Technical Monitor. MCAIR established the design configuration of the test nozzles and provided detailed drawings of the test apparatus. Fabrication and assembly of the test nozzle and associated test hardware were performed at NASA Ames. The experimental test program was carried out by NASA Ames personnel with MCAIR support. The tests were conducted at the Ames remote static test site during the period between 26 June 1976 and 20 July 1976. Data reduction and analysis of the test results were performed by MCAIR, and are documented in this report.

A description of the test apparatus is provided in Section 2 and the test program and procedure are presented in Section 3. The results and discussion of results are presented in Section 4, and the conclusions derived from the test program are set forth in Section 5.

2. EXPERIMENTAL APPARATUS

The experimental apparatus utilized in this test program consisted of the LF336/J85 turbotip lift fan system, a thrust calibration nozzle, a "boilerplate" version of the "D" vented vectoring nozzle, associated test instrumentation, a data acquisition system, and the NASA Ames static test facility. A description of each is presented below.

2.1 LF336/J85 TURBOTIP LIFT FAN SYSTEM

The LF336/J85 lift fan system used in the nozzle test program was designed and built by General Electric for NASA under Contract NAS2-4130. The LF336 fan, shown schematically in Figure 2-1, is a single stage, turbotip, fan-in-wing design with a fan diameter of 91.44 cm (36 in.) and an aerodynamic design pressure ratio of 1.3. The LF336 fan flow is 98.88 kg/sec (218 lb/sec) when operating at a 100% design speed of 6047 rpm. The LF336 tip turbine is an axial flow, impulse turbine fed by a 360-degree double entry scroll. The turbine is designed to accept the full exhaust flow of a J85-GE-5 General Electric turbojet engine at military power setting. Figure 2-2 summarizes the LF336/J85 system performance.

The LF336 fan map characteristics as determined by General Electric are shown in Figure 2-3 and were used to establish the test nozzle exit areas. Figure 2-4 is a curve of corrected thrust versus corrected fan speed for the LF336 as originally defined by General Electric when operating in the lift fan mode.

2.2 THRUST CALIBRATION NOZZLE

Calibration of the LF336/J85 lift fan system with a near ideal thrust performance nozzle was performed with four different nozzle exit areas to establish the undistorted nozzle pressure ratio-specific nozzle corrected flow characteristics of the test propulsion system and to establish baseline thrust performance levels to which the vectoring nozzle performance could be compared. The thrust calibration nozzle was designed by MCAIR and fabricated at NASA Ames.

Figure 2-5 presents a schematic of the thrust calibration nozzle which consists of a cylindrical outer duct and sinusoidal shaped hub centerbody which transitions the exhaust flow from an annular cross section at the nozzle entrance station to a circular cross section at the nozzle exit station. At the nozzle entrance station, the outer wall diameter is 107.2 cm (42.22 in.) and the hub centerbody diameter is 47.75 cm (18.8 in.). The hub centerbody is aligned with the fan aft hub and is supported off the outer wall by means of two struts

FIGURE 2-1
GENERAL ELECTRIC LF336 TURBOTIP FAN

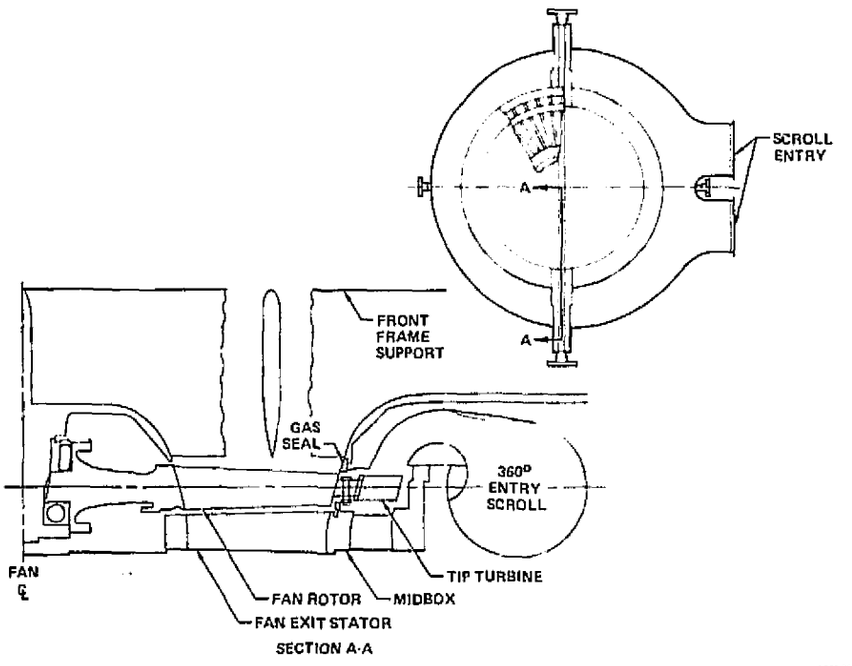

FIGURE 2-2
LF336/J85 DESIGN PERFORMANCE SUMMARY

FAN FLOW, KG/SEC, (LB/SEC)	98.88 (218)
FAN PRESSURE RATIO	1.3
BYPASS RATIO	5.0
RPM	6,047
FAN TIP SPEED, M/SEC (FT/SEC)	29.56 (970)
FAN DIAMETER, CM, (IN.)	91.44 (36)
RADIUS RATIO	.0.475
TURBINE INLET FLOW, KG/SEC (LB/SEC)	20.01 (44.12)
TURBINE INLET PRESSURE, N/CM^2 (PSIA)	21.95 (31.84)
TURBINE INLET TEMPERATURE, ^{O}K, (R^{O})	950.6 (1,711)
TURBINE DISCHARGE PRESSURE RATIO	1.118
TURBINE DISCHARGE TEMPERATURE, ^{O}K (R^{O})	833 (1,500)
FAN THRUST, N, (LB)	19,688 (4,426)
TURBINE THRUST, N, (LB)	4,982 (1,120)
TOTAL THRUST, N, (LB)	24,670 (5,546)

GP76-0867-30

FIGURE 2-3
LF336 FAN MAP CHARACTERISTICS

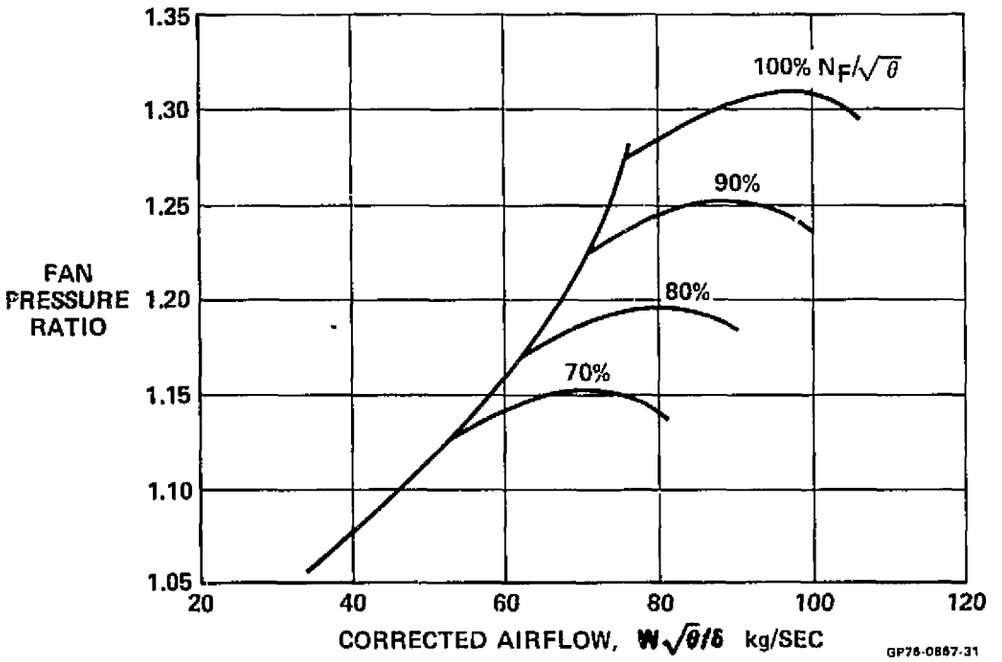

FIGURE 2-4
LF336 THRUST PERFORMANCE
Lift Fan Mode

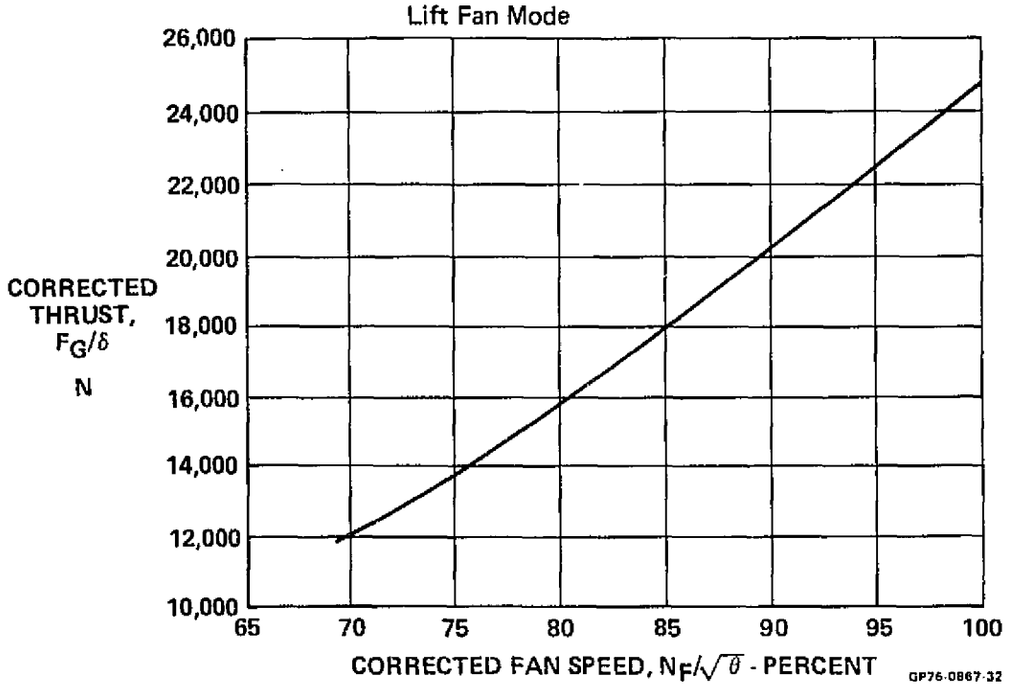

FIGURE 2-5
THRUST CALIBRATION TEST NOZZLE

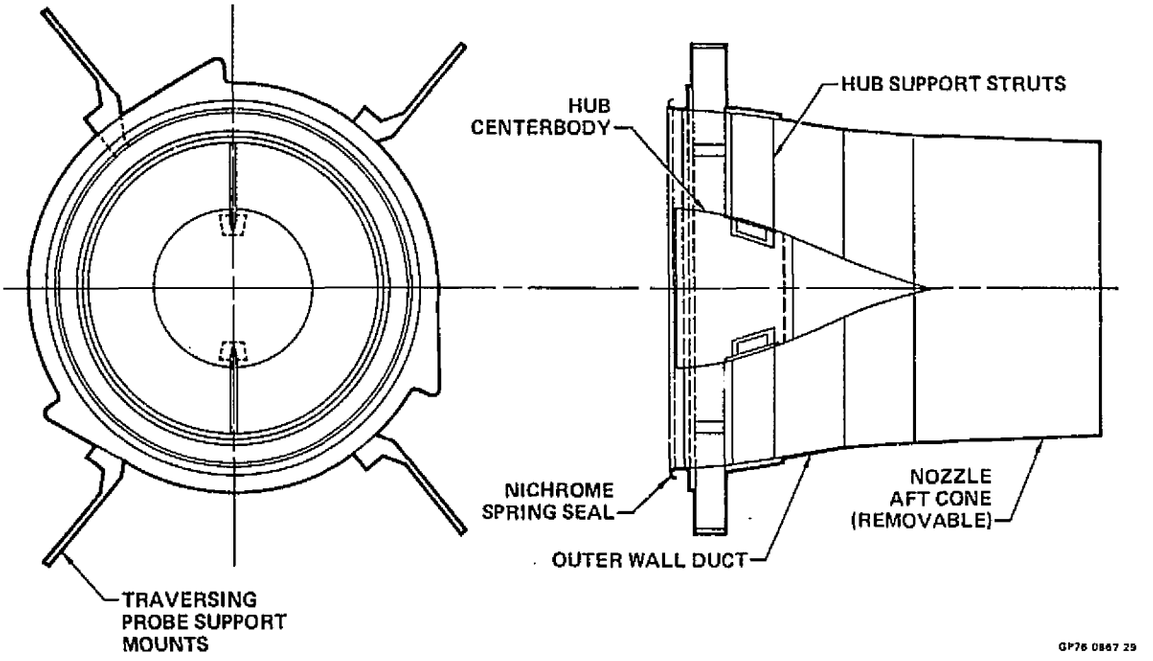

which span the annular flow passage. The struts incorporate a chord length of 12.55 cm (4.94 in.), a thickness to chord ratio of 0.10, and a double circular arc cross section.

The nozzle exit area is varied by means of removable nozzle aft cones. A total of four aft cone sections were fabricated which provide nozzle exit areas of 6730, 6285, 5935, and 5485 cm^2.

Four support mounts for radial traversing probes are circumferentially located on the outer duct element at a station 15.24 cm (6 in.) downstream of the nozzle entrance station. The four probes are located on diameters oriented ±39° from the horizontal plane.

The entire thrust calibration assembly was mounted to a supporting framework by means of a series of struts and brackets which prevented transfer of nozzle loads to the fan. A series of nichrome leaf seals was attached to the outer duct element at the entrance station to minimize gas leakage at the fan/nozzle interface.

2.3 "D" VENTED TEST NOZZLE

The "boilerplate" test nozzle geometry is shown schematically in Figure 2-6. The test nozzle consists of six elements: a nozzle entrance support ring, a fixed structure element, two movable hood elements, and two "D" shaped spacers.

The nozzle entrance ring incorporates the strut mounted hub centerbody, the mounts for the four entrance traversing probes, and a single longitudinal support beam for the combination yaw vane-closure door assembly. The hub centerbody geometry and traversing probe locations are identical to that used for the thrust calibration nozzle described above. The yaw vane-closure door assembly is simulated by a single door for these tests rather than a split vane assembly as proposed for the full scale geometry. The yaw vane is hinged to the support beam, the combination of which forms an articulated foil section with a chord length of 67.06 cm (26.40 in.) and a thickness-to-chord ratio of 0.13. The nozzle entrance ring transitions the fan exhaust flow from an annular cross section at the nozzle entrance to a "D" shaped cross section at the venting lip location and is the primary element through which the nozzle loads are transferred to the supporting framework.

The fixed structure element is an open sided shell element which in combination with the closure doors defines the cruise nozzle internal flow geometry. A thrust reduction modulation (TRM) port is located in the aft-top region of the fixed element. The port open area is sized at 1580 cm^2 (245 in^2). Test

FIGURE 2-6
BOILER PLATE "D" VENTED TEST NOZZLE

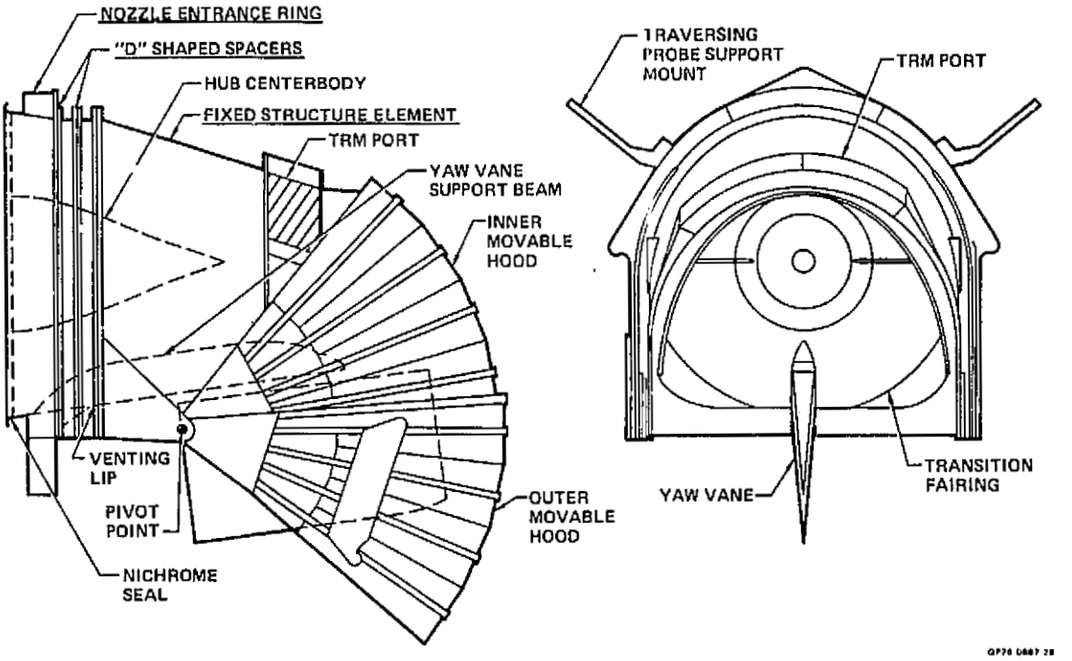

hardware was fabricated to permit variation of the open area between full open and closed in three equal increments. The support pivot for the two movable hoods is located in the lower portion of the fixed element at a distance 59.10 cm (23.27 in.) below the nozzle entrance centerline and 46.23 cm (18.2 in.) downstream of the nozzle entrance station.

The two movable hood elements are "D" shaped in cross section. The internal widths of the inner and outer hoods are 110.05 cm (43.72 in.) and 116.13 cm (44.72 in.) respectively. The mean radius of curvature of the two elements as measured from the pivot point is 53.95 cm (21.24 in.). Each of the hood elements possess an arc angle of 47° and allow geometric deflection angles up to 132°.

The "D" shaped spacer elements are designed to insert between the nozzle entrance ring and fixed structure element and thereby provide variability in VTO nozzle exit area.

The VTO nozzle exit area is further varied by means of removable transition fairings and venting lip extension plates. The transition fairings are located in the two lower corners formed at the venting lip station and provided an improved internal flow contour in this region. Addition of the transition fairings served to decrease the VTO exit area.

The venting lip extension plates are flat plate elements which span the nozzle width and effectively extend the venting lip downstream. Two lip extension plates, one 12.7 cm (5.0 in.) in length and one 25.4 cm (10 in.) were fabricated and tested. The "D" vented test nozzle was designed by MCAIR and fabricated at NASA Ames.

2.4 ASSOCIATED TEST INSTRUMENTATION

The LF336 fan, J85 gas generator, test nozzles, and test stand were instrumented for measurement of fan system and nozzle performance and for monitoring of the total system during the conduct of the tests. The primary test variables were system gross thrust, thrust direction and line of application, total nozzle mass flow, nozzle entrance total pressure and total temperature ratios, internal pressure and wall temperature distributions. Gross thrust, thrust direction, and line of application were determined by means of three load cells which are mounted below the fan/nozzle test assembly in a triform arrangement as indicated in Figure 2-7.

FIGURE 2-7
FAN NOZZLE TEST GEOMETRY

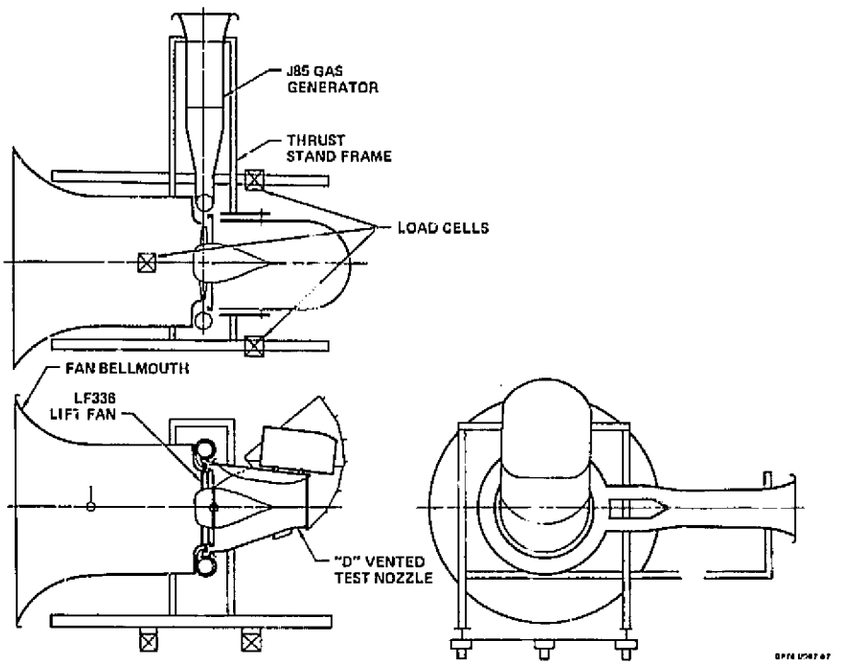

Each load cell was a 3-component strain gauge balance, with 26,690 N (6000 lb) normal force, 17,793 N (4000 lb) axial force, and 13,345 N (3000 lb) side force capability. The load cells were oriented with the normal force elements parallel with the vertical direction and the axial force elements with the horizontal direction. The nominal accuracy of the load cells was estimated by NASA to be ±1% of full scale. Total nozzle mass flow was established by means of calibrated bellmouth inlets on both the gas generator and fan and flowmeter measurement of fuel flow. The nozzle pressure and total temperature ratios were established through radial surveys at the nozzle entrance with four traversing total pressure and total temperature probes. The pressure and temperature radial distributions were integrated over the entrance flow area to yield average pressure and temperature data for both the fan and turbine regions. The average values for the fan and turbine were then mass flow weighted to provide nozzle pressure ratio and temperature data. The integration procedure is described in Appendix A.

Nozzle internal pressure measurements were obtained by means of a series of wall pressure taps located around the nozzle periphery. Wall temperature measurements were established by means of thermocouples attached to the outside surface of the nozzle structure. The locations of the wall pressure and temperature instrumentation on the thrust calibration nozzle and "D" vented nozzle are shown in Figures 2-8 and 2-9. A detailed list of the test instrumentation is provided in Figure 2-10.

2.5 DATA ACQUISITION SYSTEM

The experimental test parameters were measured, digitized, and recorded on paper punch tape utilizing a VIDAR Corporation digital data system. This system is comprised of analog signal conditioning, an integrating digital voltmeter, and a Teletype Paper-Tape punch. A total of 99 data recording channels are available with this system. The first 20 channels of the VIDAR system are multiple scan channels and the remaining channels are single scan. For this test a total of 60 channels were utilized. During a recording sequence, the first 20 channels were recorded a total of 48 times and the last 40 channels were recorded once. The total time for one data recording sequence was approximately 90 seconds.

The multi-scan channels were selected to record the primary performance data such as fan speed, nozzle flow, traversing probe information, and load cell axial and normal force components. Due to the 20 multi-scan channel

FIGURE 2-8
THRUST CALIBRATION NOZZLE PRESSURE AND TEMPERATURE INSTRUMENTATION

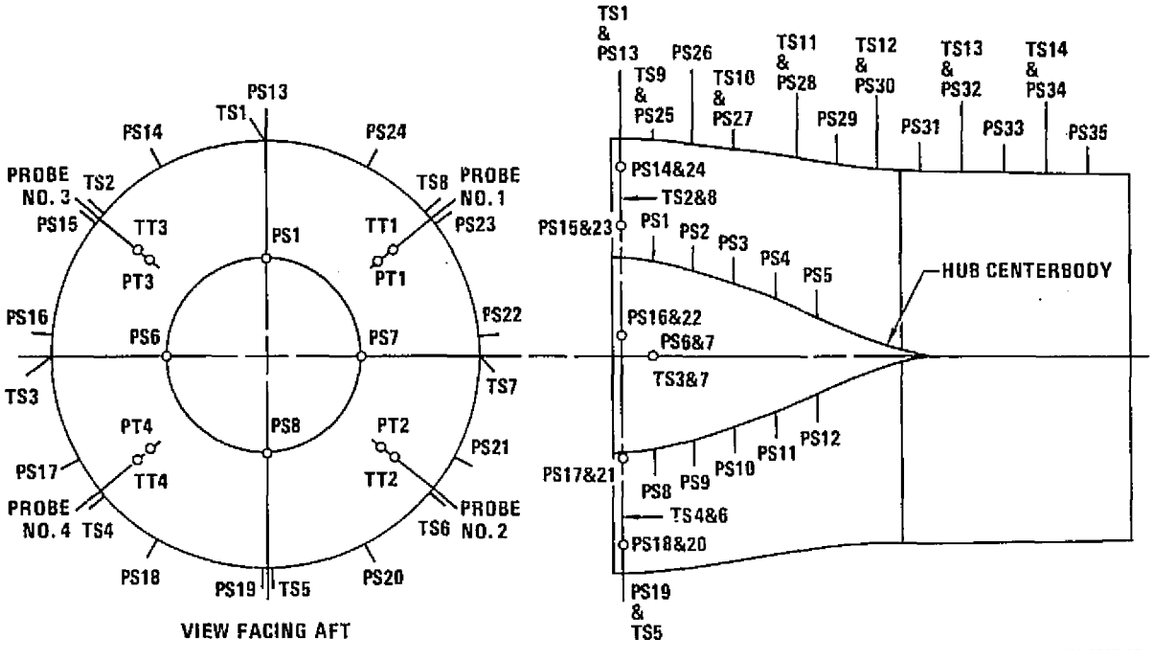

FIGURE 2-9
"D" VENTED NOZZLE WALL PRESSURE AND TEMPERATURE INSTRUMENTATION

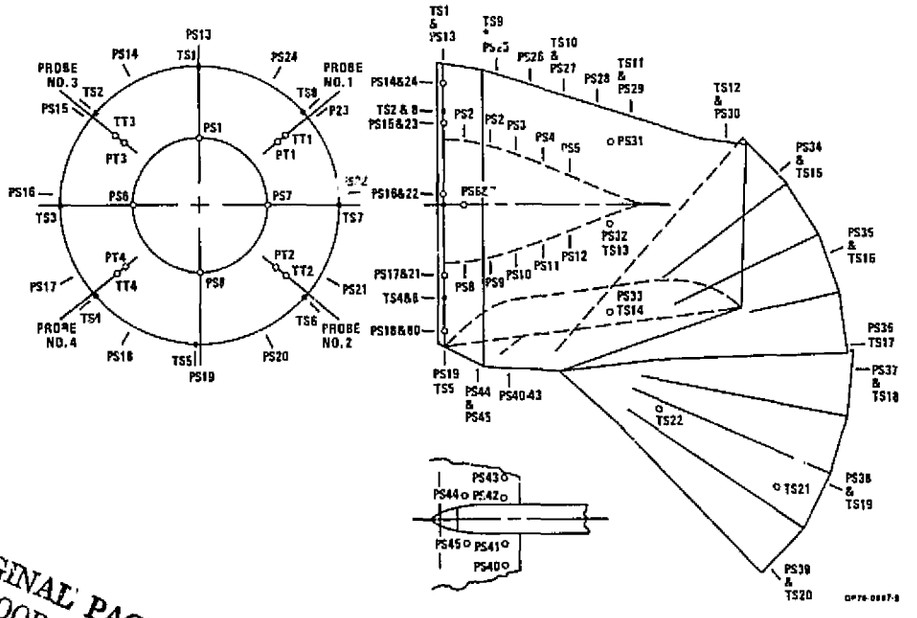

FIGURE 2-10
TEST INSTRUMENTATION SUMMARY

PARAMETER	SYMBOL	NO.	MEASUREMENT DEVICE	RECORDING MODE
AMBIENT CONDITIONS				
AMBIENT TEMPERATURE	TA	1	HG THERMOMETER	PANEL
AMBIENT PRESSURE	PA	1	HG BAROMETER	PANEL
WIND VELOCITY	VA	1		PANEL
J85 GAS GENERATOR				
RPM	NG	2	TACHOMETER	PANEL/VIDAR
THROTTLE POSITION	TP	1		PANEL
FUEL PRESSURE	PF	1	PRESS. GAUGE	PANEL
FUEL FLOW	WF	1	FLOWMETER	VIDAR
FUEL TEMPERATURE	TWF	1	TEMP GAUGE	VIDAR
BLEED VALVE POSITION	BVO	1		VIDAR
OIL PRESSURE	–	1	PRESS GAUGE	PANEL
BELLMOUTH STATIC PRESSURE	PBG	1	S/V NO. 1	VIDAR
BELLMOUTH INLET TEMPERATURE	TGI	1	THERMOCOUPLE	VIDAR
EXHAUST GAS TEMPERATURE	EGT	4	THERMOCOUPLE	PANEL (1)/VIDAR (3)
EXHAUST GAS PRESSURE	EGP	1	PRESS TRANSDUCER	VIDAR
VIBRATION				
COMPRESSOR VERTICAL	CV	1	ENG STRAIN GAUGE	PANEL
LF336 FAN				
RPM	NF	2	TACHOMETER	PANEL/VIDAR
ROLLER BEARING TEMPERATURE	TRB	2	THERMOCOUPLE	PANEL
BALL BEARING TEMPERATURE	TBB	2	THERMOCOUPLE	PANEL
FAN VIBRATION				
HUB HORIZONTAL	FH	1	FAN STRAIN GAUGE	PANEL
HUB AXIAL	FA	1	FAN STRAIN GAUGE	PANEL
BELLMOUTH STATIC PRESSURE	PBF	1	S/V NO. 1	VIDAR
BELLMOUTH INLET TEMPERATURE	TF1-TF4	4	THERMOCOUPLE	VIDAR
INLET STATIC PRESSURES	PSBM	12	S/V NO. 1	VIDAR

GP76-0867-36

FIGURE 2-10 (Continued)
TEST INSTRUMENTATION SUMMARY

PARAMETER	SYMBOL	NO.	MEASUREMENT DEVICE	RECORDING MODE
THRUST CALIBRATION NOZZLE				
ENTRANCE TRAVERSE PROBES NO. 1, 2, 3, 4				
RADIAL POSITION	R1-R4	4	POSITION TRANSDUCER	VIDAR
TOTAL PRESSURE	PT1-PT4	4	PRESSURE TRANSDUCER	VIDAR
TOTAL TEMPERATURE	TT1-TT4	4	THERMOCOUPLE	VIDAR
HUB WALL PRESSURES	PS1-PS12	12	S/V	VIDAR
NOZZLE WALL PRESSURES	PS13-PS35	23	S/V	VIDAR
NOZZLE WALL TEMPERATURES	TS1-TS14	14	THERMOCOUPLES	VIDAR
"D" VENTED NOZZLE				
ENTRANCE TRAVERSE PROBES NO. 1, 2, 3, 4				
RADIAL POSITION	R1-R4	4	POSITION TRANSDUCER	VIDAR
TOTAL PRESSURE	PT1-PT4	4	PRESSURE TRANSDUCER	VIDAR
TOTAL TEMPERATURES	TT1-TT4	4	THERMOCOUPLES	VIDAR
HUB WALL PRESSURES	PS1-PS12	12	S/V	VIDAR
NOZZLE WALL PRESSURES	PS13-PS45	33	S/V	VIDAR
NOZZLE WALL TEMPERATURES	TS1-TS22	22	THERMOCOUPLES	VIDAR
THRUST STAND				
BALANCE NO. 1, 2, 3				
AXIAL FORCE ELEMENTS	FX1-FX3	3	STRAIN GAUGE	VIDAR
SIDE FORCE ELEMENTS	FY1-FY3	3	STRAIN GAUGE	VIDAR
NORMAL FORCE ELEMENTS	FZ1-FZ3	3	STRAIN GAUGE	VIDAR

GP76-0867-37

limitation, the load cell side force components were recorded on single scan channels. As a consequence, at each test point the axial and normal forces were recorded 48 times whereas the side forces were recorded once.

The paper tape data records were processed at NASA Ames on the 40 x 80 wind tunnel data computer which converted the raw test data to engineering test parameters.

2.6 NASA AMES STATIC TEST FACILITY

The nozzle tests were conducted at the NASA-Ames Research Center Outside Static Test Facility, designated as test site number N-249. This site is used primarily to evaluate static performance of powered models prior to entry into the NASA-Ames 40 x 80 wind tunnel. This facility includes an enclosed trailer that serves as the control room and houses the data acquisition systems. Auxiliary equipment located at the site includes an engine starter unit, 400 cycle A/C power unit, and fuel tanker.

For this program, the nozzle test rig comprised of the fan inlet bellmouth, LF336 fan, J85 gas generator and supporting framework was mounted on the three load cells and orierted with the fan axis horizontal and approximately 230 cm (90 in.) above the ground plane. The vectoring nozzle was oriented to exhaust the vectored flow upwards in the vertical direction. Figures 2-11 and 2-12 are photographs of the nozzle test rig with the thrust calibration nozzle attached. Figures 2-13 through 2-16 show the "D" vented test nozzle in the low speed cruise configuration (doors open), 75° geometric hood position (intermediate vectoring, ≈45°), 112° geometric hood position (≈90° vectoring), and 132° geometric hood position (reverse vectoring, 117°) respectively.

Figure 2-17 shows the thrust reduction modulation port in the full open position, and Figure 2-18 shows the simulated ground plane as it was being positioned over the test nozzle for ground effects tests.

FIGURE 2-11
THRUST CALIBRATION NOZZLE ON TEST RIG (REAR QUARTER VIEW)

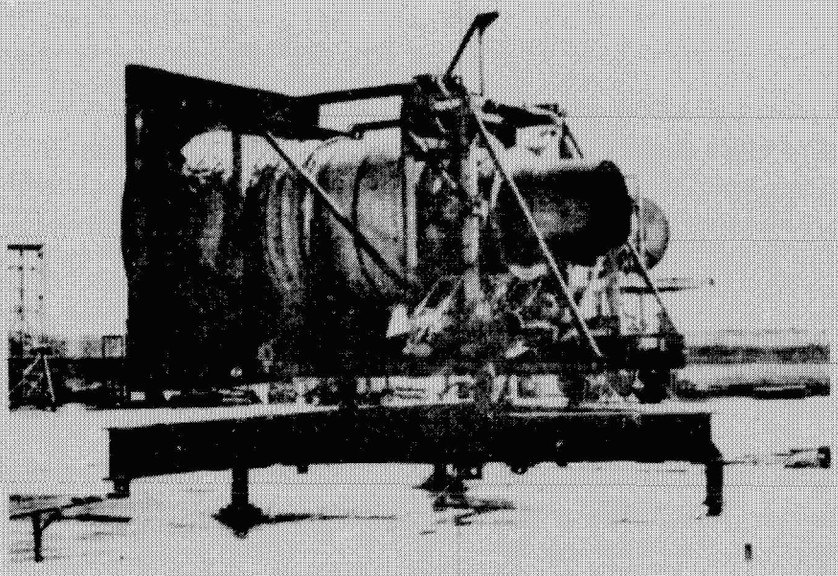

FIGURE 2-12
THRUST CALIBRATION NOZZLE ON TEST RIG (FORWARD QUARTER VIEW)

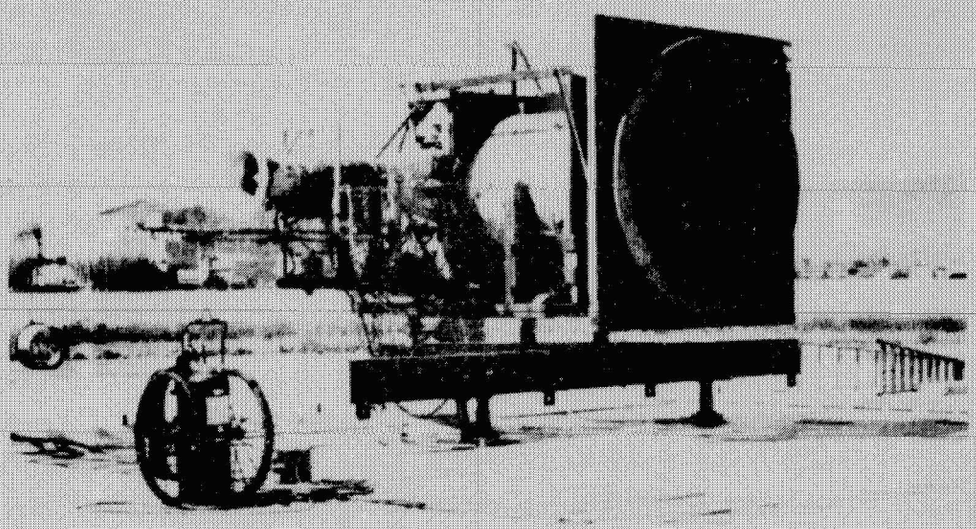

FIGURE 2-13
"D" VENTED TEST NOZZLE ON TEST RIG, 0^{o} GEOMETRIC POSITION

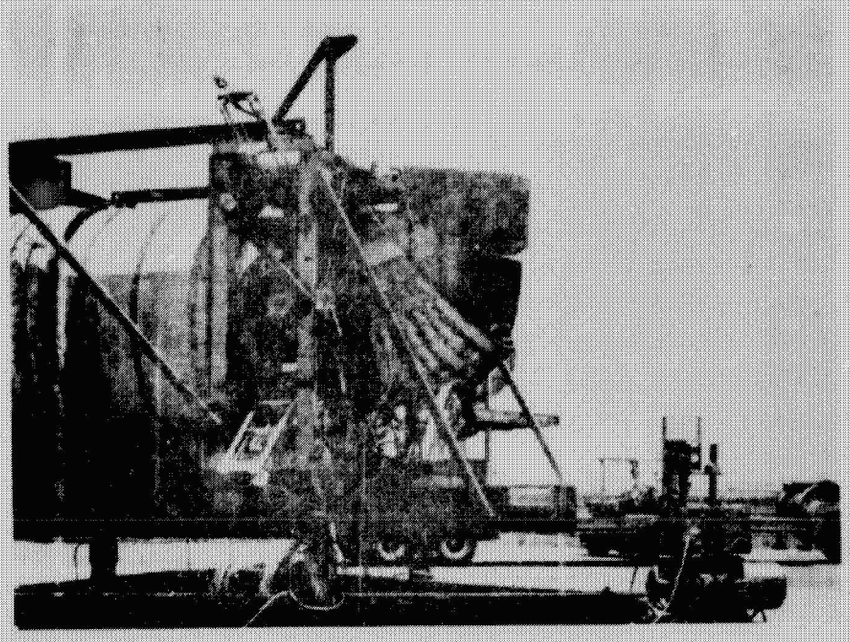

FIGURE 2-14
"D" VENTED TEST NOZZLE ON TEST RIG, 75^{o} GEOMETRIC POSITION

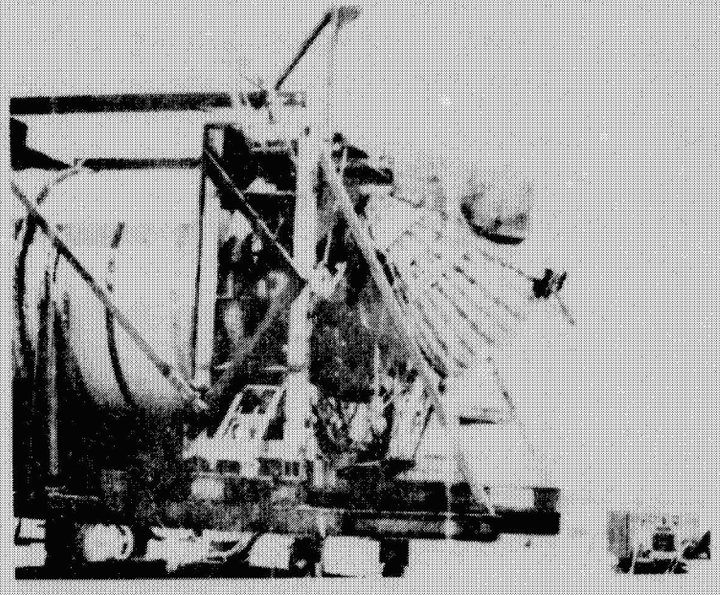

FIGURE 2-15
"D" VENTED TEST NOZZLE ON TEST RIG (112° GEOMETRIC POSITION)

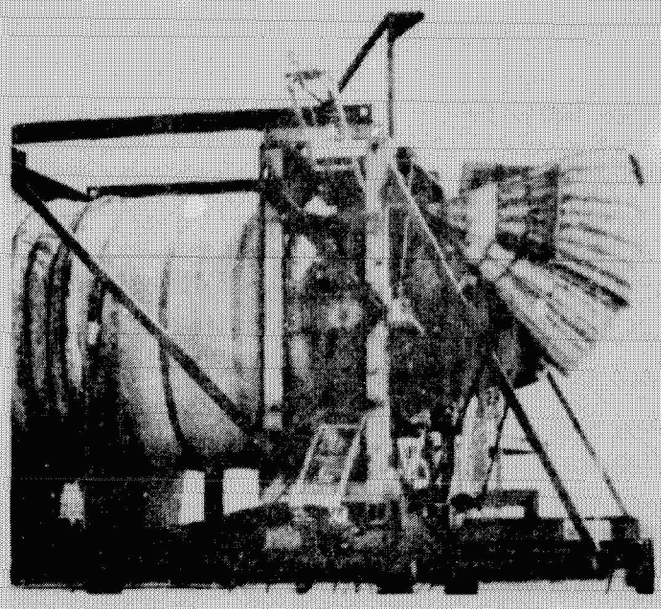

FIGURE 2-16
"D" VENTED TEST NOZZLE ON TEST RIG (132° GEOMETRIC POSITION)

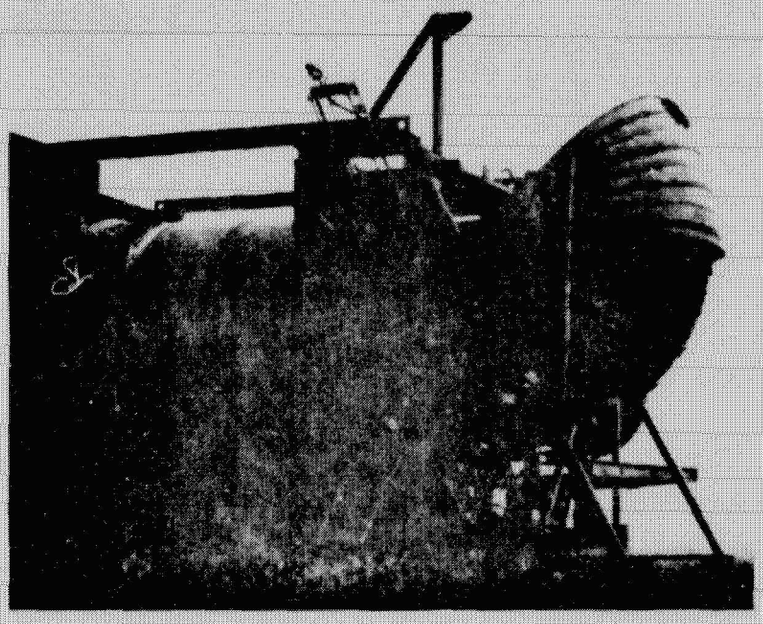

FIGURE 2-17
"D" VENTED TEST NOZZLE WITH TRM PORT 100% OPEN

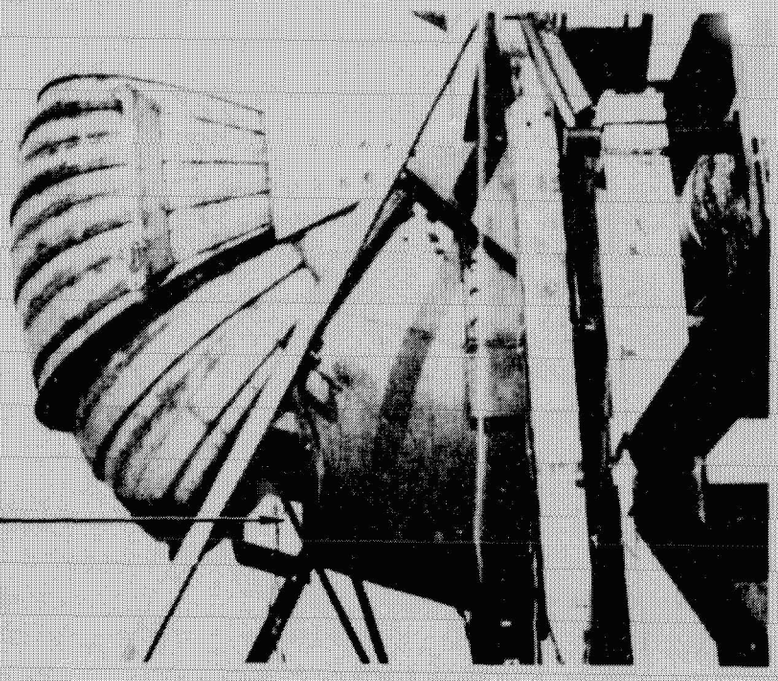

FIGURE 2-18
SIMULATED GROUND PLANE OVER "D" VENTED TEST NOZZLE

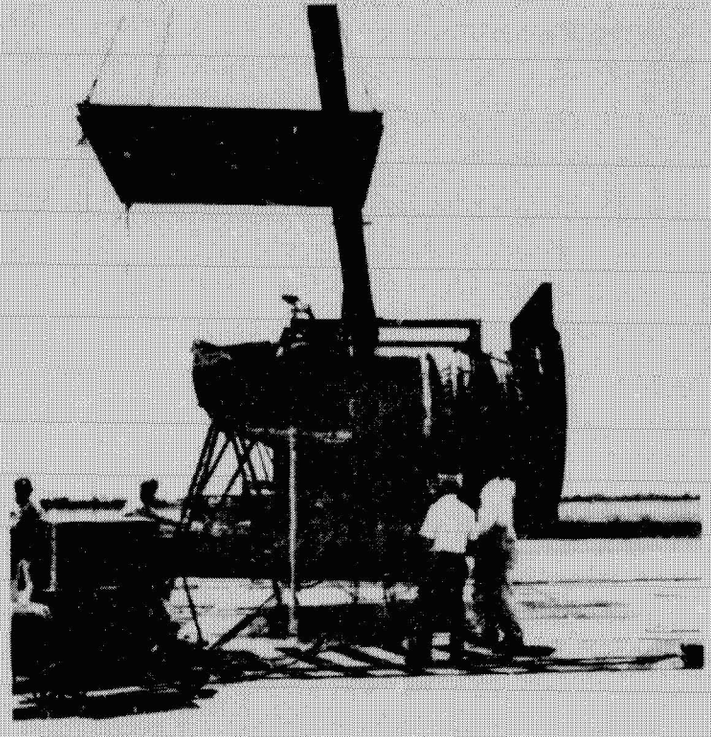

3. TEST PROGRAM PROCEDURE AND DATA ACCURACY

The procedure followed during the test program and an assessment of data accuracy are presented in this section.

Initially the nozzle tests were to be conducted with the fan/nozzle test rig mounted on a hydraulic lift platform with the nozzle exhausting downward. This arrangement, used in previous nozzle tests at NASA-Ames (Reference 2), allows the nozzle ground height to be easily varied for ground effects testing. The initial tests of the "D" vented nozzle on the hydraulic lift platform rig indicated a severe fan reingestion problem with this arrangement. Reingestion of the deflected nozzle exhaust flow as observed in this test arrangement is illustrated in Figure 3-1 and prevented stable control of the LF336 fan speed. The initial tests were terminated after foreign object damage was detected on the LF336 tip turbine section. During the period required to acquire and replace the LF336 tip turbine, the nozzle test rig was reconfigured to the test arrangement described in Section 2.

The complete test program is summarized in the test run summary shown in Figure 3-2. Upon completion of the first five test runs with the thrust calibration nozzle, minor foreign object damage was again detected on the LF336 tip turbine section. The fan was removed from the test rig for detailed inspection, which revealed damage to 8 of the 21 turbine carrier segments. The damaged carriers were replaced with four new carrier elements and four carrier elements which had been previously used. The fan was reassembled in the test rig and the remainder of the test program was completed without incident. Due to the condition of the LF336 tip turbine carriers, the maximum fan speed was restricted to 90%.

3.1 TEST PROGRAM PROCEDURE

The tests were initiated each day during the pre-dawn period to take advantage of low wind conditions which normally existed during this period. The majority of the test runs were made with ambient wind velocities below five knots. For each test run the propulsion system was started and brought to an idle fan speed of 50% (3000 RPM) for a five-minute warm-up period, after which the fan speed was increased in five increments to 90% (5400 RPM). After completion of data acquisition at 90% fan speed, the fan speed was reduced to the idle setting for a three-minute cool-down period and then shut down. Fan

FIGURE 3-1
SCHEMATIC OF NOZZLE EXHAUST REINGESTION ON HYDRAULIC LIFT TEST ARRANGEMENT

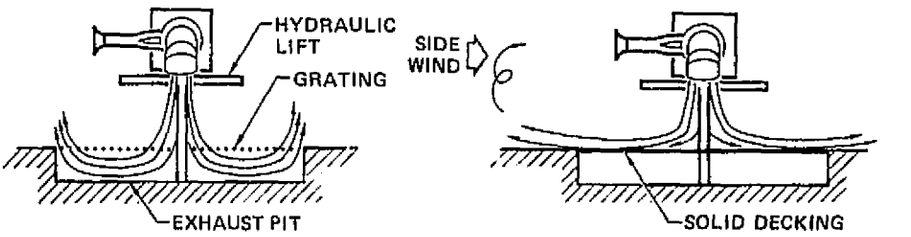

INITIAL TEST ARRANGEMENT SEVERE REINGESTION

MODIFIED TEST ARRANGEMENT REDUCED REINGESTION

PROBLEM:

REINGESTION OF NOZZLE EXHAUST PREVENTS OPERATION OF FAN AT CONSTANT SPEED

SOLUTION:

- ROTATE NOZZLE 180° AND EXHAUST FLOW UPWARDS
- LOCATE GROUND PLANE ABOVE TEST STAND TO EVALUATE GROUND EFFECTS

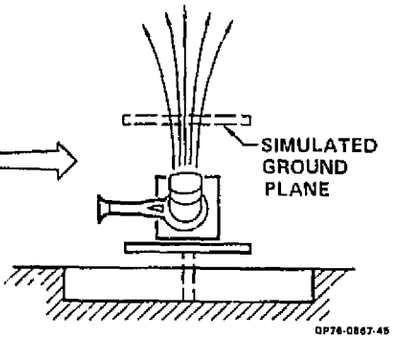

QP76-0867-45

FIGURE 3-2
SUMMARY OF TEST RUNS

RUN NO.	NOZZLE CONFIGURATION	PURPOSE
00	TCN, A_{NOZ} = 6730 cm^2	SYSTEM CHECKOUT
1	TCN, A_{NOZ} = 6730 cm^2	THRUST AND MASS FLOW CALIBRATION OF LF338/J85 FAN SYSTEM
2	TCN, A_{NOZ} = 6285 cm^2	
3	TCN, A_{NOZ} = 5935 cm^2	
4	TCN, A_{NOZ} = 5485 cm^2	
5	TCN, A_{NOZ} = 5485 cm^2	
6	DVN, 0° GEO POSITION	LONGITUDINAL VECTORING PERFORMANCE 2 "D" SPACERS INSTALLED
7	DVN, 0° GEO POSITION	
8	DVN, 75° GEO POSITION	
9	DVN, 90° GEO POSITION	
10	DVN, 132° GEO POSITION	
11	DVN, 112° GEO POSITION	
12	DVN, 112° GEO POSITION TRANSITION FAIRING INSTALLED	VTO PERFORMANCE
13	DVN, 112° GEO POSITION TRM 33% OPEN	THRUST REDUCTION MODULATION PERFORMANCE
14	DVN, 112° GEO POSITION TRM 100% OPEN	
15	DVN, 112° GEO POSITION 15° YAW VANE DEFLECTION	YAW VECTORING PERFORMANCE
16	DVN, 112° GEO POSITION h/DF = 2.97	GROUND EFFECTS PERFORMANCE
17	h/DF = 1.30	
18	h/DF = 1.60	
19	h/DF = 1.93	
20	DVN, 112° GEO POSITION NO. 1 LIP EXTENSION	VTO PERFORMANCE
21	DVN, 112° GEO POSITION NO. 2 LIP EXTENSION	
22	DVN, 112° GEO POSITION 15° YAW VALVE DEFLECTION	YAW VECTORING AND SPOILAGE PERFORMANCE
23	10° YAW VANE D DEFLECTION	
24	DVN, 90° GEO POSITION 15° YAW VANE DEFLECTION	
25	15° YAW AND TRIM 100% OPEN	
26	DVN, 75° GEO POSITION 15° YAW VANE DEFLECTION	
27	DVN, 0° GEO POSITION	REPEATABILITY, RUN 6 & 7
28	DVN, 112° GEO POSITION	LONGITUDINAL VECTORING PERFORMANCE SPACERS REMOVED
29	DVN, 90° GEO POSITION	
30	DVN, 0° GEO POSITION	
31	DVN, 0° GEO POSITION	REPEATABILITY, RUN 30

TCN - THRUST CALIBRATION NOZZLE
DVN - "D" VENTED NOZZLE

and nozzle performance data were recorded at seven test points which corresponded to nominal fan speeds of 50%, 70%, 75%, 80%, 85%, 90%, and 50%.

At each test point, data was recorded by means of the VIDAR data acquisition system and also fan and engine panel instrumentation were manually recorded. Concurrent with the initiation of the VIDAR data recording sequence, the nozzle entrance traversing probe drive system was actuated which simultaneously drove each of the four entrance traversing probes. The probe radial drive speed was selected to provide a complete inward and outward traverse of the combined fan/turbine annular flow region during the approximate 90-second period required for the VIDAR system to record the multiscan channels a total of 48 times. With this arrangement the entrance probes were recorded a total of 48 times during the inward and outward traverses.

3.2 DATA ACCURACY

The probe drive speed was somewhat faster than that required to achieve valid steady state pressure and temperature recording at each radial position. The above conclusion is based upon a comparison of the pressure and temperature profiles recorded during the inward and outward probe traverses, a typical case of which is shown in Figure 3-3. As is shown, pressure and temperature lags are evident primarily in the high gradient region behind the turbine midbox. For the purpose of establishing a mean set of profile data, the inward and outward data traverses were separately curve fitted and the two curve fits were then averaged in the integrations to define average values of the nozzle entrance pressure and temperature ratios.

At each test point, the axial and normal load cell elements were recorded 48 times, whereas the side force elements were recorded only once. Figure 3-4 is a plot of the 48 normal force readings for each load cell, recorded during Run 21, at a fan speed of 89.5%. Considerable variation of the load cell normal force readings about the mean values is evident which suggests that the nozzle rig was undergoing a low frequency oscillation. Typical variations of the axial force readings about the mean values are shown in Figure 3-5 as recorded during Run 7 at a fan speed of 88.58%. The peak-to-peak differences on the axial components were generally lower than that observed on the normal force elements. The overall accuracy of the axial and normal force measurements is difficult to assess due to the lack of calibration apparatus at the remote test site and the obvious difficulties in holding environmental conditions constant at an outside facility. Pre-test checkouts of the load cell system

FIGURE 3-3
TYPICAL NOZZLE ENTRANCE PRESSURE AND TEMPERATURE RADIAL PROFILE MEASUREMENTS

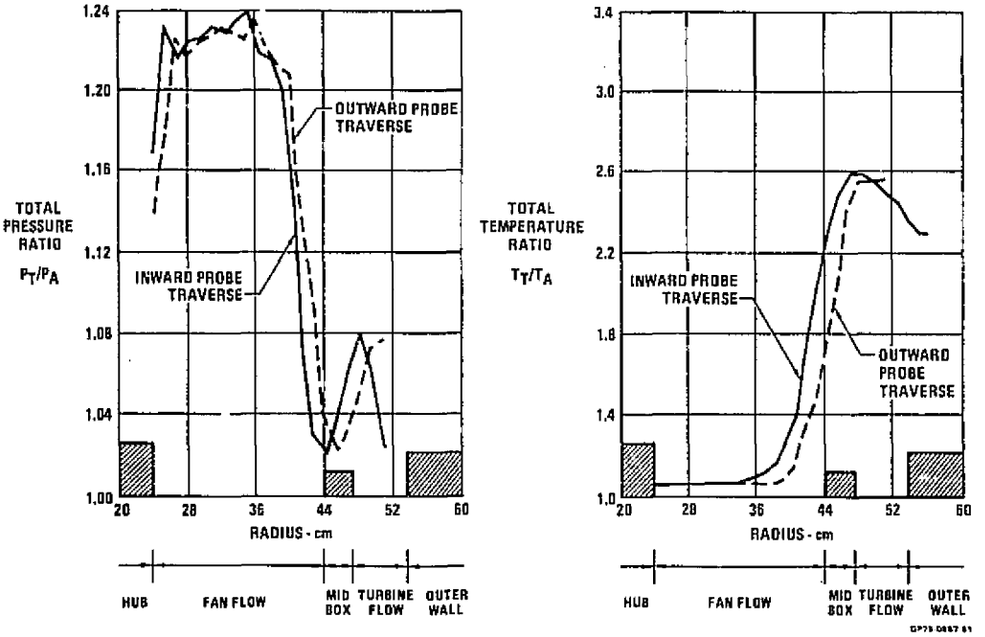

FIGURE 3-4
VARIATION OF LOAD CELL NORMAL FORCE READINGS DURING A RECORDING SEQUENCE

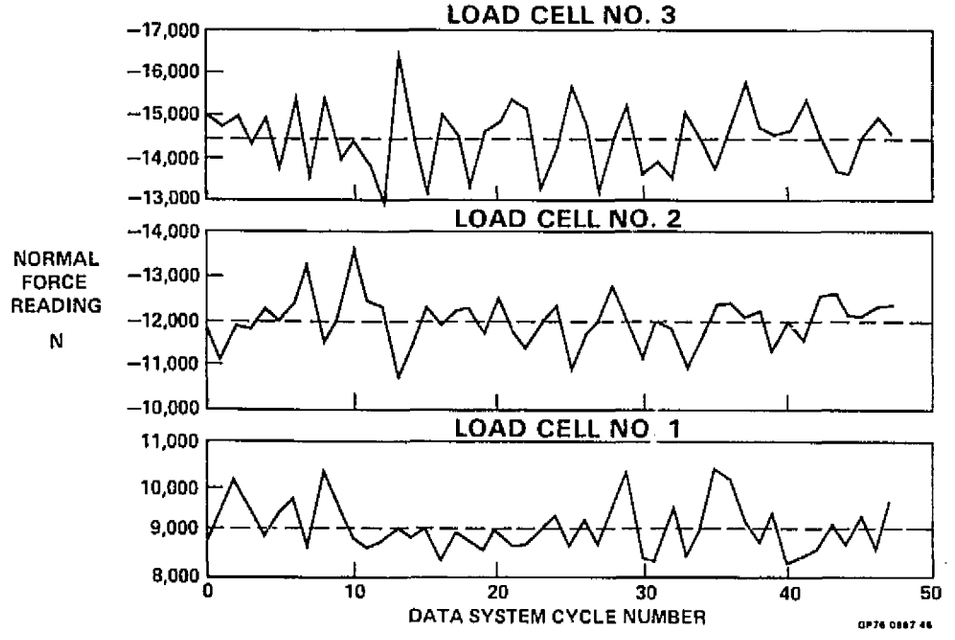

FIGURE 3-5
VARIATION OF LOAD CELL AXIAL FORCE READINGS
DURING A RECORDING SEQUENCE

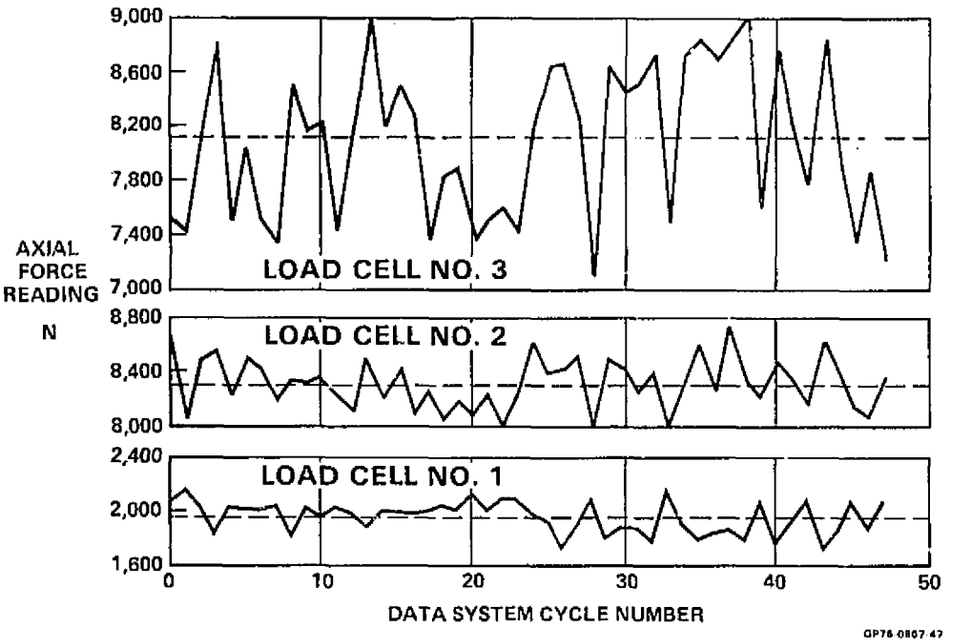

were carried out by applying a horizontal force to the nozzle rig through the fan centerline by means of a cable and pulley arrangement with a calibrated dynamometer. The results of these tests showed agreement between the load cell reading and the dynamometer reading within one-half of one percent. Runs 6, 7, and 27 were conducted on different days with the same nozzle hardware and provide a measure of the thrust measurement repeatability. Figure 3-6 presents the corrected thrust versus fan speed performance for these three runs and indicates that the thrust measurement repeatability was within ±1%. Runs 30 and 31 were carried out with the same nozzle test hardware on the same day; however, the sequence of data recording was reversed in that the fan was brought from idle to 90% fan speed and then decreased in 5% increments rather than starting at 70% fan speed with increasing increments. The corrected thrust versus fan speed performance for these two runs is shown in Figure 3-7 and again the thrust measurement repeatability is shown to be within 1%.

The uncertainties in the side force measurements are considered to be quite large, primarily because these readings were recorded only once per data point and the evidence from the axial and normal force measurements that a large number of readings were required to obtain representative average values. A total of 20 runs were conducted with the exit yaw vane undeflected where a zero net side force was expected. The actual side force angle, ψ, readings recorded during these test runs are plotted in summary form on Figure 3-8. The data in Figure 3-8 indicated that a variation of $\pm 8°$ in the side force angle was obtained with a mean value of 0.33°. A total of five runs were made with the yaw vane geometric deflection at either 10° or 15° which according to small scale tests should have produced a side force angle of 6.5° and 9.0°, respectively. The side force readings recorded on these five tests are indicated on Figure 3-8 by the closed symbols. The average of these readings indicates a net side force of -1.58° which is less than the expected value. Since the uncertainty in the side force measurement was of an equal magnitude as the expected result, it is concluded that the experimental setup was inadequate to perform the desired measurement.

FIGURE 3-6
THRUST MEASUREMENT REPEATABILITY, RUNS 6, 7, 27

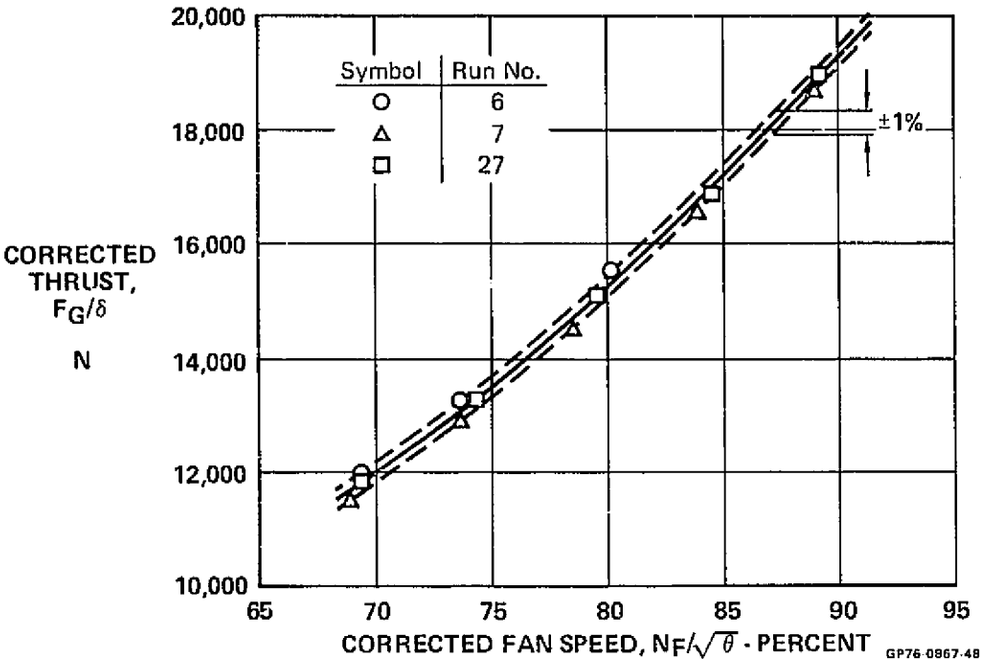

FIGURE 3-7
THRUST REPEATABILITY, RUNS 30 AND 31

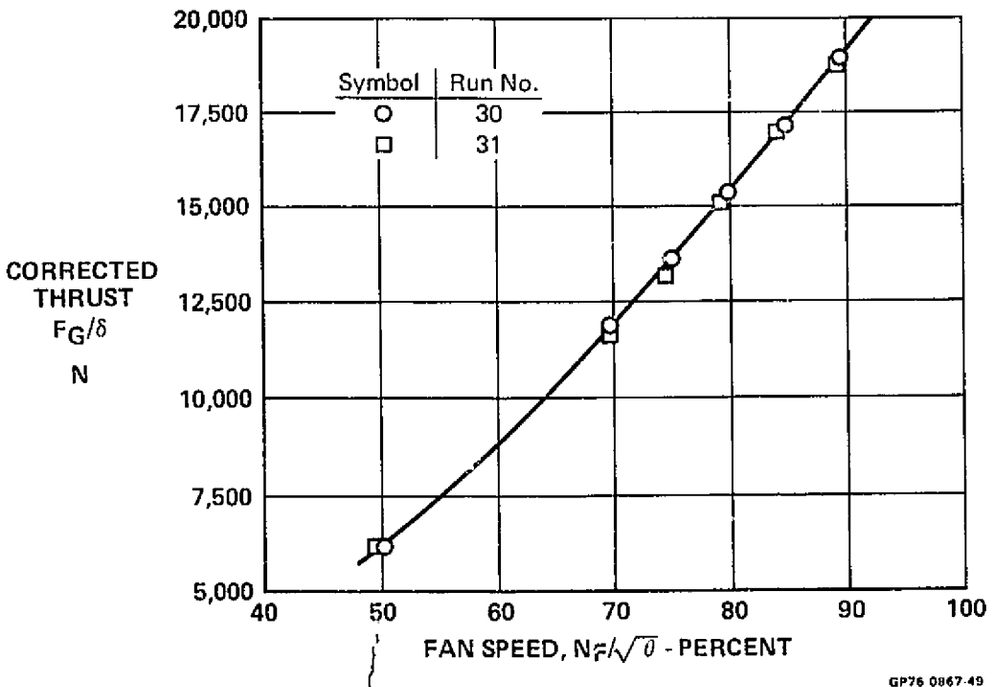

FIGURE 3-8
SUMMARY OF SIDE FORCE ANGLE MEASUREMENTS

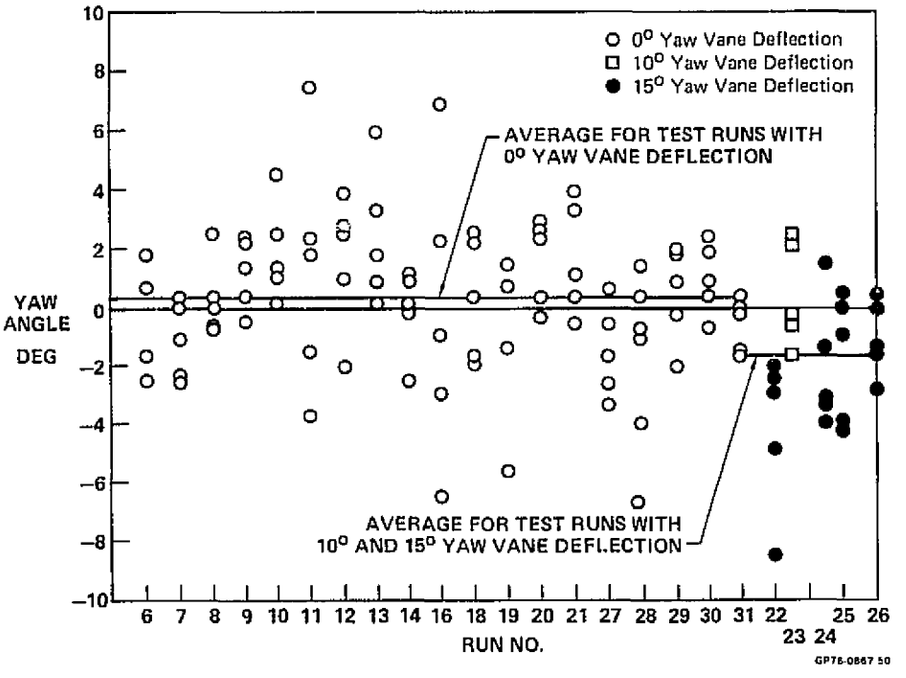

4. RESULTS AND DISCUSSION OF RESULTS

The experimental data obtained during the tests of the thrust calibration and "D" vented test nozzles were reduced to yield nozzle performance data which were then compared with similar information obtained via small scale nozzle tests. The test results and the scale effect comparisons are presented below.

4.1 THRUST CALIBRATION NOZZLE TESTS

The thrust calibration nozzle tests were conducted to establish the reference thrust performance levels of the LF336 test system with near ideal nozzles and to determine the specific nozzle entrance corrected flow characteristics of the LF336 fan operating with a nozzle in the confluent mode (combined fan and turbine flows).

4.1.1 THRUST PERFORMANCE - The corrected thrust versus corrected fan speed characteristics obtained during the thrust calibration nozzle test results are shown in Figure 4-1. Also plotted on Figure 4-1 are the General Electric performance characteristics which were originally measured without an exit nozzle attached to the LF336 fan. The thrust levels obtained with the largest nozzle exit area were slightly higher than the G.E. data, whereas the three smaller exit areas yielded performance below the G.E. quoted performance. The G.E. performance is presented primarily for trend comparisons since the condition of the fan was different between the present tests and the G.E. tests.

The measured corrected fan flow versus corrected fan speed is depicted in Figure 4-2 and shows the expected increase in flow as the nozzle exit area is increased.

The radial distributions of total pressure ratio at the nozzle entrance as measured with the four traversing probes are shown in Figure 4-3 for the largest nozzle exit area (6730 cm^2) configuration at a corrected fan speed of 84.5%. Figure 4-4 illustrates the total temperature ratio distributions for this test point. Examination of the total pressure profile data indicates that the fan flow was slightly asymmetric in the circumferential direction and that a greater asymmetry existed in the turbine flow region. The turbine total pressures were reduced on the side opposing the entrance to the turbine scroll and reflect the additional scroll losses expected for this region of the turbine. The radial pressure data further show the existence of significant total pressure losses in the fan hub and tip regions. The tip total pressure losses are accentuated by hot gas leakage from the turbine flow into the fan stream at the forward seal location. The total temperature distributions indicate

FIGURE 4-1
THRUST CALIBRATION NOZZLE, THRUST vs FAN SPEED PERFORMANCE

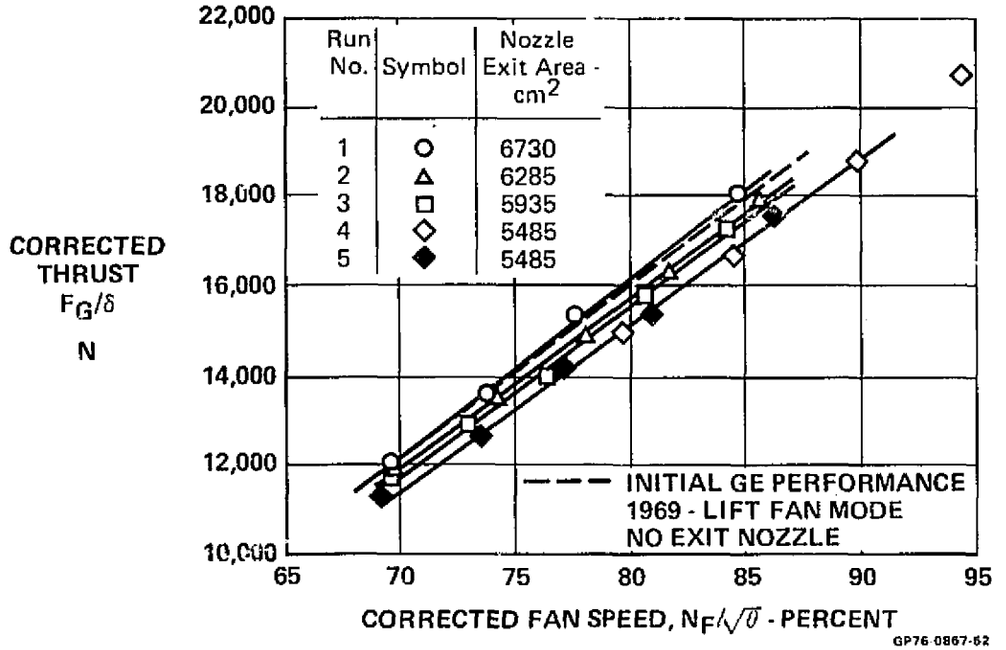

FIGURE 4-2
THRUST CALIBRATION NOZZLE, FAN FLOW vs FAN SPEED CHARACTERISTICS

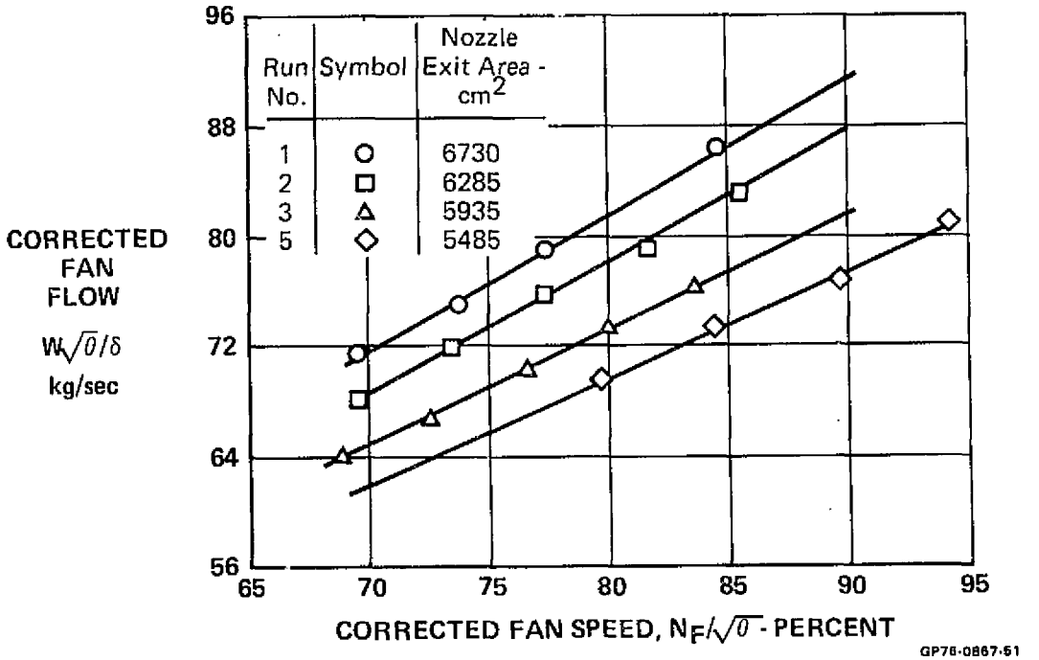

FIGURE 4-3
THRUST CALIBRATION NOZZLE, ENTRANCE TOTAL PRESSURE DISTRIBUTION
A_{NOZ} = 6730 cm^2, $N_F/\sqrt{\theta}$ = 84.55%

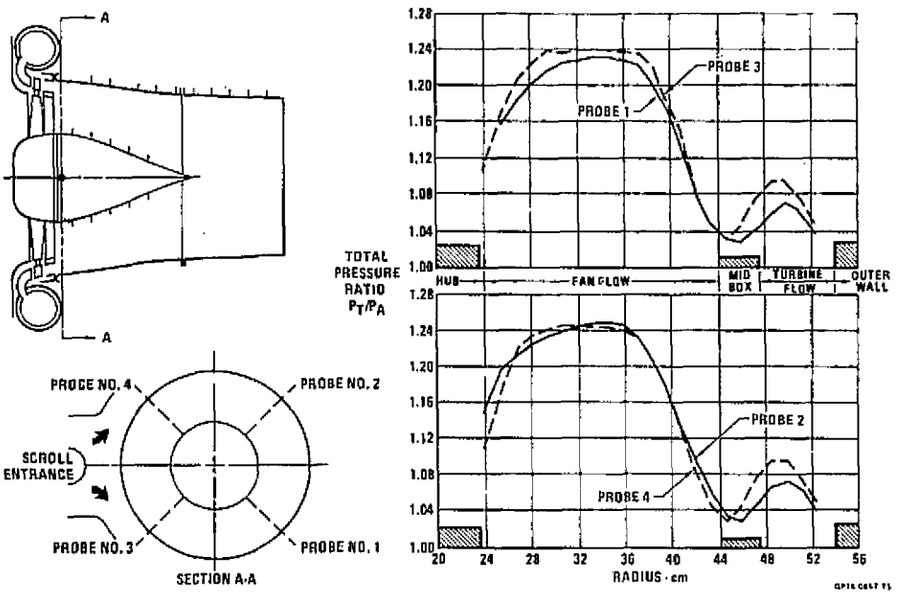

FIGURE 4-4
THRUST CALIBRATION NOZZLE,
ENTRANCE TOTAL TEMPERATURE DISTRIBUTION
A_{NOZ} = 6730 cm^2 $N_F/\sqrt{\theta}$ = 84.55%

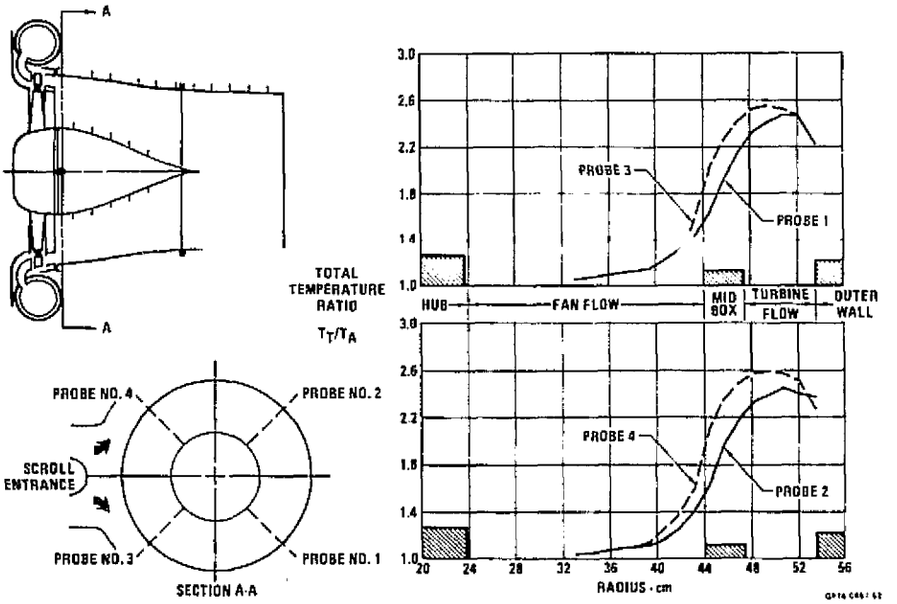

leakage into the fan stream to a radial distance of approximately one fan chord length. The temperature distributions also exhibit a similar circumferential asymmetry as seen in the pressure data. Figures 4-5 and 4-6 show the radial pressure and temperature distribution at 89.53% fan speed for the smallest nozzle exit area, 5485 cm^2.

The radial distributions of total pressure and temperature were area integrated over the fan and turbine flow regions to define average values for the two streams. The average properties for the two streams were then mass flow weighted to provide nozzle entrance conditions at each test point. The integration and mass weighting procedure is outlined in Appendix A.

The sum of the fan and turbine flows was corrected with respect to the nozzle entrance total conditions to provide nozzle corrected flow data. The nozzle pressure ratio-corrected flow characteristics for the LF336/J85 system as determined from the thrust calibration nozzle tests are shown in Figure 4-7. The NPR versus corrected flow data are used to enter the small scale vectoring nozzle VTO performance map and thereby establish nozzle performance estimates for the large scale system. Figure 4-8 shows the measured thrust data as a function of nozzle corrected flow and represents the reference thrust performance of the LF336/J85 system.

4.1.2 WALL PRESSURE AND TEMPERATURE MEASUREMENTS - Figure 4-9 shows a typical set of internal pressure measurements recorded during the thrust calibration nozzle tests. The data plotted are for the smallest nozzle exit area, at a fan speed of 89.53%. The circumferential distribution on the hub centerbody and outer duct wall at the nozzle entrance station is relatively independent of the angle, γ; however, a radial pressure gradient between the hub and outer wall exists which is indicative of an inward turning of the flow around the hub centerbody. The axial distributions indicate that the radial gradient reverses approximately midway along the centerbody.

Figure 4-10 depicts the wall temperature measurements for the same test configuration. The wall temperature data at the nozzle entrance exhibit the same circumferential variations as recorded on the traversing temperature probes. The nozzle skin temperatures decreased as the flow progressed to the nozzle exit, indicating some mixing of the fan and turbine flows.

4.2 "D" VENTED NOZZLES LONGITUDINAL THRUST VECTORING TESTS

The longitudinal thrust vectoring tests were initiated with the nozzle in the low speed cruise configuration, 0° geometric hood position, yaw vane-

FIGURE 4-5
THRUST CALIBRATION NOZZLE, ENTRANCE TOTAL PRESSURE DISTRIBUTIONS
A_{NOZ} = 5485 cm^2, $N_F/\sqrt{\theta}$ = 89.53%

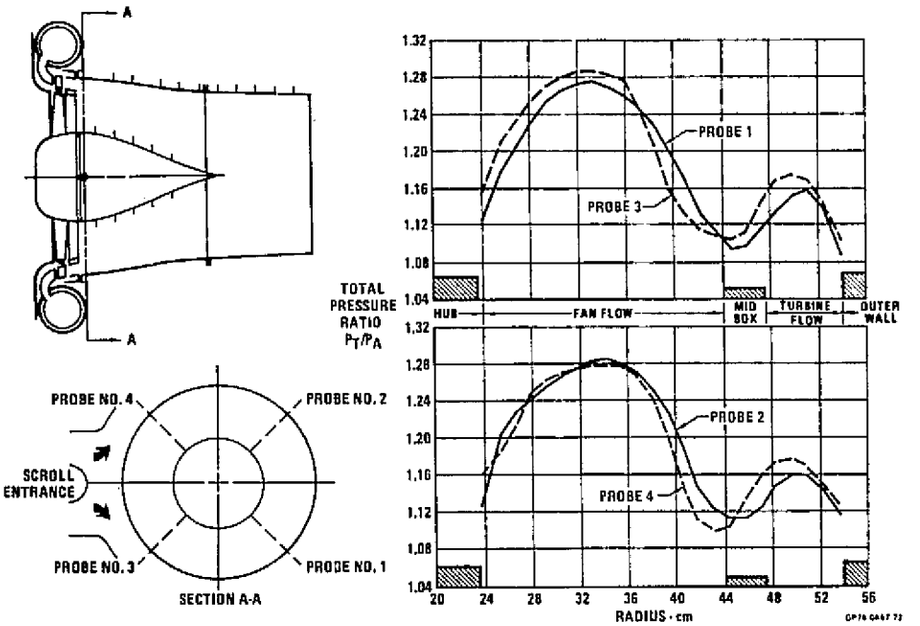

FIGURE 4-6
THRUST CALIBRATION NOZZLE, ENTRANCE TOTAL TEMPERATURE DISTRIBUTIONS
A_{NOZ} = 5485 cm^2 $N_F/\sqrt{\theta}$ = 89.53%

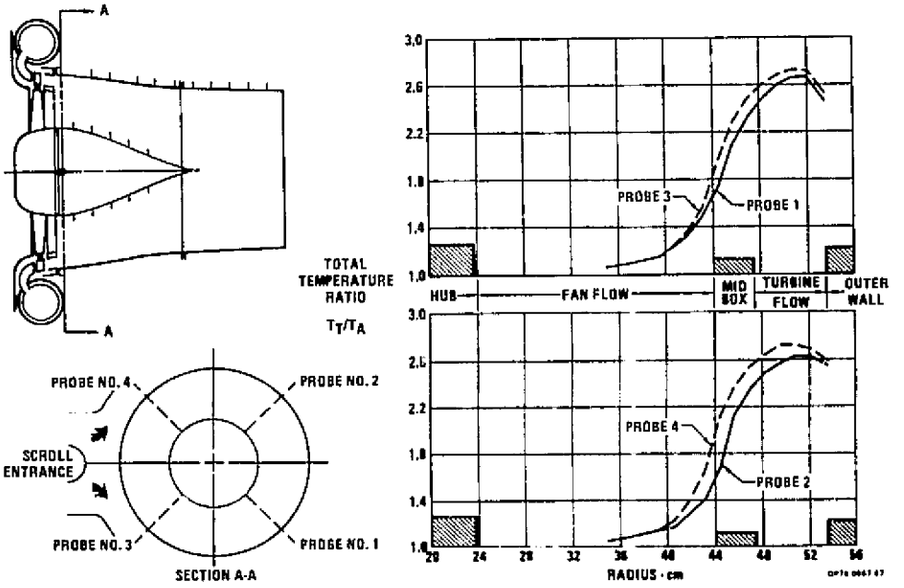

FIGURE 4-7
THRUST CALIBRATION NOZZLE, NOZZLE PRESSURE RATIO - CORRECTED FLOW CHARACTERISTICS

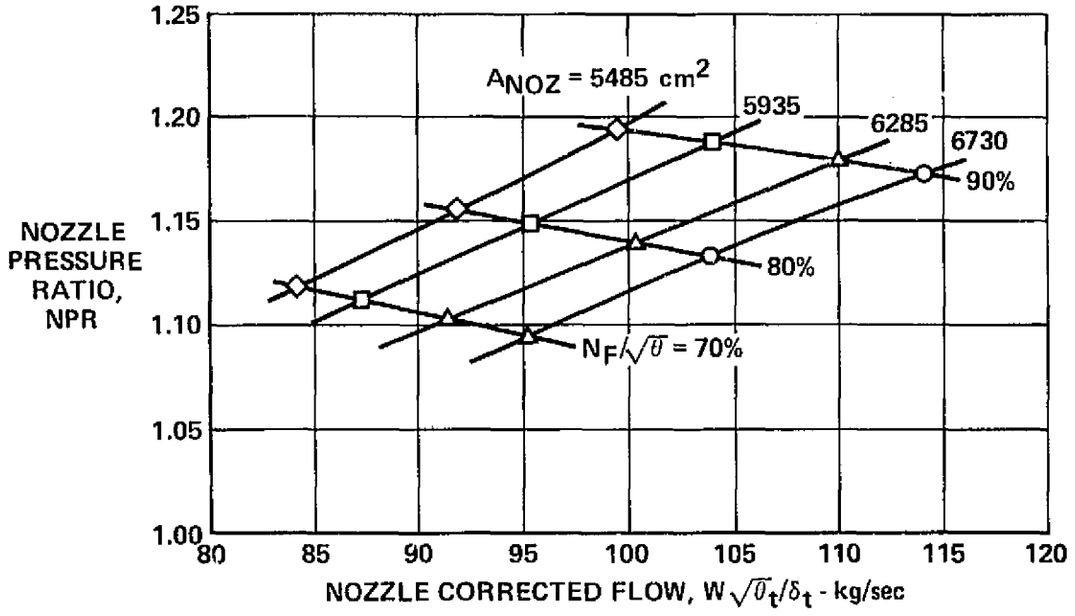

FIGURE 4-8
THRUST CALIBRATION NOZZLE, CORRECTED THRUST vs NOZZLE CORRECTED FLOW

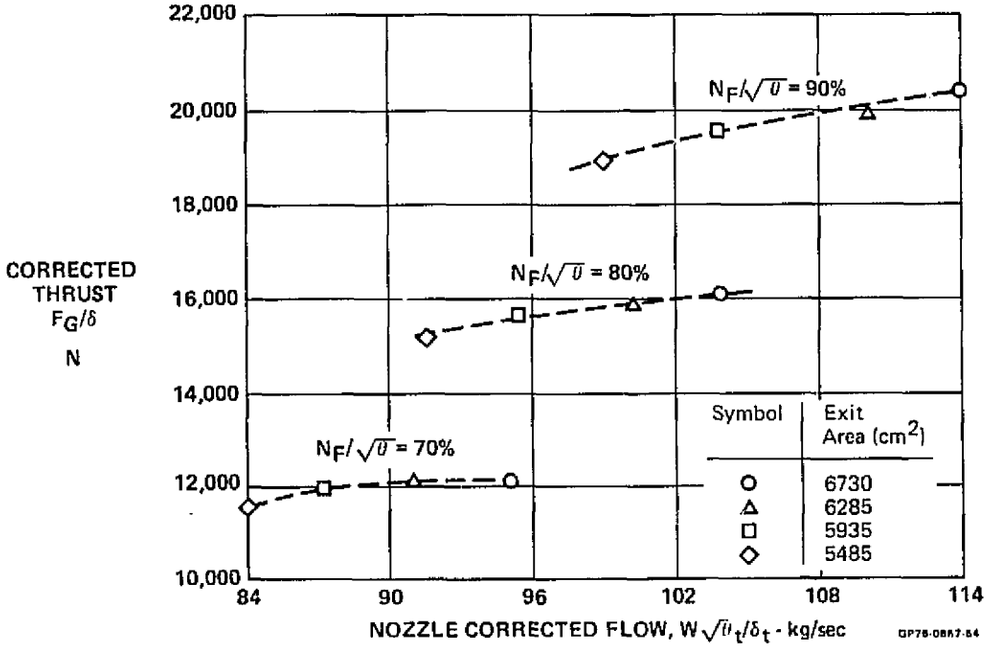

FIGURE 4-9
THRUST CALIBARTION NOZZLE, WALL PRESSURE DISTRIBUTIONS
A_{NOZ} = 5485 cm^2

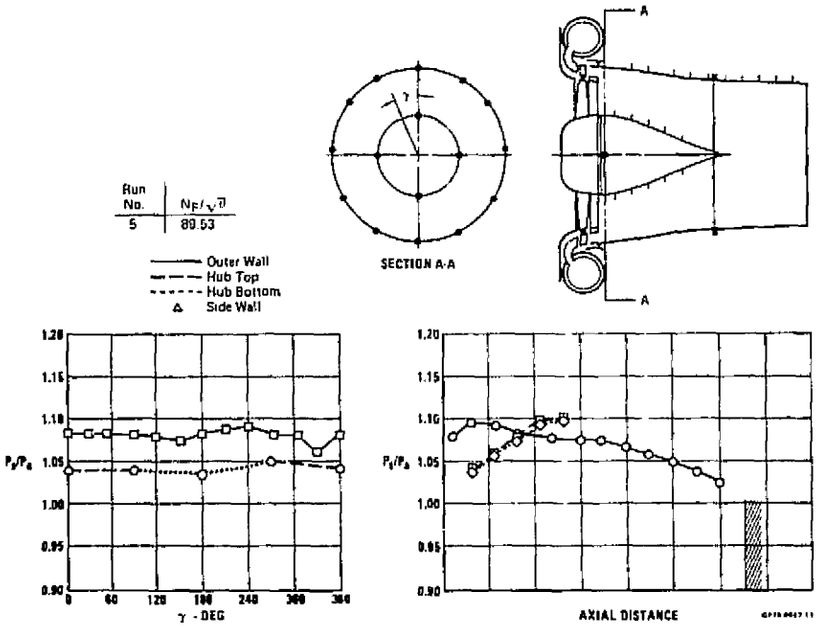

FIGURE 4-10
THRUST CALIBRATION NOZZLE, WALL TEMPERATURE DISTRIBUTIONS
A_{NOZ} = 5485 cm^2 $N_F/\sqrt{\theta}$ = 89.53%

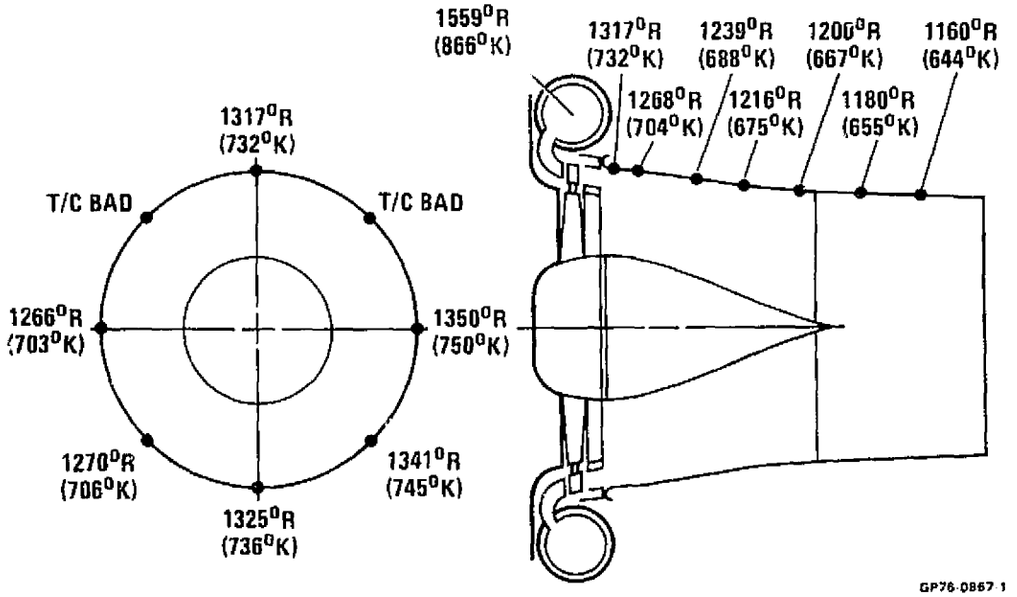

closure doors open and two "D" shaped spacers installed. With the two spacers, the nozzle geometry provided the largest VTO nozzle exit area. Subsequent tests were conducted with the movable hoods at geometric angles of 75°, 90°, 112° and 132°. The geometric hood angle of 112° produced thrust vectoring near 90° and at this position the transition fairing and two venting lip extension plates were installed and tested. The transition fairings and lip extensions produced a three step variation in the nozzle exit area. The two "D" shaped spacers were removed which produced a fifth nozzle exit area. Tests at geometric positions of 112°, 90° and 0° were carried out with the two spacers removed.

4.2.1 THRUST PERFORMANCE - Figure 4-11 presents the resultant thrust versus fan speed performance measured for the geometric positions of 0°, 75°, 90°, 112° and 132° with the two spacers installed. Corresponding corrected fan flow data is shown in Figure 4-12. Resultant thrust decreased as the hood rotation angle was varied between 0° and 132°, whereas fan flow increased slightly between 0° and 75° and then decreased for the larger hood angles. The fan flow measurements indicate that the maximum effective flow area of the "D" vented nozzle configuration occurs at the intermediate geometric hood positions. Installation of the transition fairings and lip extension plates in the nozzle at the 112° geometric position produced an increase in resultant thrust and a decrease in fan flow as depicted in Figures 4-13 and 4-14. The thrust and fan flow measurements recorded for the test with the two "D" shaped spacers removed is shown in Figures 4-15 and 4-16.

The nozzle entrance total pressure and temperature measurements recorded at geometric positions of 0°, 75°, 90° and 112° with the two spacers installed are shown in Figures 4-17 through 4-24. In general, rotation of the hood elements from 0° to 112° produced a change in turbine flow total pressure distributions. At 112° geometric positions the total pressure at the top of the nozzle is higher than that recorded on the bottom of the nozzle which is slightly upstream of the nozzle venting lip. Figures 4-25 and 4-26 illustrate for comparison purposes the entrance total pressure data for the thrust calibration nozzle and the "D" vented nozzle at the 0° and 112° geometric positions. As shown, the primary effect of the vectoring nozzle is to introduce circumferential distortion in the turbine flow region.

Nozzle corrected flow data were calculated using the entrance flow measurements for each of the longitudinal test runs and are presented on Figure 4-27

FIGURE 4-11
"D" VENTED NOZZLE, LONGITUDINAL VECTORING PERFORMANCE
THRUST vs FAN SPEED

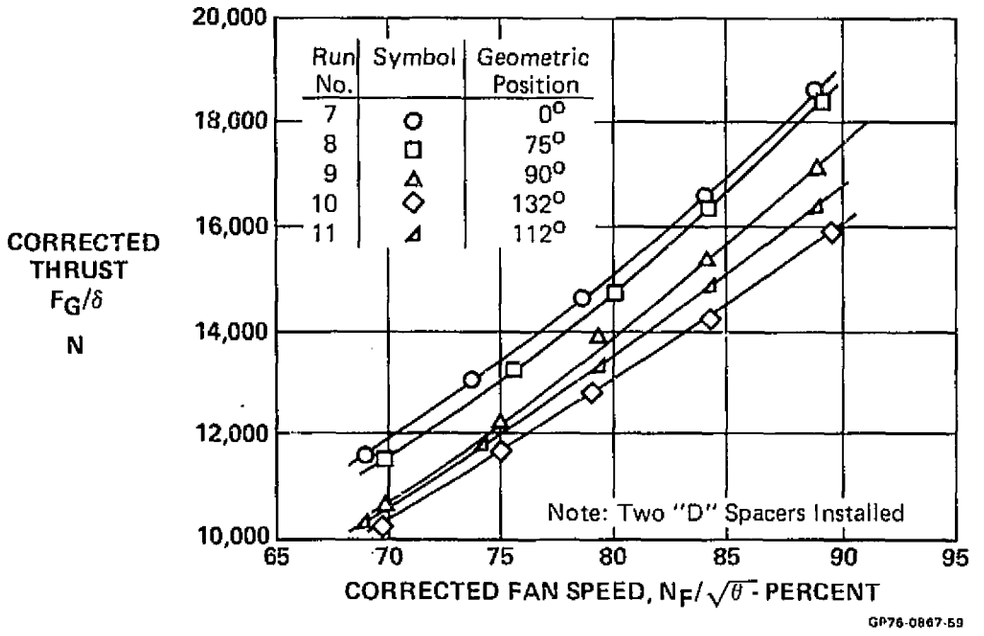

FIGURE 4-12
"D" VENTED NOZZLE, LONGITUDINAL VECTORING PERFORMANCE
FAN FLOW vs FAN SPEED

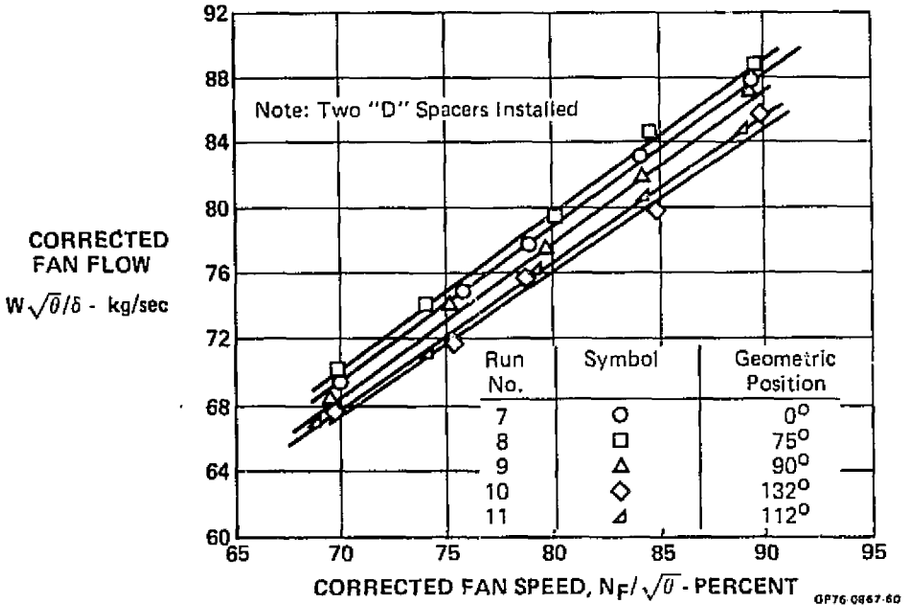

FIGURE 4-13
"D" VENTED NOZZLE, VTO PERFORMANCE, THRUST vs FAN SPEED

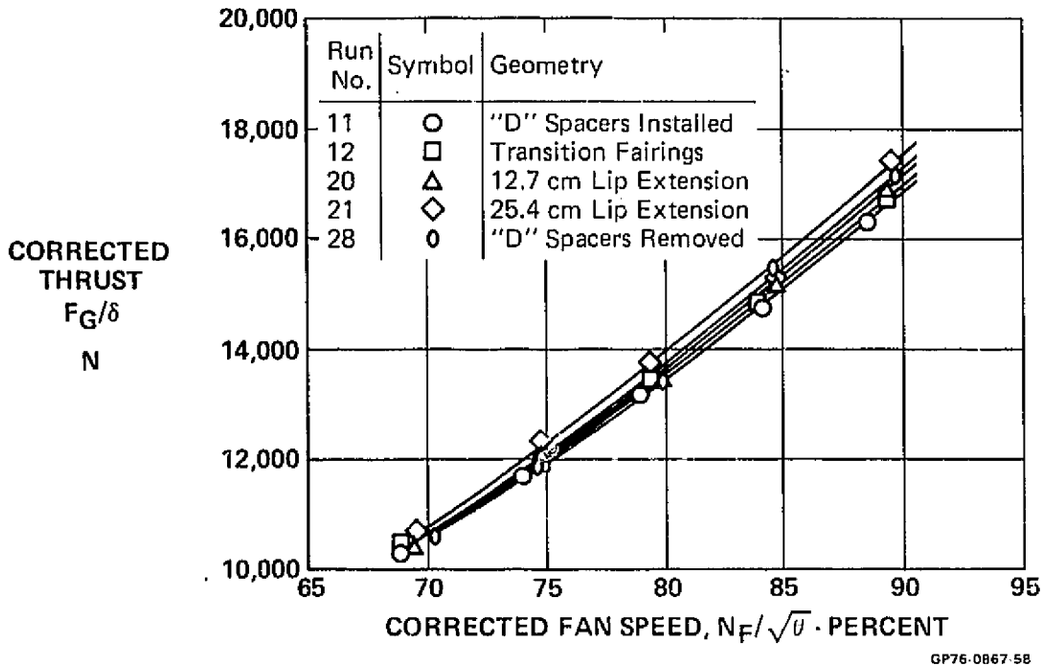

FIGURE 4-14
"D" VENTED NOZZLE, VTO PERFORMANCE FAN FLOW vs FAN SPEED

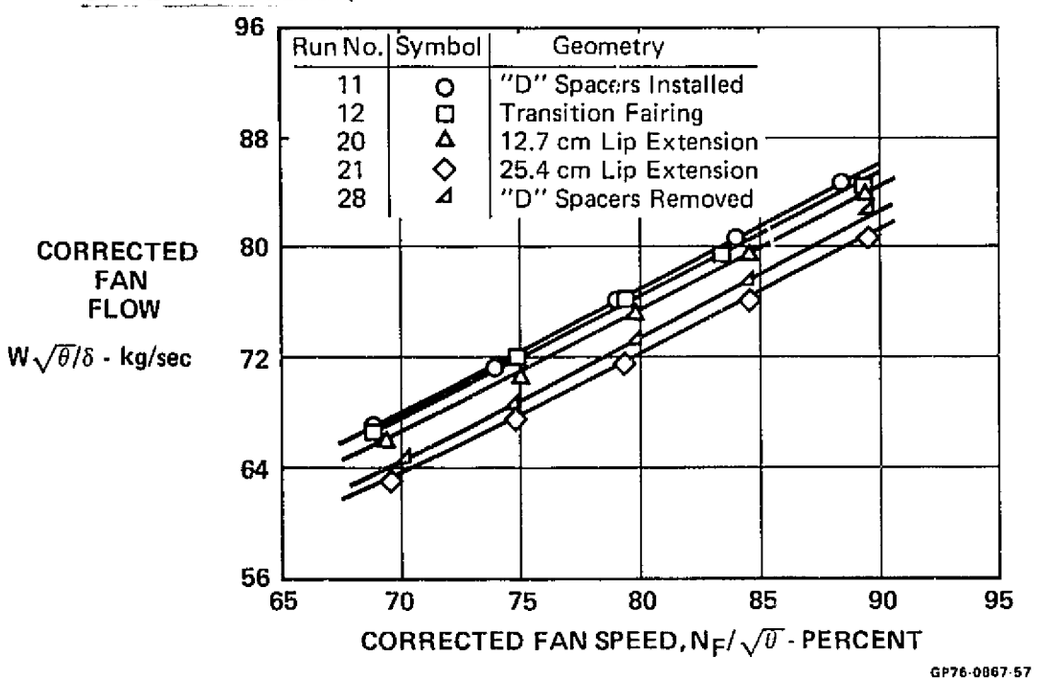

FIGURE 4-15
"D" VENTED NOZZLE LONGITUDINAL PERFORMANCE, THRUST vs FAN SPEED

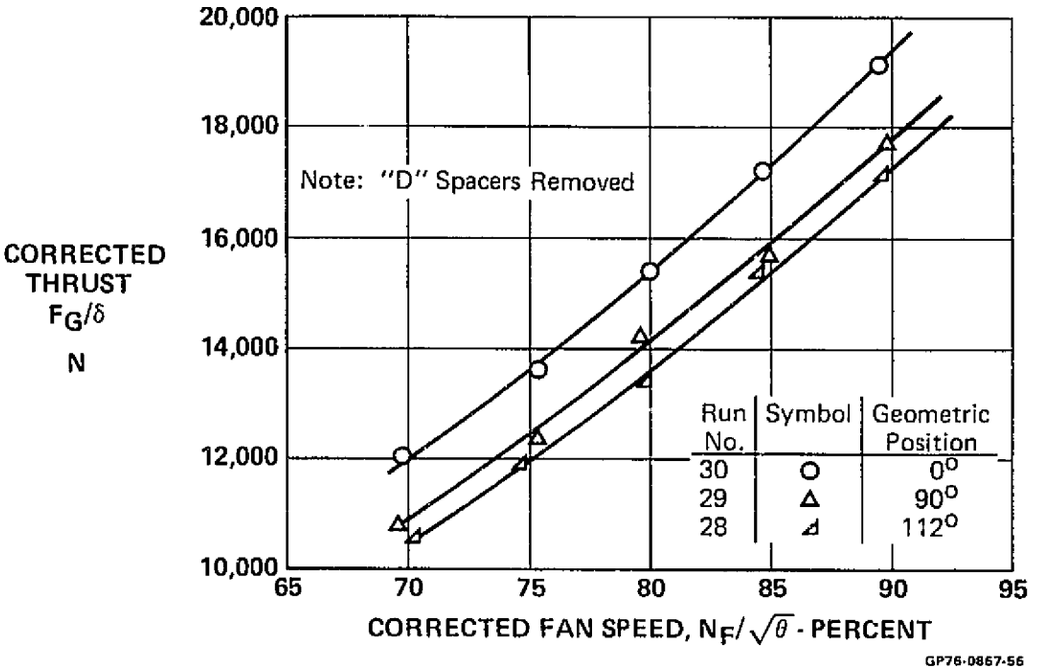

FIGURE 4-16
"D" VENTED NOZZLE, LONGITUDINAL PERFORMANCE FAN FLOW vs FAN SPEED

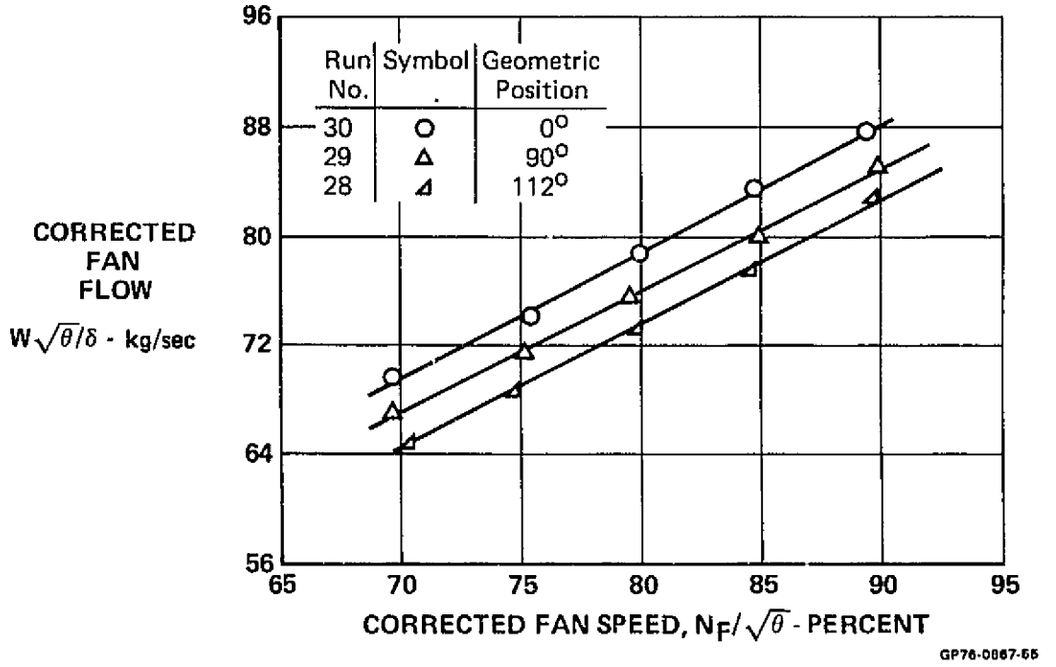

FIGURE 4-17
"D" VENTED NOZZLE, ENTRANCE TOTAL PRESSURE DISTRIBUTIONS,
0° GEOMETRIC POSITION
$N_F/\sqrt{\theta}$ = 88.85%

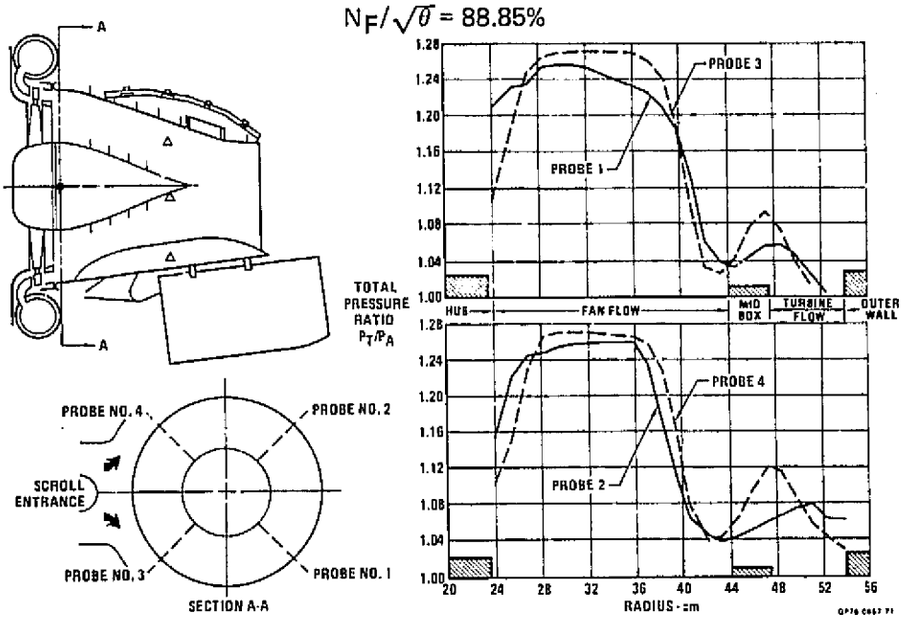

FIGURE 4-18
"D" VENTED NOZZLE, ENTRANCE TOTAL TEMPERATURE DISTRIBUTIONS,
0° GEOMETRIC POSITION
$N_F/\sqrt{\theta}$ = 88.85%

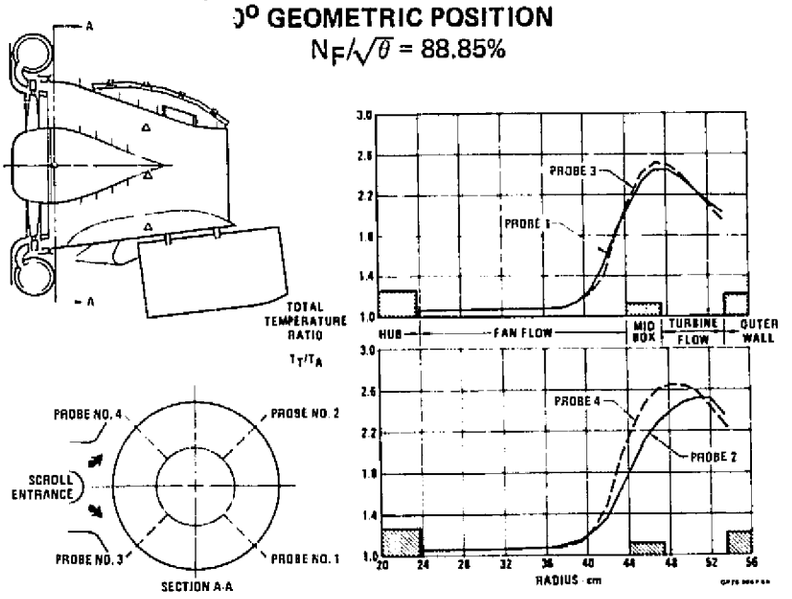

FIGURE 4-19
"D" VENTED NOZZLE, ENTRANCE TOTAL PRESSURE DISTRIBUTIONS,
75° GEOMETRIC POSITION
$N_F/\sqrt{\theta}$ = 89.15%

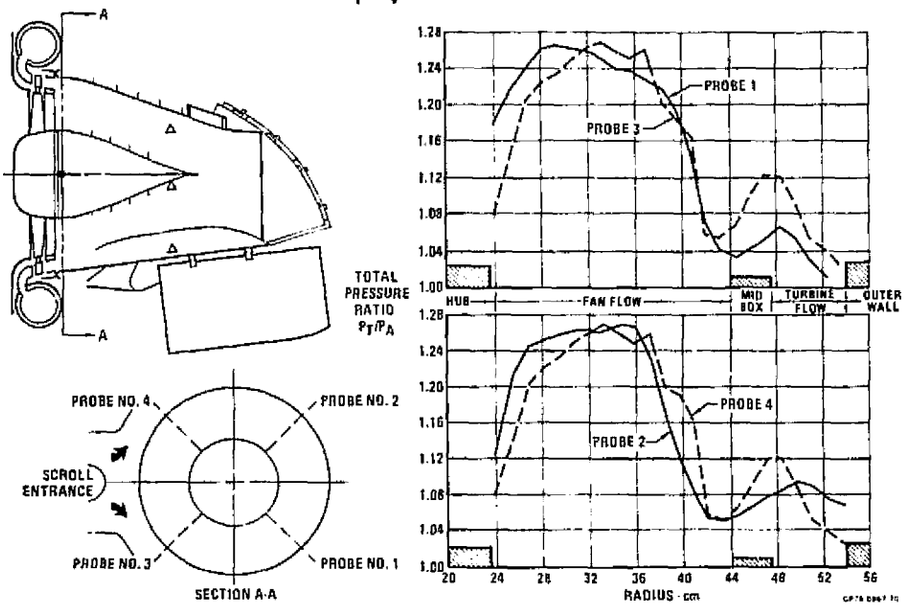

FIGURE 4-20
"D" VENTED NOZZLE, ENTRANCE TOTAL TEMPERATURE DISTRIBUTIONS,
75° GEOMETRIC POSITION
$N_F/\sqrt{\theta}$ = 89.15%

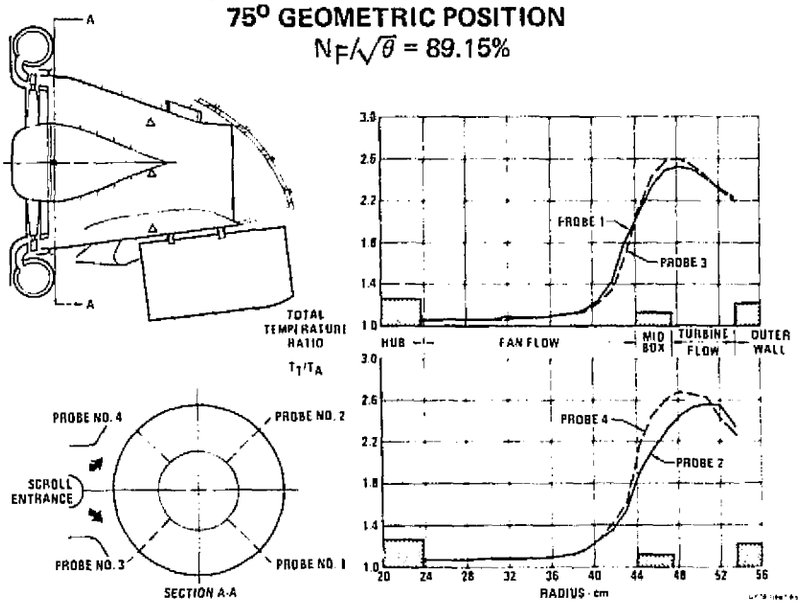

FIGURE 4-21
"D" VENTED NOZZLE, ENTRANCE TOTAL PRESSURE DISTRIBUTIONS, 90° GEOMETRIC POSITION
$N_F/\sqrt{\theta}$ = 88.86%

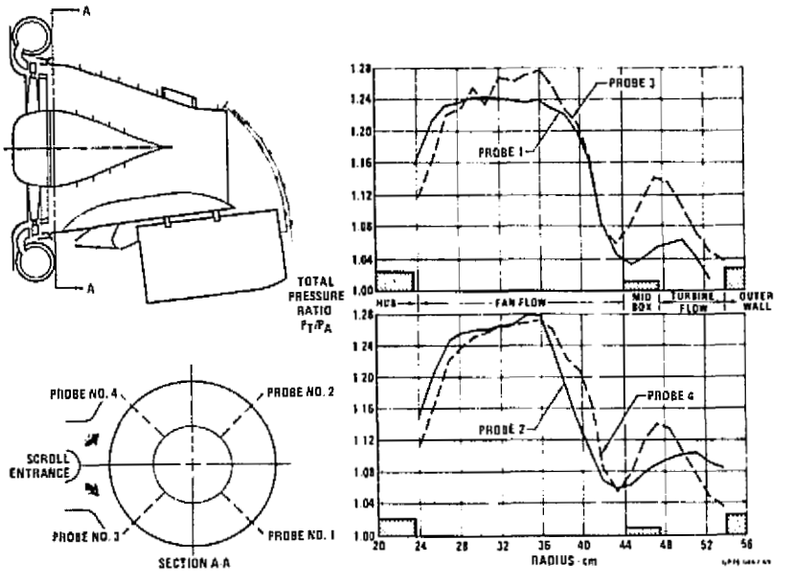

FIGURE 4-22
"D" VENTED NOZZLE, ENTRANCE TOTAL TEMPERATURE DISTRIBUTIONS, 90° GEOMETRIC POSITION
$N_F/\sqrt{\theta}$ = 88.86%

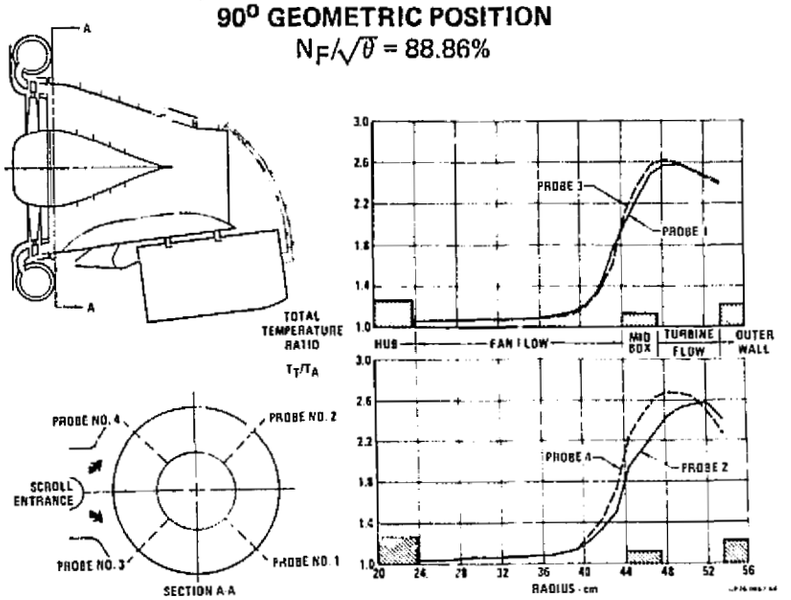

FIGURE 4-23
"D" VENTED NOZZLE, ENTRANCE TOTAL PRESSURE DISTRIBUTIONS,
112° GEOMETRIC POSITION
$N_F/\sqrt{\theta}$ = 88.54%

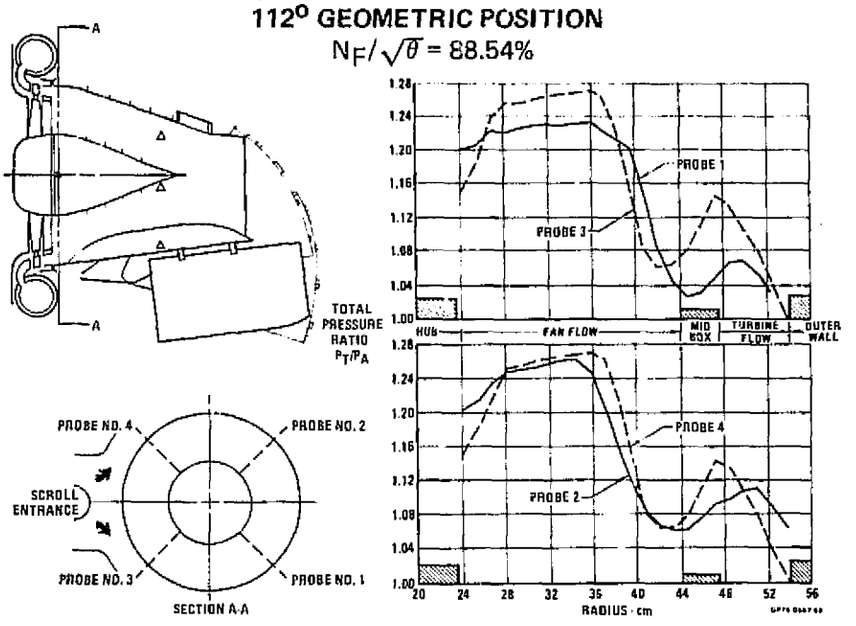

FIGURE 4-24
"D" VENTED NOZZLE, ENTRANCE TOTAL TEMPERATURE DISTRIBUTIONS,
112° GEOMETRIC POSITION
$N_F/\sqrt{\theta}$ = 88.54%

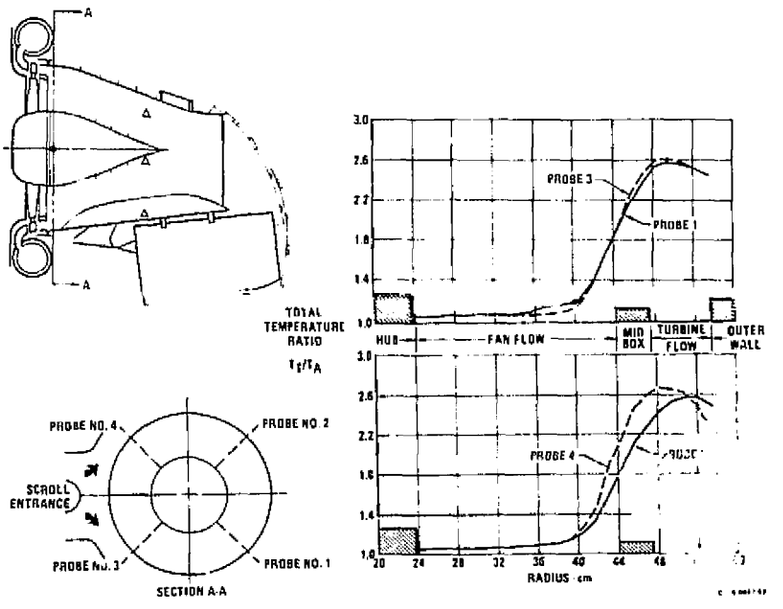

FIGURE 4-25
COMPARISON OF ENTRANCE TOTAL PRESSURE DISTRIBUTIONS ON THRUST CALIBRATION NOZZLE AND "D" VENTED NOZZLE (0°)

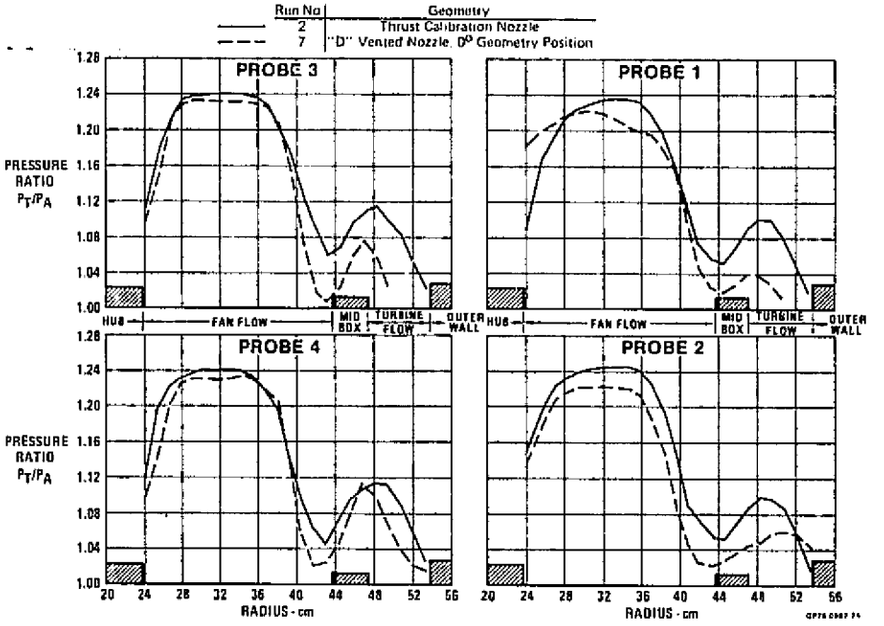

FIGURE 4-26
COMPARISON OF ENTRANCE TOTAL PRESSURE DISTRIBUTIONS ON THRUST CALIBRATION NOZZLE AND "D" VENTED NOZZLE (112°)

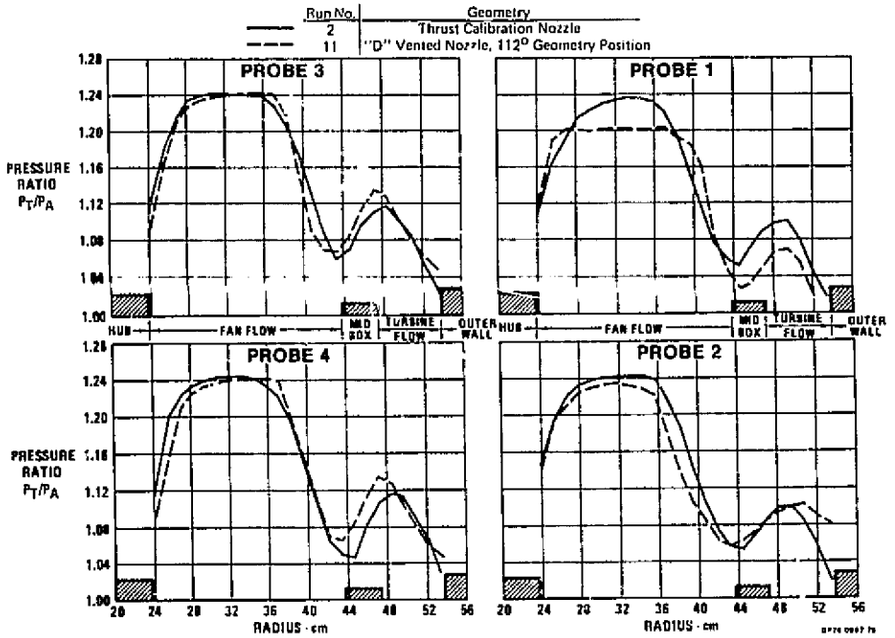

in terms of corrected thrust versus nozzle corrected flow. Also plotted on Figure 4-27 is the reference thrust data obtained with the thrust calibration nozzle for corrected fan speeds of 70, 80 and 90 percent. Figure 4-27 illustrates the effects of hood rotation angle and VTO exit area changes on thrust and the resultant variation of nozzle corrected flow during thrust vectoring.

The thrust data obtained with the "D" vented nozzle were divided by the reference thrust values at the corresponding corrected nozzle flow in order to define nozzle thrust coefficient data. Figure 4-28 shows the thrust coefficient data as a function of thrust vector angle and is based on the 90% fan speed data. Also shown on Figure 4-28 is the small scale vectoring performance estimates for the large scale "D" vented nozzle. Agreement within one to two percent is indicated. Comparison of the large scale VTO performance with small scale test data is shown in Figure 4-29 in terms of thrust coefficient versus specific nozzle corrected flow. The solid curve represents the estimated LF336/"D" vented nozzle performance and was obtained via the NPR - nozzle corrected flow characteristics measured with the thrust calibration nozzles and discussed in Section 4.1. The VTO thrust coefficient data obtained by variation of the nozzle VTO exit area are shown as the solid symbols and again indicates agreement within one to two percent over the range of test variables.

The relationship between the thrust vector angle and the geometric hood position is shown on Figure 4-30 for both the LF336 tests and previous small scale tests. The large scale tests produced a slightly different characteristic in that less flow turning was produced at intermediate hood angles and greater turning near the VTO position. This effect may be due to the difference in nozzle entrance conditions which was uniform for the small scale tests and non-uniform for the large scale tests.

The thrust vector line of application was defined by the perpendicular distance (R_o) between the thrust vector direction and the pivot for the rotating hood elements. The distance, R_o, was experimentally determined via the load cell axial and normal components and a knowledge of the load cell locations with respect to the hood pivot. Figure 4-31 shows the variation of R_o as a function of vectoring angle as recorded during the longitudinal thrust vectoring tests. In the 0° geometric position the thrust vector lies slightly below the fan centerline and at the 112° geometric position the thrust vector falls slightly aft of the hood center of curvature.

FIGURE 4-27
"D" VENTED NOZZLE, LONGITUDINAL VECTORING PERFORMANCE, THRUST vs NOZZLE CORRECT FLOW
$N_F/\sqrt{\theta} = 90\%$

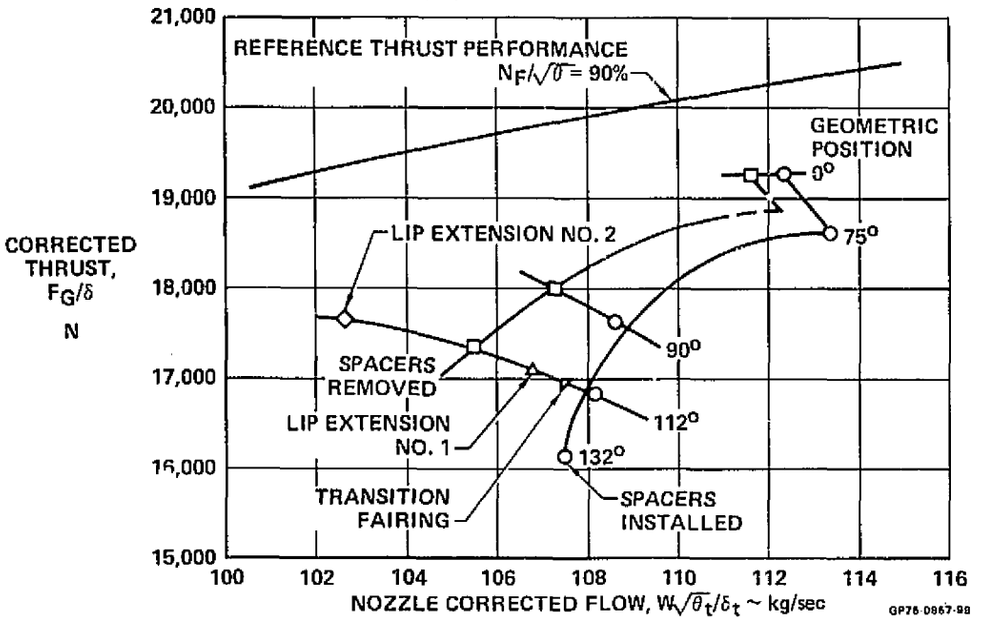

FIGURE 4-28
"D" VENTED NOZZLE, LONGITUDINAL VECTORING PERFORMANCE, THRUST COEFFICIENT vs VECTOR ANGLE

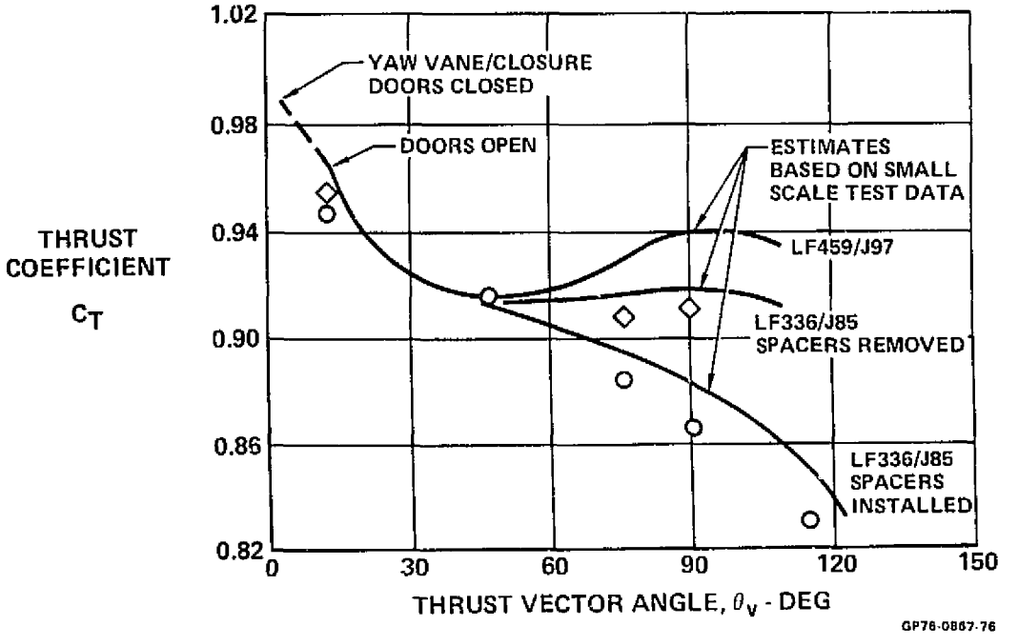

FIGURE 4-29
"D" VENTED NOZZLE, VTO PERFORMANCE THRUST COEFFICIENT
vs SPECIFIC NOZZLE CORRECTED FLOW

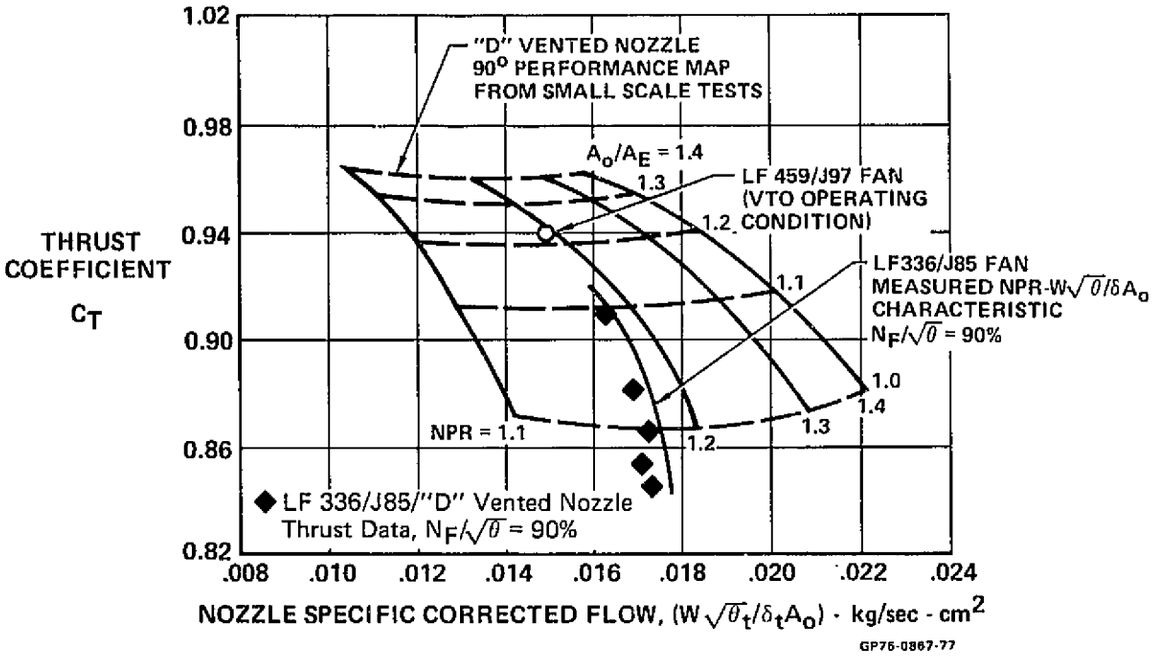

FIGURE 4-30
"D" VENTED NOZZLE, THRUST VECTOR ANGLE vs NOZZLE GEOMETRIC ANGLE

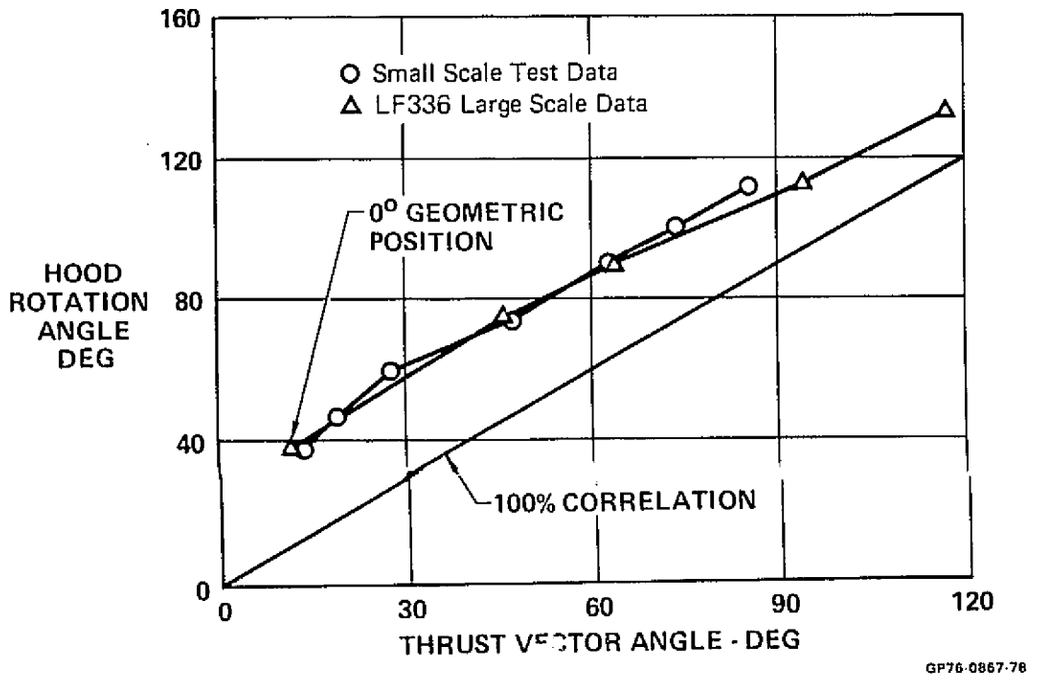

FIGURE 4-31
"D" VENTED NOZZLE, THRUST VECTOR LINE OF APPLICATION vs THRUST VECTOR ANGLE

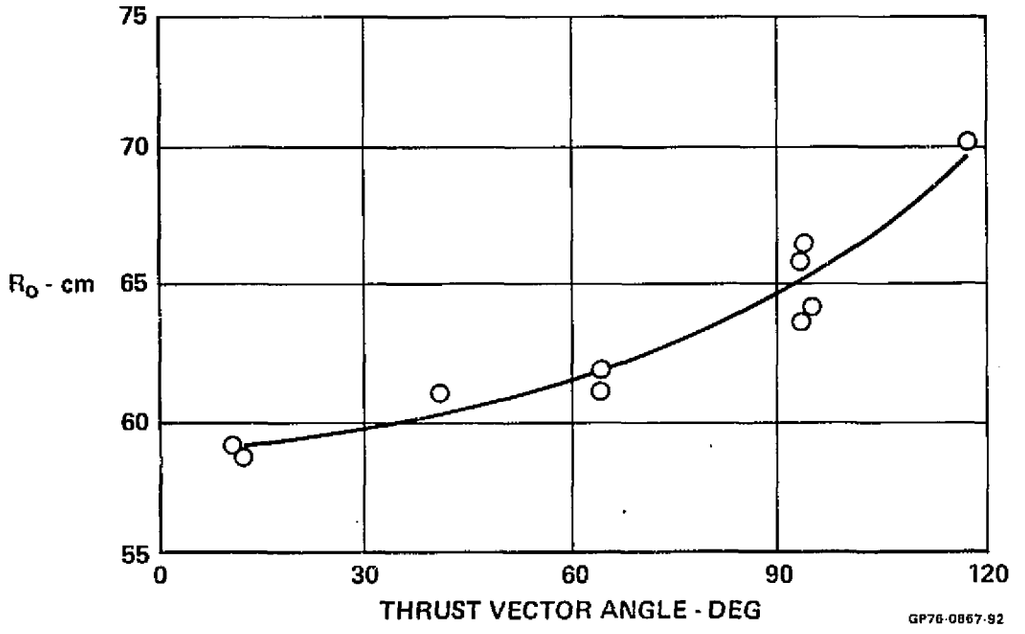

4.2.2 WALL PRESSURE AND TEMPERATURE MEASUREMENTS - Figures 4-32 through 4-36 illustrate the internal wall pressure distributions recorded during the thrust vectoring tests for the configuration with two spacers installed. In general the pressure distributions do not change significantly in character as the vector angle is varied. The pressure levels do vary in a manner consistent with the change in nozzle flow rate with vector angle. The nozzle entrance circumferential pressure distribution shows a radial gradient between the outer wall and the hub centerbody as was the case with the thrust calibration nozzle. However, with the "D" vented nozzle a circumferential gradient from the top to bottom exists which is indicative of a net downward turning of the flow at this station in the same direction as the deflected exit flow. Thus it is concluded that the "D" vented vectoring nozzle introduces a static pressure distortion at the fan exit. The axial wall pressure distributions show the characteristic increase in wall pressure to near stagnation values as the flow proceeds through the rotating hoods and then a decrease to ambient at the nozzle exit.

The corresponding wall temperature distributions are shown in Figures 4-37 through 4-41. The wall temperatures at the nozzle entrance station also show a circumferential nonuniformity which increases as the vectoring angle is increased. A gradient from top to bottom of approximately 150°K exists at the 132° geometric position. The temperature distribution throughout the nozzle fixed element and in the movable hood elements indicate that significant mixing of the fan and turbine exhaust flows takes place within the nozzle. The maximum temperature recorded on the movable elements was 720°K and occurred on the inner hood near the junction with the fixed structure elements. The wall temperatures decrease rapidly from this point to the nozzle exit station. For the 112° geometric position, the nozzle exit wall temperature was 309°K which is approximately the temperature of the fan exit flow.

4.3 "D" VENTED NOZZLE GROUND EFFECTS TESTS

A total of 4 test runs were conducted with the ground plane positioned over the nozzle test rig for the purpose of establishing the performance of the "D" vented nozzle in ground effect. The tests were run with the nozzle in the 112° geometric position and at ground plane heights of 272 centimeters (107 inches), 177 centimeters (69.5 inches), 146 centimeters (57.5 inches) and 119 centimeters (46.7 inches). The ground plane height was measured from the hood pivot point on the "D" vented nozzle.

FIGURE 4-32
"D" VENTED NOZZLE, WALL PRESSURE DISTRIBUTIONS,
0° GEOMETRIC POSITION
$N_F/\sqrt{\theta}$ = 88.85%

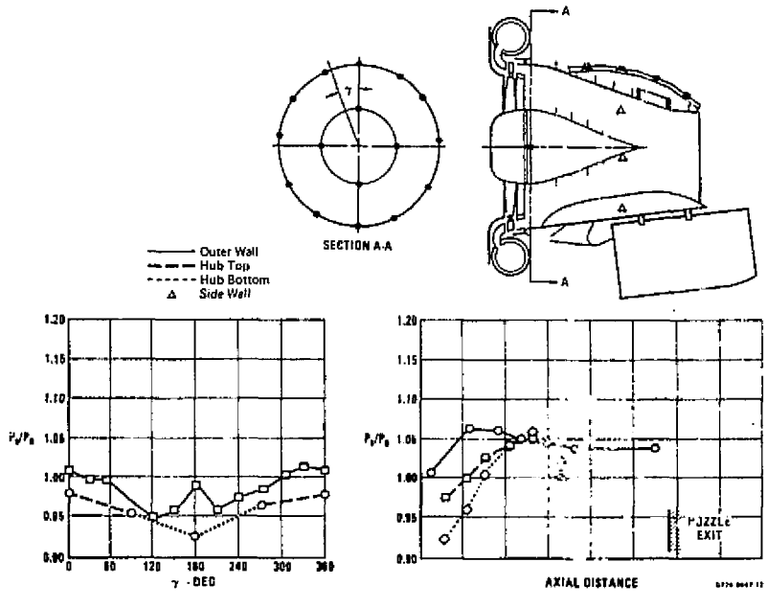

FIGURE 4-33
"D" VENTED NOZZLE, WALL PRESSURE DISTRIBUTIONS,
75° GEOMETRIC POSITION
$N_F/\sqrt{\theta}$ = 89.15%

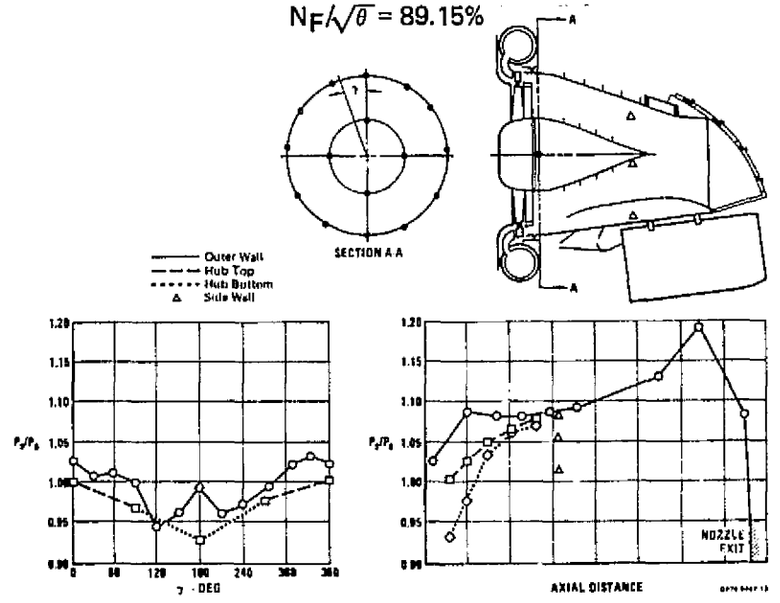

FIGURE 4-34
"D" VENTED NOZZLE, WALL PRESSURE DISTRIBUTIONS, 90° GEOMETRIC POSITION
$N_F/\sqrt{\theta}$ = 88.86%

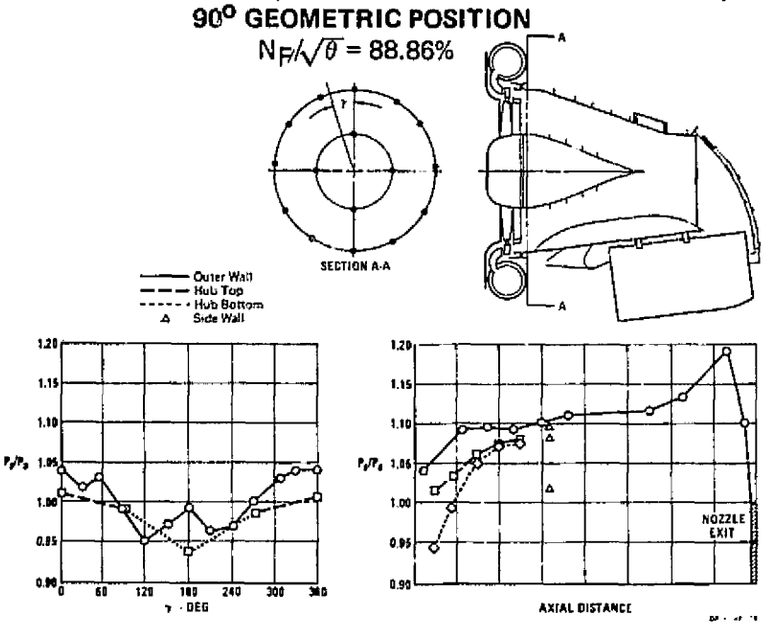

FIGURE 4-35
"D" VENTED NOZZLE WALL PRESSURE DISTRIBUTIONS, 112° GEOMETRIC POSITION
$N_F/\sqrt{\theta}$ = 88.54%

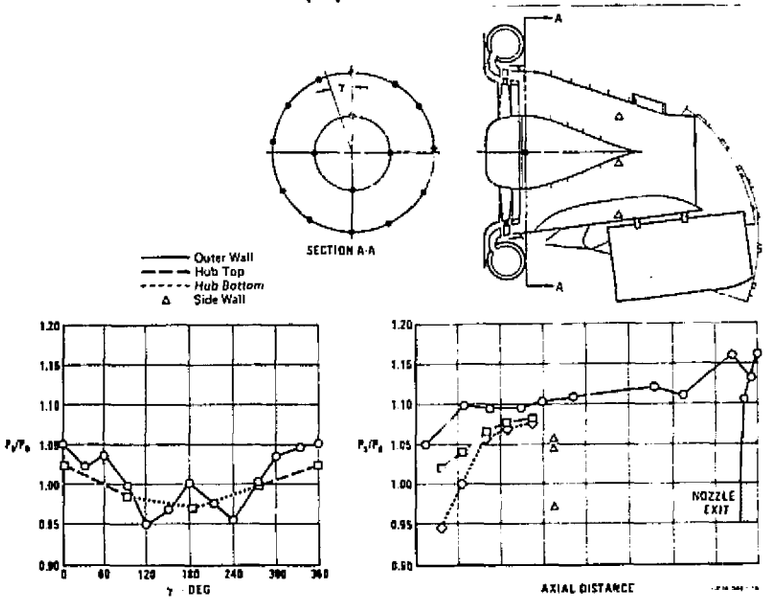

FIGURE 4-36
"D" VENTED NOZZLE, WALL PRESSURE DISTRIBUTIONS,
132° GEOMETRIC POSITION
$N_F/\sqrt{\theta}$ = 89.5%

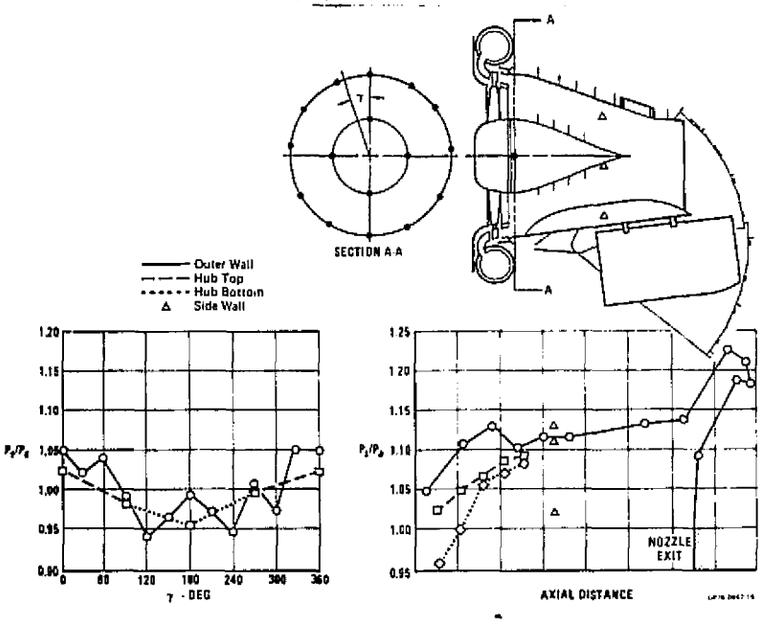

FIGURE 4-37
"D" VENTED NOZZLE, WALL TEMPERATURE DISTRIBUTIONS,
0° GEOMETRIC POSITION
$N_F/\sqrt{\theta}$ = 88.85%

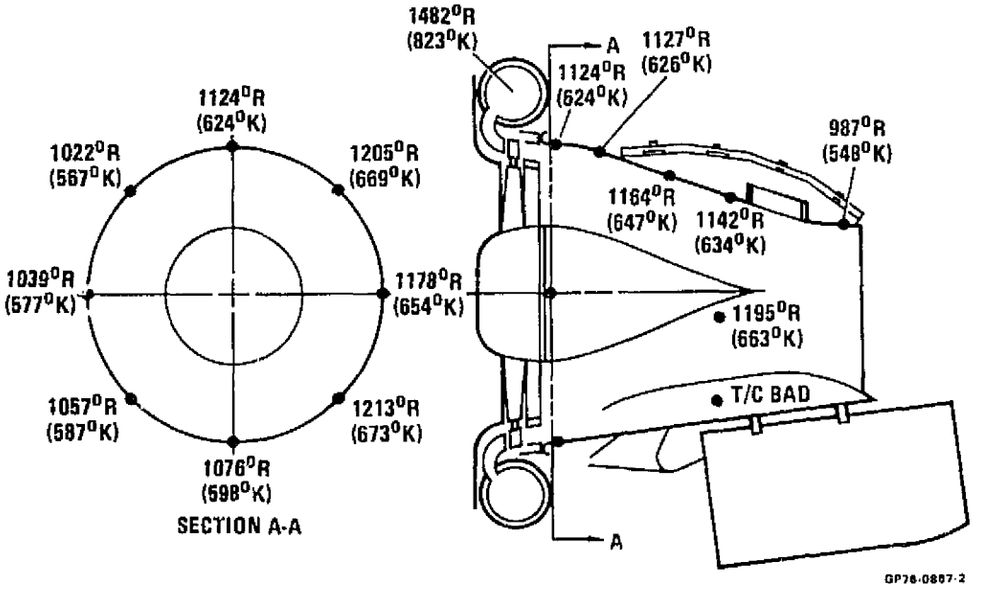

FIGURE 4-38
"D" VENTED NOZZLE, WALL TEMPERATURE DISTRIBUTIONS,
75° GEOMETRIC POSITION
$N_F/\sqrt{\theta}$ = 89.15%

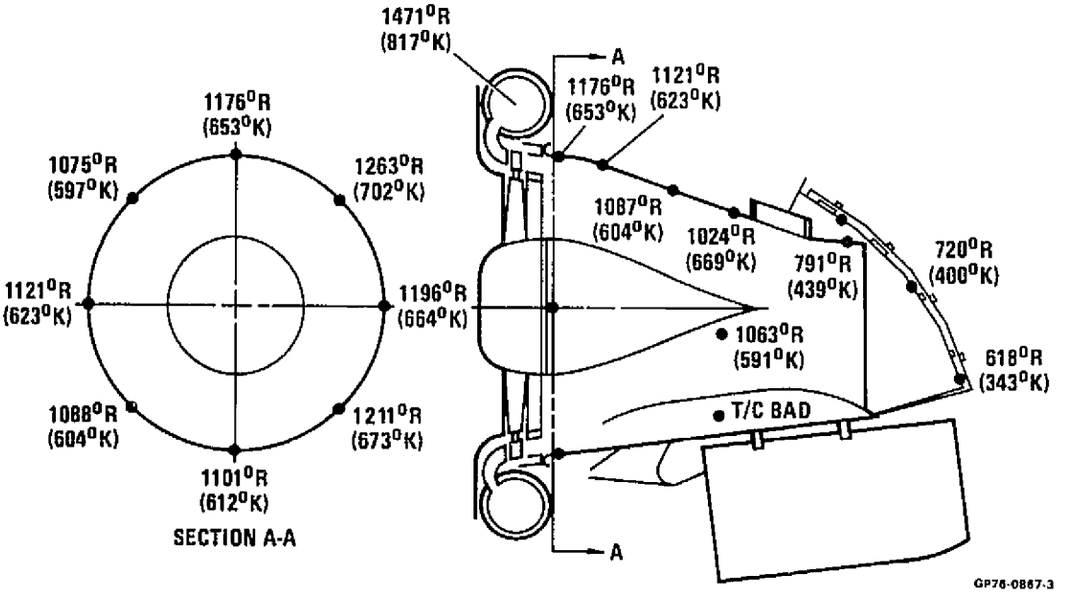

FIGURE 4-39
"D" VENTED NOZZLE, WALL TEMPERATURE DISTRIBUTIONS,
90° GEOMETRIC POSITON
$N_F/\sqrt{\theta}$ = 88.86%

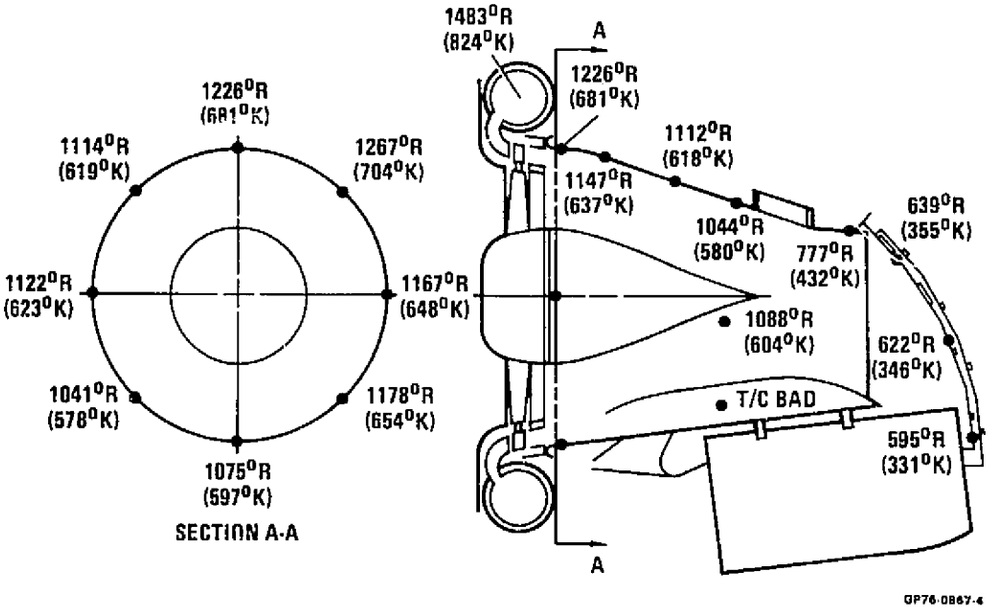

FIGURE 4-40
"D" VENTED NOZZLE, WALL TEMPERATURE DISTRIBUTIONS,
112° GEOMETRIC POSITION
$N_F/\sqrt{\theta}$ = 88.54%

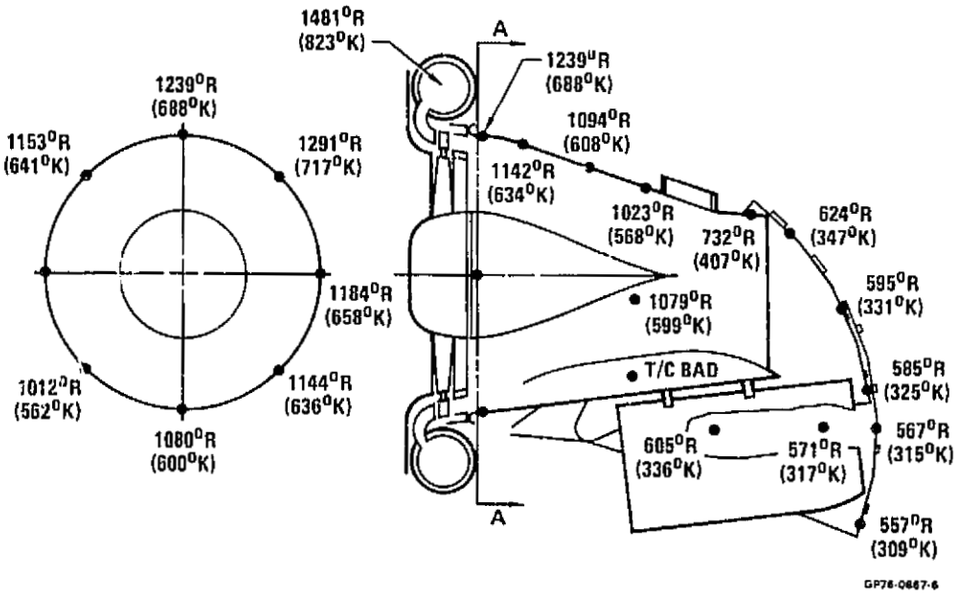

FIGURE 4-41
"D" VENTED NOZZLE, WALL TEMPERATURE DISTRIBUTIONS,
132° GEOMETRIC POSITION
$N_F/\sqrt{\theta}$ = 89.35%

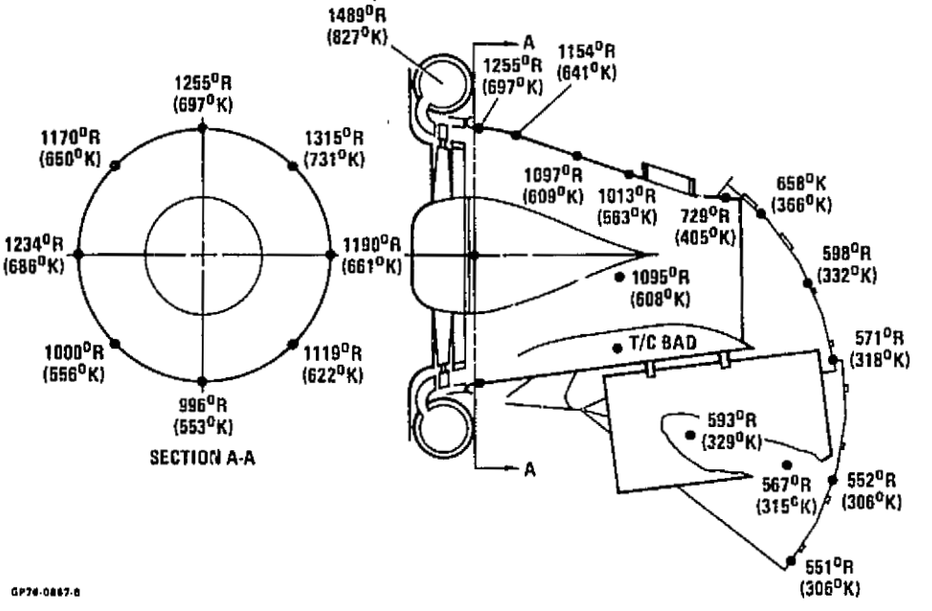

Reingestion of the nozzle exhaust flow into the fan and gas generator inlets was indicated during each of ground plane tests. Figure 4-42 shows the recorded temperature rise at both the gas generator and fan inlets as a function of ground height to fan diameter ratio. At the lowest ground height, foam insulation material which was attached to the fan inlet bellmouth was torn away by the deflected exhaust flow. This test was terminated after the 70% fan speed data was recorded to prevent possible damage to the fan due to reingestion of the insulation material.

Figure 4-43 presents the thrust versus fan speed characteristics recorded during the ground effects test runs and also out of ground effect data on the nozzle for comparison purposes. A definite loss in thrust is indicated at the low fan speeds as the ratio h/D_F was reduced however, the shape of the thrust versus fan speed curves indicate an increase in thrust at a fan speed of 90%. Figure 4-44 is a plot of fan flow versus fan speed recorded during the ground effects tests and indicates that the fan flow increased approximately 10% at $h/D_F = 1.6$ compared to the out of ground effect value. Figure 4-45 illustrates the ground effects data in terms of thrust versus nozzle corrected flow. At 90% fan speed, thrust and nozzle flow increased whereas at reduced speeds thrust decreased and nozzle flow increased. This increase in nozzle flow is indicative of an increase in effective nozzle exit area with decreasing values of h/D_F. This effect is in contrast with conventional exhaust nozzle performance in ground effect which generally exhibits a decrease in effective area. The "D" vented nozzle, out of ground effect is not a full flowing nozzle in that the exit region adjacent to the venting lip is void of exhaust flow and also acts as an inlet region for entrainment of ambient air into the exhaust flow. The measured ground effects data suggests that in ground effect the impinging exhaust pressure field causes the open region near the venting lip to become effective as exhaust flow area.

Small scale pressurized tests of the "D" vented nozzle and a conventional full flowing nozzle are shown in Figure 4-46. These data show the expected decrease in flow for the conventional nozzle and no change in mass flow down to $h/D = .5$ for the "D" vented nozzle.

The difference between the small and large scale nozzle tests is no doubt attributable to the presence of the fan and the out of ground effect nozzle exit area sizing point. In either case the vented lower elbow corner in this nozzle

FIGURE 4-42
FAN AND GAS GENERATOR TEMPERATURE RISE DURING
GROUND EFFECTS TESTS

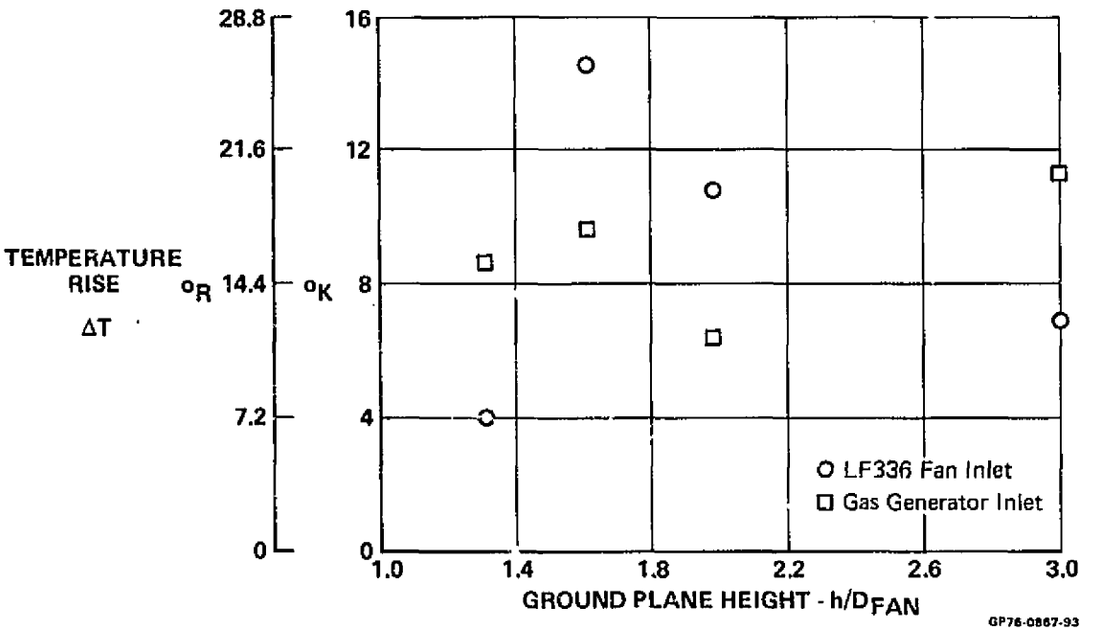

FIGURE 4-43
"D" VENTED NOZZLE, GROUND EFFECT PERFORMANCE,
THRUST vs FAN SPEED CHARACTERISTICS

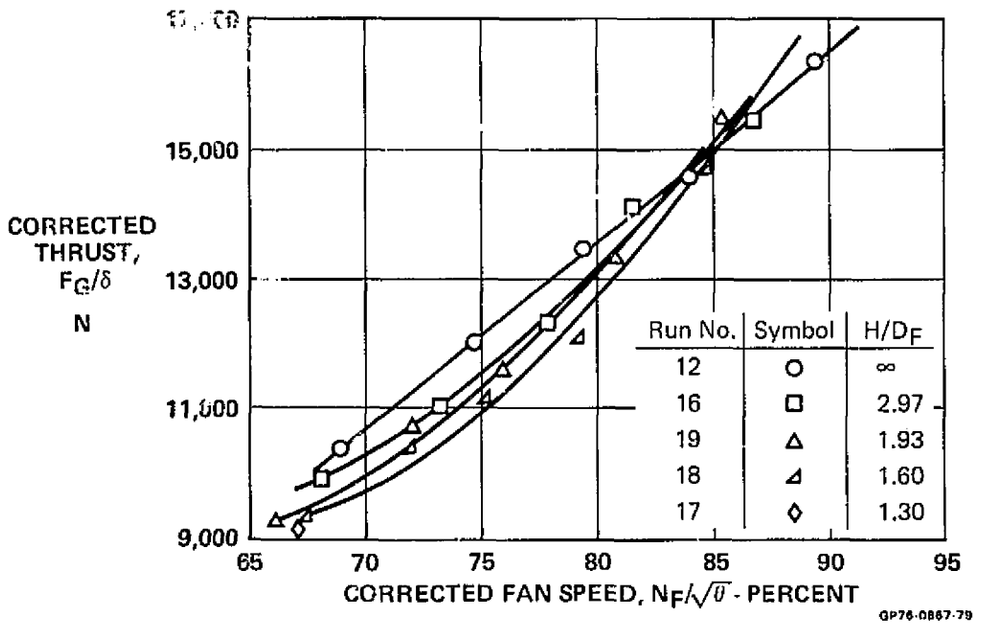

FIGURE 4-44
"D" VENTED NOZZLE, GROUND EFFECT PERFORMANCE,
FAN FLOW vs FAN SPEED CHARACTERISTICS

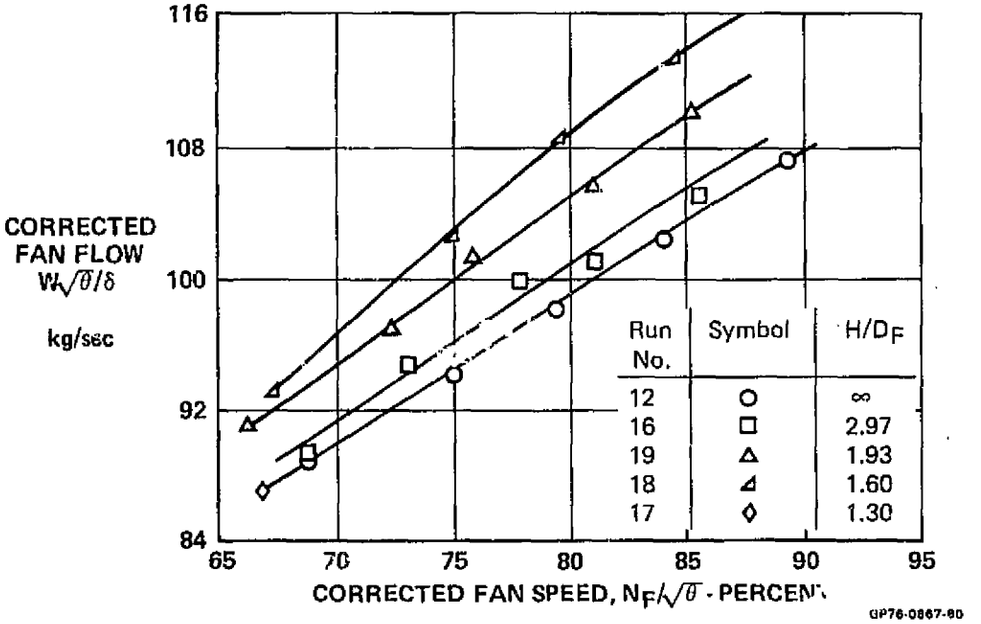

FIGURE 4-45
"D" VENTED NOZZLE, GROUND EFFECT PERFORMANCE,
THRUST vs NOZZLE CORRECTED FLOW

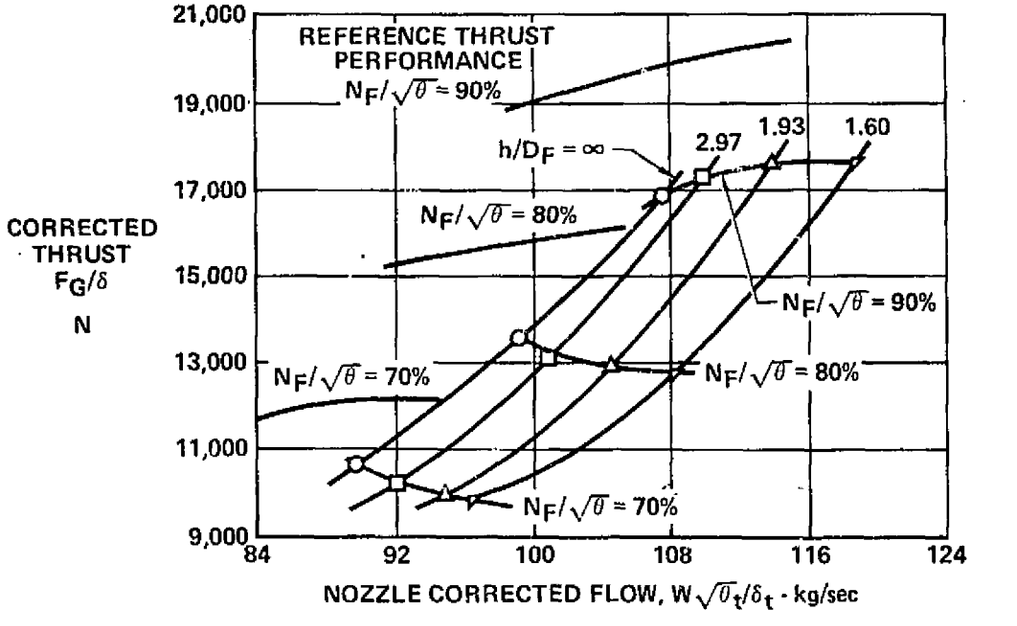

FIGURE 4-46
"D" VENTED NOZZLE, GROUND EFFECT MASS FLOW PERFORMANCE
Small Scale Test Data

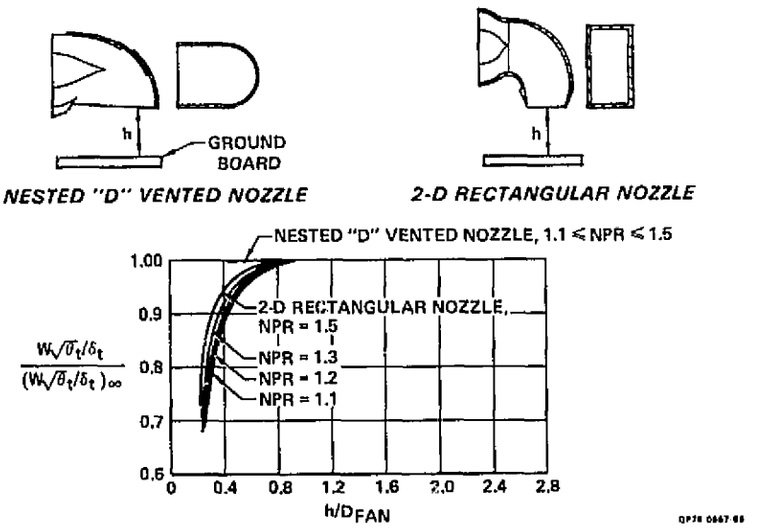

design appears to be self relieving with respect to exit area when operating in ground effect. The significance of this feature on thrust performance in ground effect is a function of the fan design characteristics and the out of ground effect nozzle sizing point. The variation of thrust performance in ground effect with fan speed recorded on LF336 tests indicates further that the nozzle pressure ratio is also an important parameter affecting ground effect performance.

4.4 "D" VENTED NOZZLE, THRUST REDUCTION MODULATION TESTS

Thrust reduction modulation was investigated during three test runs: two runs with the nozzle position at 112° and one run at the 90° geometric position. Two positions of the TRM port, 33% and 100% open, were evaluated at the 112° nozzle position, whereas the combination of spoilage and yaw vectoring was tested during the 90° geometric run.

Thrust versus fan speed performance recorded with the nozzle at 112° and the TRM port closed, 33% open and 100% open is shown on Figure 4-47. Corresponding fan flow data is presented in Figure 4-48 and shows that opening the TRM port appears as an increase in nozzle effective area. Thrust versus nozzle corrected flow information is shown on Figure 4-49 and was used to establish the thrust coefficient data of Figure 4-50. Figure 4-50 shows the nozzle thrust coefficient as a function of the ratio of TRM open area to nozzle entrance area. Small scale TRM performance for the "D" vented nozzle is also shown on Figure 4-50 for comparison. General agreement between the large and small scale performance was obtained for variation of the TRM port open area ratio. The deviation between large scale and small scale performance at the closed port position is primarily associated with the difference in specific nozzle corrected flow for the two tests.

The performance obtained with the nozzle at the 90° geometric position with the TRM port full open and the yaw vane deflected 15° is also shown on Figure 4-50 and indicates a nozzle thrust coefficient of 0.76.

4.5 "D" VENTED NOZZLE, YAW VECTORING TESTS

Several tests were conducted with the exit yaw vane deflected either 10° or 15°, for the purpose of establishing the yaw vectoring capability of the "D" vented nozzle. As discussed in Section 3, post test analysis revealed the side force measurement technique to be inadequate to define the side force angle. Resultant thrust and fan flow data were obtained during the yaw vectoring tests. Figure 4-51 shows the resultant thrust versus fan speed data for yaw vane

FIGURE 4-47
"D" VENTED NOZZLE, TRM PERFORMANCE,
THRUST vs FAN SPEED CHARACTERISTICS

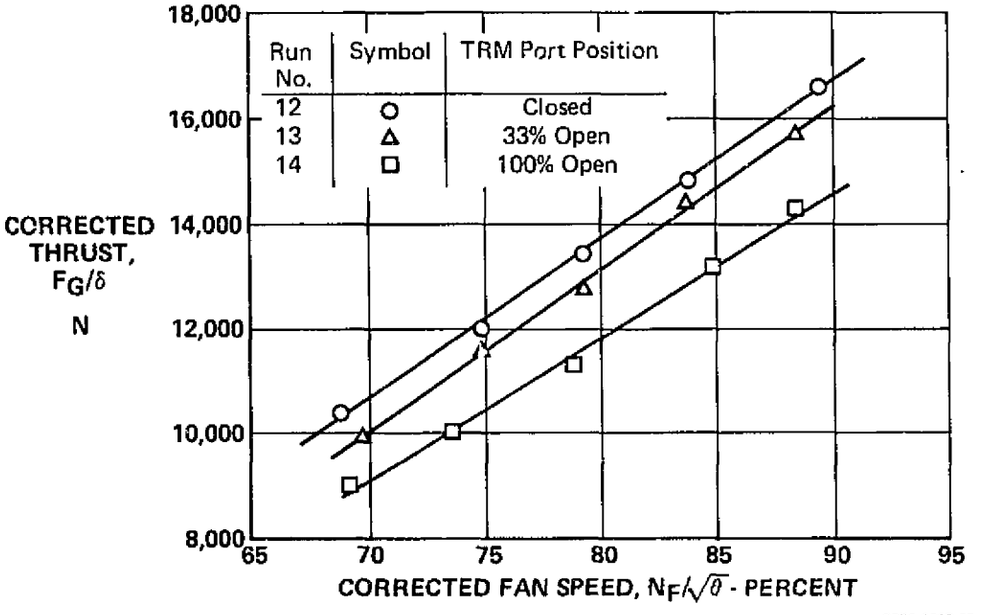

FIGURE 4-48
"D" VENTED NOZZLE, TRM PERFORMANCE, FAN FLOW
vs FAN SPEED CHARACTERISTICS

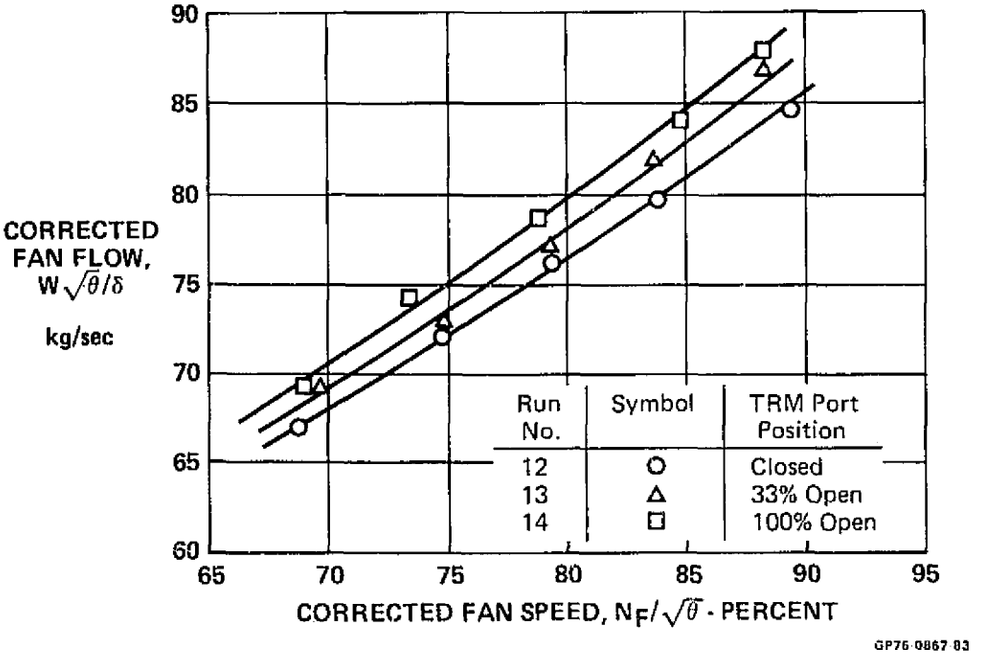

FIGURE 4-49
"D" VENTED NOZZLE, TRM PERFORMANCE, THRUST vs NOZZLE CORRECTED FLOW

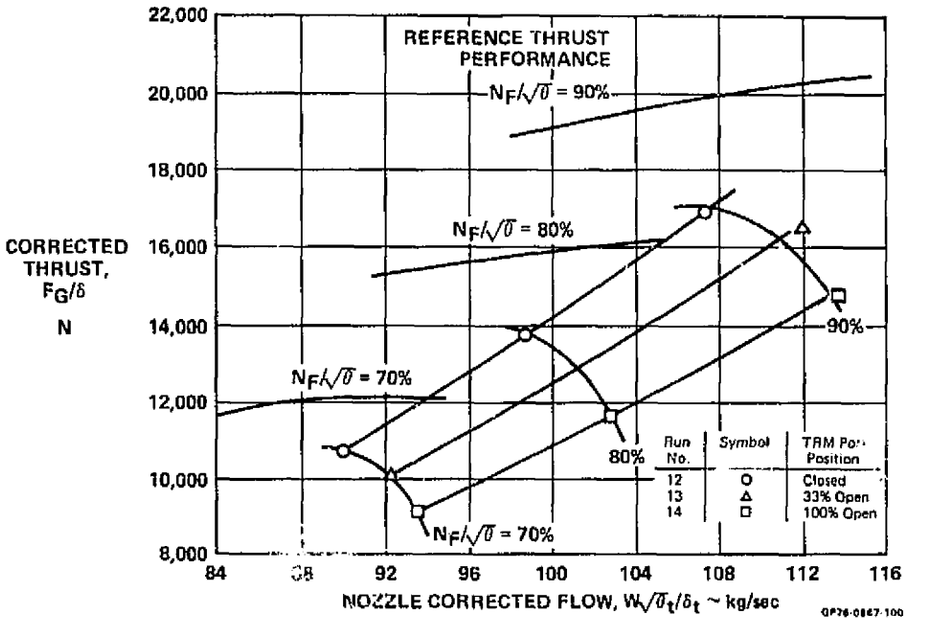

FIGURE 4-50
"D" VENTED NOZZLE, TRM PERFORMANCE THRUST COEFFICIENT AS A FUNCTION OF TRM PORT OPEN AREA

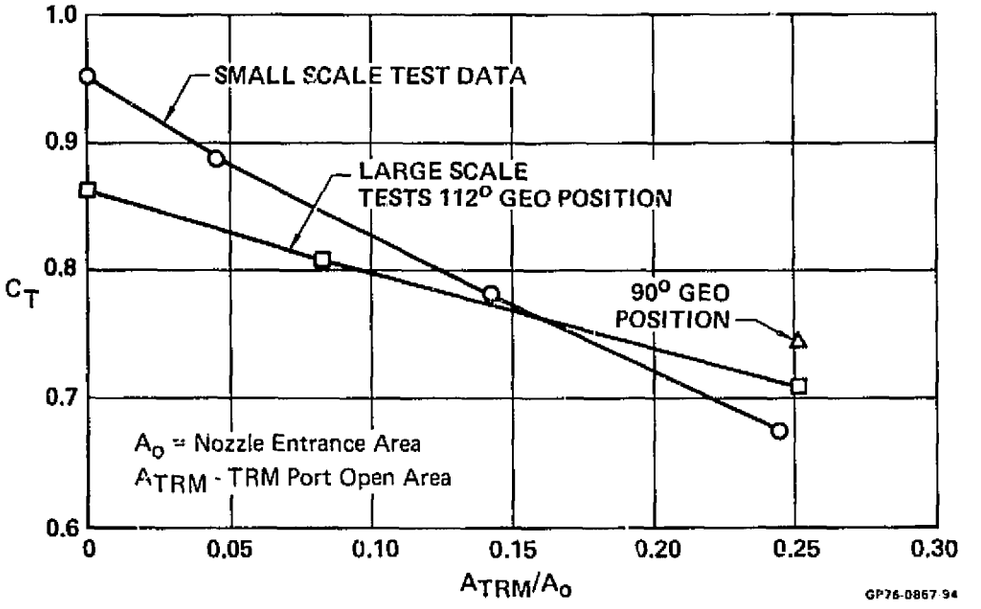

FIGURE 4-51
"D" VENTED NOZZLE, YAW VECTORING PERFORMANCE, 112° GEOMETRIC POSITION, THRUST vs FAN SPEED CHARACTERISTICS

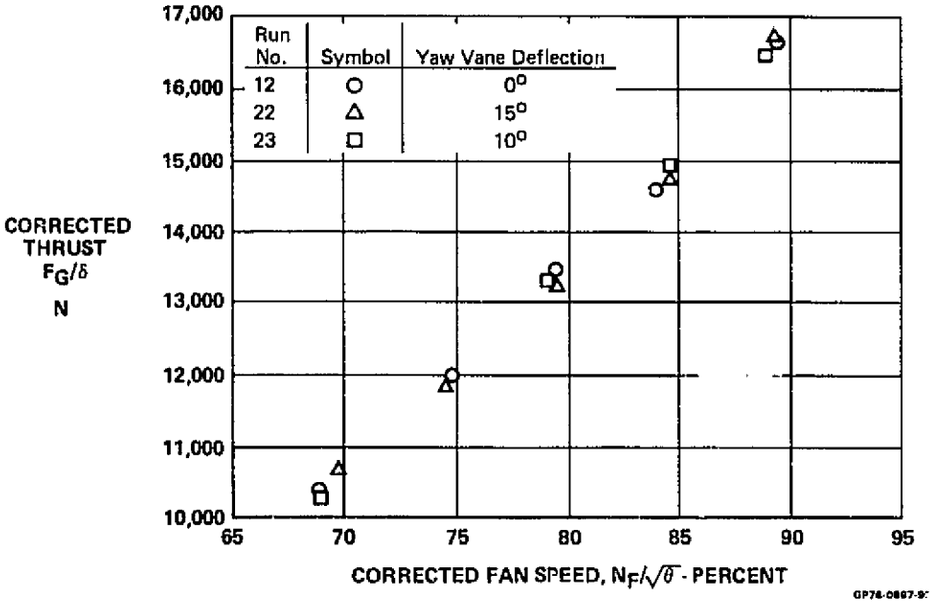

deflections of 0°, 10°, and 15° at the 112° nozzle position. Corresponding fan flow data is plotted in Figure 4-52. No discernible changes in resultant thrust or fan flow were recorded for the range of yaw vane deflections tested. A similar result was obtained at a nozzle position of 75° with the yaw vane at 15° deflection as shown in Figures 4-53 and 4-54.

FIGURE 4-52
"D" VENTED NOZZLE, YAW VECTORING PERFORMANCE, 112° GEOMETRIC PERFORMANCE, FAN FLOW vs FAN SPEED CHARACTERISTICS

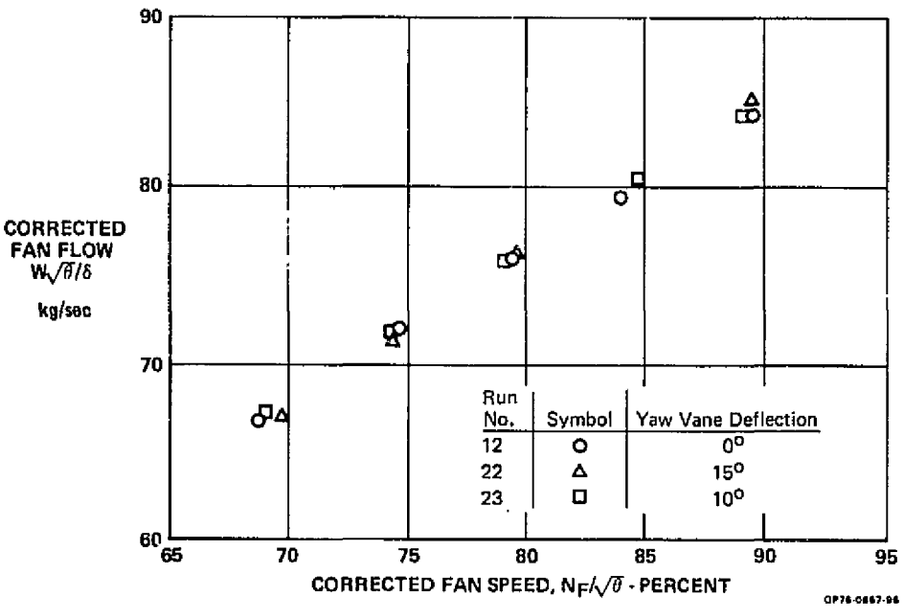

FIGURE 4-53
"D" VENTED NOZZLE, YAW VECTORING PERFORMANCE, 75° GEOMETRIC POSITION, THRUST vs FAN SPEED CHARACTERISTICS

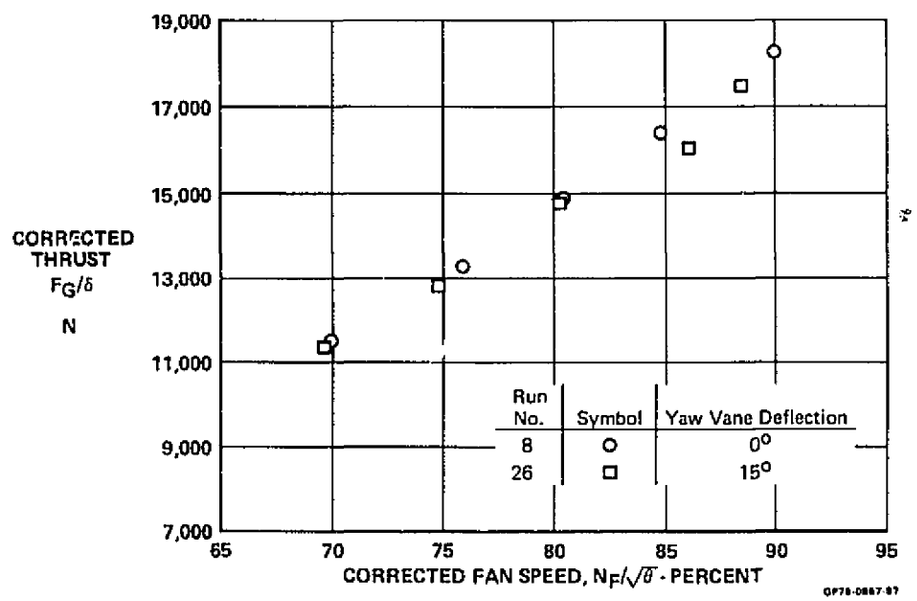

FIGURE 4-54
"D" VENTED NOZZLE, YAW VECTORING PERFORMANCE, 75° GEOMETRIC POSITION, FAN FLOW vs FAN SPEED CHARACTERISTICS

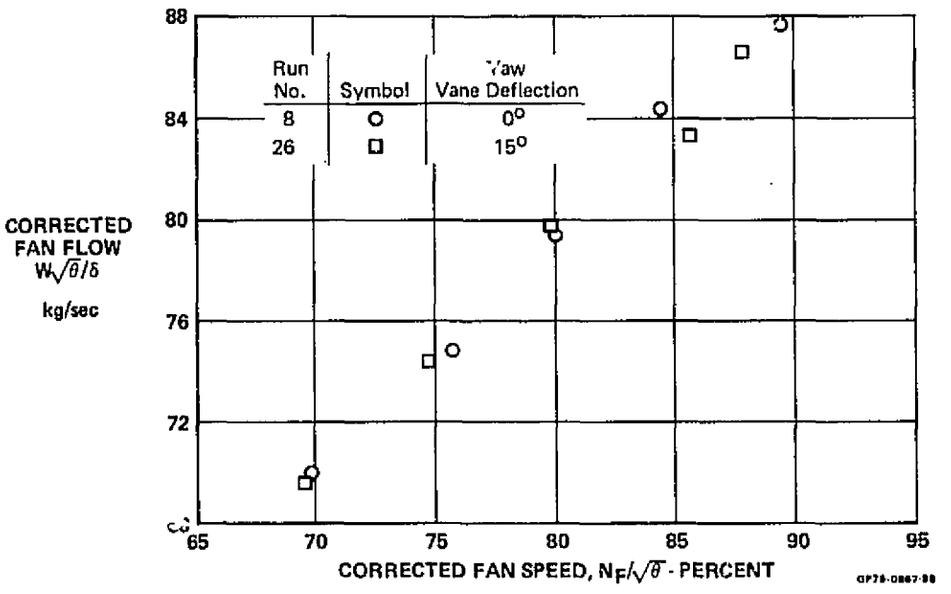

5. CONCLUSIONS

The large scale tests of the boilerplate "D" vented nozzle were conducted to establish vectoring performance "in" and "out" of ground effect, thrust spoilage capability, fan/nozzle compatibility, and nozzle wall temperature distributions and to obtain a comparison of large scale nozzle performance with small scale test data. The conclusions derived as a result of the large scale tests are presented below:

- Longitudinal and VTO thrust vectoring performance of the "D" vented nozzle, out of ground effect, is strongly dependent upon nozzle pressure ratio and nozzle corrected flow. Comparison of the large scale vectoring performance with small scale test data showed good agreement, within 1% to 2%, and indicates that nozzle scale effects between 4.5% and 60% are small.
- In ground effect, the vented lower corner of the "D" vented configuration provides a self-relieving exit area feature which can be used to reduce or eliminate back pressure effects on the propulsion system. The "D" vented nozzle with the LF336/J85 system produced an increase in vertical thrust performance at the maximum fan speed (90%) as the ground plane height to fan diameter ratio (h/D_F) was reduced to 1.6. A decrease in vertical thrust was measured at reduced fan speeds as h/D_F was reduced.
- Thrust reduction modulation by porting exhaust flow through the top of the nozzle is an effective method to reduce vertical thrust levels for aircraft control purposes. Reduction of the nozzle thrust coefficient to a value of 0.7 was demonstrated on the LF336 fan system. General agreement between large and small scale TRM performance was obtained.
- The compatibility of the "D" vented nozzle with a turbotip fan system was demonstrated by the successful completion of all vectoring and control function tests with no detectable adverse effects on fan operation. Close coupled vectoring of the turbotip fan exhaust from 0° to 117° was accomplished with little distortion of the fan exit total pressure or temperature distributions. Circumferential distortion of fan exit static pressure distribution and turbine exit flow total conditions was introduced by the vectoring nozzle, the result

of which implies nonuniform work extraction by the tip turbine. The variation in turbine work extraction caused by the nozzle is well within the distortion tolerances of turbotip fan systems as evidenced by successful test operation of turbotip fans with 180° partial arc turbine admission.

- The structural temperatures within the "D" vented nozzle are rapidly reduced below the tip turbine exhaust temperature level as a result of mixing processes within the nozzle. For the LF336 tests the maximum temperature recorded on the two movable hood elements was approximately 400°K (260°F).
- The capability of the "D" vented nozzle to accomplish side force vectoring was not demonstrated due to insufficient test instrumentation. No loss in resultant thrust performance was recorded during deflection of the exit yaw vane up to 15°.
- The large scale performance tests have confirmed the validity of the small scale performance data base for the "D" vented nozzle. Application of this data base to advanced turbotip fan systems such as the General Electric LCF459/J97 system indicates that the "D" vented nozzle will provide an efficient lift/cruise thrust vectoring system for use on an advanced lift/cruise fan V/STOL aircraft.

6. REFERENCES

1. Smith, E. G., Dors, J. C., "LCF459/J97 Estimated Performance," General Electric Report R75AE6413, July 1975.
2. Schlundt, Donald W., "Testing of Lift/Cruise Fan Exhaust Deflector," Rockwell International Report NA-75-227, March 1975.
3. Anon, "Design of a Thrust Vectoring Nozzle for V/STOL Transport Lift Cruise Fans," McDonnell Douglas Report MDC A2738, March 1974.

APPENDIX A
DATA ANALYSIS PROCEDURE

Corrected Parameters

Fan and nozzle performance was converted to corrected parametric notations. The fan correction factors were based on ambient temperature and barometric pressure measurements which were recorded during each test; thus,

$$\theta = T_A/518.67 \qquad \text{A-1}$$

$$\delta = P_A/14.696 \qquad \text{A-2}$$

Nozzle corrected flow rates were corrected to nozzle entrance total conditions where

$$\theta_t = T_T/518.67 \qquad \text{A-3}$$

$$\delta_t = P_T/14.696 \qquad \text{A-4}$$

Nozzle Mass Flow Rates

The total mass flow rate through the test nozzle was comprised of the sum of LF336 fan flow and J85 gas generator exhaust flow.

$$W_{TOT} = W_F + W_{GG} \qquad \text{A-5}$$

LF336 fan flow was established by means of the large diameter, 153.61 cm (60.5 in.) fan bellmouth. Measurements of the wall static pressures at the throat station of the bellmouth were used in conjunction with a calibration curve for this bellmouth to determine the fan flow rate. The gas generator inlet flow was established in a similar manner with a standard J85-5 bellmouth supplied by General Electric Co. The gas generator exhaust flow was computed from the sum of inlet flow, fuel flow and interstage bleed flows, where

$$W_{GG} = W_{GA} + W_F - W_{IB} \qquad \text{A-6}$$

Fuel flow was directly measured with a turbine flowmeter whereas the interstage bleed flow was determined from measurements of the bleed valve position and a calibration curve of the bleed valve geometry.

Nozzle Entrance Conditions

Average values of nozzle entrance total pressures and temperatures were computed using the radial temperature and pressure information obtained with the four nozzle entrance traversing probes. The pressure and temperature data obtained from each probe during the inward and outward traverses were separately

curve fitted and then averaged to account for the lack of adequate stabilization time at each radial position. The four curve fitted radial distributions were then used to calculate area weighted values of pressure and temperature for both the fan stream and turbine stream. The equations used for the area weighted properties are given below:

$$(P_T)_{FAN} = 2\pi \int_{R_H}^{R_M} \frac{(P_{T1} + P_{T2} + P_{T3} + P_{T4})}{4\ A_{FAN}}\ rdr \qquad A-7$$

$$(T_T)_{FAN} = 2\pi \int_{R_H}^{R_M} \frac{(T_{T1} + T_{T2} + T_{T3} + T_{T4})}{4\ A_{FAN}}\ rdr \qquad A-8$$

where

$$A_{FAN} = 2\pi \int_{R_H}^{R_M} rdr \qquad A-9$$

and

$$(P_T)_{TURBINE} = 2\pi \int_{R_M}^{R_T} \frac{(P_{T1} + P_{T2} + P_{T3} + P_{T4})}{4\ A_{TURBINE}}\ rdr \qquad A-10$$

$$(T_T)_{TURBINE} = 2\pi \int_{R_M}^{R_T} \frac{(P_{T1} + P_{T2} + P_{T3} + P_{T4})}{4\ A_{TURBINE}}\ rdr \qquad A-11$$

where

$$A_{TURBINE} = 2\pi \int_{R_M}^{R_T} rdr \qquad A-12$$

The area weighted fan and turbine properties were then used to obtain mass weighted nozzle entrance properties as given below:

$$(P_T)_{NOZ} = [(P_T)_{FAN}\ W_{FAN} + (P_T)_{TURBINE}\ W_{GG}]/W_{TOT} \qquad A-13$$

$$(T_T)_{NOZ} = [(T_T)_{FAN}\ W_{FAN} + (T_T)_{TURBINE}\ W_{GG}]/W_{TOT} \qquad A-14$$

and

$$NPR = (P_T)_{NOZ}/P_A \qquad A-15$$